Single- and Multi-Transducer Arrays Employing Nanoparticle Interface Layers as Vapor Detectors for a Microfabricated Gas Chromatograph

By

Lindsay Kay Wright

A dissertation submitted in partial fulfillment
of the requirements for the degree of
Doctor of Philosophy
(Chemistry)
in the University of Michigan
2015

Doctoral Committee:

Professor Edward T. Zellers, Chair
Professor Xudong Fan
Professor Adam Matzger
Associate Professor Anne McNeil

DEDICATION

To my Uncle Chris, Aunt Carla, and my grandfathers

ACKNOWLEDGMENTS

I would first like to thank my advisor, Prof. Edward T. Zellers, for his patience, guidance, and support through this journey. I have benefited from his insight and scientific expertise and have become a better scientist and scholar as a result. Next, I would like to express my gratitude to my dissertation committee members, Dr. Adam Matzger, Dr. Anne McNeil, and Dr. Xudong Fan for their insight, support, ideas, and time put forth during all of the milestones to my Ph.D.

I would also like to acknowledge the Zellers' group, current and past members, for their ideas, support, and collaborations. A special thanks to those who have trained me and whom I have worked alongside with the most: Forest Bohrer, Gustavo Serrano, Will Collin, Kee Scholten, Thitiporn Sukaew, and Jonathan Bryant.

I would like to acknowledge the sources of funding that supported this research: the Department of Homeland Security, Science and Technology Directorate under Cooperative Agreement 06-G-024, the WIMS^2 Center, which is sponsored by the Engineering Research Centers Program of the National Science Foundation under award number ERC-9986866, the National Science Foundation under award number ECCS 1128157, as well as the NIOSH and Rackham Merit Fellowships.

Those mentioned above have helped me along my journey to becoming a Ph.D., but I would also like to pay tribute to those that gave me the desire to begin this endeavor in the first place. A special thanks to the Chemistry Department at Washington & Jefferson College for planting the seed of scientific curiosity in me. I would like to especially thank Dr. Steven

Malinak for his constant encouragement, Dr. Robbie Iuliucci for allowing me to see the possible avenues that chemistry would let me explore, and Dr. Michael Leonard for his continuous training, support, and insight with science and life.

Finally, I would like to thank my loved ones. I thank my Mom and Dad for their constant love, support, and encouragement. I know that my accomplishments are your accomplishments and I feel most successful when I have made you proud. Mom- I thank you for my stubbornness that has helped me to push through just about any obstacle that comes my way. Dad- I thank you for your work ethic and the courage to make my own decisions. To my brother, Jonathan- I would like to thank you for initiating my love-hate relationship with the realm of science by first introducing me to dry ice as a child. To my grandmothers- I thank you for the constant love and words of encouragement and I hope that I may continue to make you proud. I would like to thank my in-laws, Pamela and Joseph, for their love and support as well. Lastly, I thank my loving husband, Andrew. Words cannot express what all you have done for me for the majority of the last decade, from putting your dreams on hold so that I may pursue mine to helping me to believe in myself. I thank you for all of the love, support, and encouragement you have shown and continue to show me.

TABLE OF CONTENTS

LIST OF FIGURES

LIST OF TABLES

LIST OF APPENDICES

ABSTRACT

This body of research focuses on improving microsensor arrays used as detectors in Si-microfabricated gas chromatographs (μGC) for the determination of volatile organic compounds (VOCs). By means of such improvements, μGC technology should find wider application in homeland security, disease diagnosis, and environmental monitoring. The microsensors considered here all employ thiolate-monolayer-protected gold nanoparticles (MPN) as vapor sorptive interface layers. The central hypothesis is that by altering the MPN ligand, core size, and/or the underlying transducer, the diversity of responses to VOCs provided by microsensor arrays with MPN interfaces can be improved. The first study evaluated a single transducer (ST) array of MPN-coated chemiresistors (CR) as a μGC detector for three semi-volatile markers of the explosive 2,4,6-trinitrotoluene in the presence of alkane interferences of similar volatility. The effects of flow rate and temperature on chromatographic resolution, sensitivity, and limits of detection (LOD) were assessed. Under optimized conditions, a complete analysis required < 2 minutes, targets were separated from interferences, unique response patterns were obtained, and LODs were ≤ 4 ng. In the second study, data from four MPN-coated CRs and four similarly coated thickness shear mode resonators (TSMR) were combined to compare ST and multi-transducer (MT) arrays with respect to response diversity for a set of five VOCs and their binary mixtures. Extended disjoint principal regression (EDPCR) analysis was coupled with Monte Carlo simulations to assess the performance of all possible combinations of CRs and TSMRs in terms of the recognition rate (RR). The best 4-MT arrays generally outperformed the best 4-ST

arrays, but array composition was critical. In the third study, the plasmonic behavior of the MPN films was exploited by assessing the changes in the absorbance spectrum at three probing wavelengths. A set of seven MPN films of different ligand functionalities and Au core diameters between 4 and 40 nm was exposed to 6 individual vapors. Vapor discrimination was achieved both with single MPN films and arrays of just 2 films (RR > 95%). These types of sensor arrays can enhance the vapor discrimination of sorption-based detectors utilized in μGC technology, making the analysis of complex VOC mixtures possible.

CHAPTER I

INTRODUCTION TO SORPTION-BASED SINGLE- AND MULTI-TRANSDUCER AND MULTI-VARIABLE ARRAYS

1.1 Dissertation Overview

The need to quantitatively analyze volatile organic compounds (VOC) in complex mixtures is crucial to numerous problems of societal concern, including mapping/remediating environmental pollution, assessing human exposure to toxic chemicals, diagnosing disease, battling terrorism, and ensuring indoor air quality. In order to address these problems, instruments are needed that are capable of measuring VOCs in the low- or sub-parts-per-billion (ppb) concentration range, on site, often over a short time period. To meet these criteria, an instrument ideally must be small (portable), inexpensive to manufacture and operate routinely, possess the inherent sensitivity needed for these applications, and provide determinations of multiple VOCs. Unfortunately, current portable instrumentation falls short of these requirements.[1-4]

VOC monitoring instruments that have been successfully adapted for field use are based on Fourier transform and single beam infrared spectrometry (FTIR),[1-2, 5] direct-inlet mass spectrometry (MS),[6-7] ion mobility spectrometry (IMS),[8-10] and most commonly, gas chromatography (GC) with various detectors.[3-4,11-15,16-19] Research over the past 30 years has been directed at developing microfabricated gas chromatographs (μGC) for their ability to identify eluting analytes by the combination of retention time and the spectrum/pattern created

by the detector. In general, a μGC consists of a micropreconcentrator/focuser (μPCF) that captures a large sample volume, which is then thermally desorbed into a much smaller volume and sharply injected into a separation microcolumn (μcolumn) and, ultimately to the detector to identify the components of the sample mixture. Although portable GC instruments containing traditional detectors, like that of MS or IMS, have been commercially available,[4, 8-10, 11,16] several reports have focused on the use of sorption-based microsensor (μsensor) arrays as μGC detectors because of the sensitivities typically achieved with these devices and the low power of operation.[12-14] These types of μsensor arrays typically comprise one type of transducer coated with different interface materials (functionalized polymers or monolayer-protected gold nanoparticles (MPNs)) that react reversibly and differentially with a wide range of VOCs, where the ability of these single-transducer (ST) arrays to identify VOCs is dependent on the partial selectivity among the individual sensors.[12-14]

These ST arrays have the ability to recognize individual vapors among a set of 10 or more and their binary mixtures, but fall short of discriminating among the components of ternary (or higher order) mixtures, due in part to the limited range in energies that can be probed by the reversible, non-bonding types of interactions responsible for sorption-based sensor arrays.[21-23] In fact, the discrimination of mixtures of three or more vapors from their components and lower-order mixtures is generally not achievable with standalone arrays.[22-26] To overcome this limitation, arrays that combine multiple transducers (MT) with the same interface layers have been investigated in hopes that probing different properties of the same coating would aid in vapor identification/discrimination. To date, MT arrays have generally outperformed ST arrays, but have only offered modest improvements.[25-28] In addition to ST and MT arrays, another recent approach to enhancing vapor discrimination uses multi-variable (MV) sensors, in which

complementary information can be obtained from measuring multiple outputs from one sensor. These sensors increase the quality and quantity of information while simplifying the materials and equipment necessary for vapor detection.

The research presented here examines various approaches to enhancing vapor discrimination with μsensor array technologies that rely on changes in mass, volume, or optical absorbance and that utilize thiolate monolayer-protected gold nanoparticles (MPNs) as interface layers. Specific devices employed include thickness shear mode resonators (TSMRs) and chemiresistors (CRs). Additionally, optical measurements of the localized surface plasmon resonance (LSPR) were performed as a preface to using microfabricated optofluidic ring resonator (μOFRR) devices. Target vapors include common VOCs and explosive marker compounds.

Chapter 1 provides the background information and significance of this research. Chapter 2 describes a study of MPN-coated CR arrays as a μGC detector for the monitoring of marker compounds of the explosive, 2,4,6-trinitrotoluene (TNT). The variables that can affect the performance of the array, including temperature and flow rate, along with the implications of thermodynamics and kinetics of vapor sorption on the sensor response are optimized. In Chapter 3, VOC response data from four MPN-coated CRs are combined with data from four similarly coated TSMRs. The performance of all possible ST and MT arrays are compared for five individual VOCs and their binary mixtures using Monte Carlo simulations and chemometric analyses. In Chapter 4, films of MPNs containing different thiolate and dithiane ligand functionalities and/or gold core diameters are explored as interface layers for optical sensing of VOCs at multiple wavelengths. Here, the plasmonic behavior of these films is exploited by monitoring the absorbance spectra at three distinct probing wavelengths upon vapor exposure. This study evaluates which ligands and core sizes afford the best vapor discrimination and,

therefore, which should be used as interface layers on microfabricated optofluidic ring resonators (μOFRRs) developed in a parallel study. Chapter 5 highlights the major findings of this research and suggests future studies. The research presented in this dissertation contributes to the fundamental understanding of MPNs as sensor interface materials and illustrates the advantages, disadvantages, and challenges of using MPNs in ST, MT, and MV arrays for μGC detection to enhance capabilities for analyzing complex VOC mixtures.

The remainder of this chapter discusses the relevant background information for this research, including the factors related to sorption and the sensor technologies that are generally used. The discussion on the role of sorption-based sensor arrays in portable instruments, in both commercially available and research level systems, is discussed prior to the kinetics and thermodynamics of sorption-based sensor arrays. Different transducers and interface layers used in sensor arrays and the types of sensor arrays that have been studied are also discussed, followed by an overview of the chemometrics used to analyze the sensor responses.

1.2 Portable Direct-Reading Instruments

Monitoring of VOCs on-site with portable direct-reading instruments has been practiced for several decades, and numerous field-deployable VOC monitoring instruments are commercially available.[1-5, 8-11, 15-19, 29] However, current portable instruments suffer from many shortcomings. Generally, they are too costly and too large for routine implementation. Additionally, only a few can provide multi-VOC determinations, and many lack the inherent sensitivity necessary for critical applications in environmental monitoring, homeland security, and biomedical diagnostics.

The instruments capable of multi-VOC determination that have been adapted for field use generally utilize conventional technology, such as infrared (IR) spectroscopy,[1-2, 5] ion mobility spectrometry,[8-10] and gas chromatography coupled with various detectors (flame ionization detector (FID), photoionization detector (PID), thermal conductivity detector (TCD), surface acoustic wave sensors (SAW), and mass spectrometry (MS)).[3-4, 11, 15-19] Other current direct-reading monitoring systems available include so-called "electronic noses," consisting of sensor arrays whose collective patterns are used to identify VOCs.[29] However, these standalone arrays are not capable of quantitative multi-vapor analysis.[23]

Among the most commonly employed direct-reading instruments used for the detection and quantification of multiple VOCs in various applications are portable gas chromatographs (GCs), and in particular, gas chromatograph/mass spectrometry (GC/MS) systems. These systems are widely used because of their ability to identify multiple VOCs by the combination of the retention time and the fragmentation pattern/spectrum created by the MS detector. Among the commercialized portable GC/MS systems are the Griffin 460, the TRIDION-9, and the Hapsite ER which weigh in at 96, 32, and 42 lbs, respectively.[4, 11, 16] The Griffin 460 uses cylindrical ion trap (CIT) technology and can determine VOCs at the parts-per-trillion (ppt) level, but only with preconcentration.[11] The TRIDION-9 uses a miniaturized toroidal ion trap mass spectrometer[16] and the Hapsite ER uses an electron multiplier mass spectrometer,[4] both of which can determine some VOCs at the ppt-level. Although these commercially available GC/MS systems are sensitive, they are still too costly and too large, limiting their use for routine or extended on-site monitoring. There is still a need for a portable instrument that is capable of identifying and quantifying low concentrations of target vapors in complex mixtures, yet small, inexpensive, and simple enough for routine analysis.

1.3 Miniaturization of Portable Direct-Reading Instruments: A μGC Overview

Numerous efforts have been directed toward the miniaturization of common analytical instruments.[3, 13-15, 20, 30-37] This research has been made possible with the development of micro-electro-mechanical systems (MEMS) processing techniques. Although reports on MEMS-based MS,[34] IMS,[35] IR,[36-37] and GC systems[3, 13-15, 20, 30-33] have appeared in the literature, MEMS-based MS systems still suffer from low sensitivities and IR systems suffer from reduced resolution accompanying the miniaturization, i.e. smaller mirrors. The most success has come in miniaturizing GC systems, with the earliest report on a MEMS-based GC system being over 30 years ago.[30] More recently, the WIMS[2] Center at the University of Michigan has developed numerous μGC components and prototypes.[13-14, 38-40] The knowledge gained from these projects was used in the development of the μGC, dubbed INTREPID, utilized in Chapter 2 of this dissertation (Figure 1-1).

The three essential components of a μGC include a preconcentator or other injector, a separation column, and a detector (Figure 1-2). The preconcentrator/focuser (μPF) serves as both a preconcentrator and a sharp injector.[41-43] It is packed with a high surface area adsorbent to capture VOCs from a large volume of air. The VOCs collected are then thermally desorbed into the separation column in a much smaller volume which helps to increase chromatographic resolution.[41-42] The separation column is coated with a thin layer of a polymer stationary phase by either a static or dynamic coating method.[44-45] Separation is based on the partitioning between the stationary (usually polymer film) and mobile (carrier gas) phases, and restricting the column length can have negative implications on the peak capacity. With the ongoing push to reduce the overall size and power requirements, focus has been placed on utilizing microsensor arrays as detectors in μGC systems.[13-14, 20, 33, 38, 40, 46] The detector consists of a thin film of ad/absorptive

material interface layer coated on a transducer that is probed electrically, mechanically, thermally, or optically. These types of detectors rely on the reversible partitioning of the target vapor in the interface layer.

The following sections (1.4-1.7) discuss the thermodynamics and kinetics governing sorption. Included in the remainder of this chapter is a discussion on the multiple transducers and interface layers that are typically used in microsensor arrays, along with how combinations of transducers and interface layers can enhance vapor discrimination. Additionally, some of the chemometric analyses used to characterize the sensor responses are also discussed.

1.4 Sensors Employing Interface Layers for Vapor Detection

Sensors that rely on reversible vapor sorption have been studied extensively over the past couple of decades.[47-54] Arrays of these types of sensors are often used to obtain partially selective responses, where each sensor in the array responds to every analyte, but to a different extent. The collective pattern of the array, like a crude spectrum, is used to identify a particular volatile organic compound (VOC).[55-58]

A typical sorption-based sensor consists of an optical, piezoelectric, or electronic transducer coated with an interface layer (Figure 1-3). Interface layers include amorphous rubbery polymers and thiolate monolayer-protected nanoparticles (MPNs) that can be synthesized with different functional groups. These materials interact reversibly with the analytes of interest. When vapor sorption/desorption occurs, changes in the properties of the interface layer are converted into analytical signals (i.e. change in absorbance, frequency, or resistance) by the transducer. Different transducers probe different properties of the vapor-film interaction, but the response of every sensor relies primarily on the degree of partitioning within the film.

The sorption of analyte in the film can be quantified using the thermodynamic partition coefficient, *K*:

$$K = C_s/C_v \quad \textbf{(1)}$$

where C_s is the concentration of the vapor in the sorbent phase and C_v is the concentration in the vapor phase. The magnitude of *K* depends on the sum of the attractive forces (i.e. H-bonding, dipole-dipole, dispersion, and polarizability) that cause the non-bonding, reversible interaction between the vapor and the film. An increase in the sensor response results from interactions that increase the sorption of vapors into the film.

K is an equilibrium-based quantity related to the Gibbs free energy (ΔG), which allows us to write:[48]

$$\ln K = \frac{\Delta H_s}{R}\frac{1}{T} + \frac{\Delta S_s}{R} = \frac{\Delta H_{vap} - \Delta H_{mix}}{R}\frac{1}{T} + \frac{\Delta S_{vap} - \Delta S_{mix}}{R} \quad \textbf{(2)}$$

where ΔH_s is the change in enthalpy due to sorption, ΔS_s is the change in entropy due to sorption, ΔH_{vap} is the change in enthalpy due to vaporization, ΔS_{vap} is the change in entropy due to vaporization, ΔH_{mix} is the change in enthalpy due to mixing, ΔS_{mix} is the change in entropy due to mixing, *R* is the ideal gas constant, and *T* is the absolute temperature. Temperature has implications for the sensor, in that it must either be tightly controlled or accounted for when measuring the response to a given VOC.

Replacing the temperature independent term with a constant, *B*, **Eqn. 2** can then be rewritten as:

$$K = B_o e^{\frac{\Delta Hs}{RT}} = B_o e^{\frac{-(\Delta H_{cond} + \Delta H_{mix})}{RT}} \quad \textbf{(3)}$$

where B_o is a constant, and ΔH_{cond} is the heat of condensation. ΔH_{mix} is related to the difference in the cohesive energies of the analyte and film. Assuming ideal conditions, ΔH_{mix} would be

equal to zero. ΔH_{cond} is related to the saturated vapor pressure, p_v^o, of the solvent via the Clausius-Clapeyron equation:

$$p_v^o = A_o e^{\frac{-\Delta H_{vap}}{RT}} = A_o e^{\frac{\Delta H_{cond}}{RT}} \quad \textbf{(4)}$$

where A_o is a constant. Substituting **Eqn. 4** into **Eqn. 3**,

$$K_i = A_i \frac{1}{p_v} \quad \textbf{(5)}$$

where A_i is a constant and K_i is the ideal partition coefficient, shows that K is inversely proportional to the p_v of the analyte.

Although K is mostly determined by the p_v of the analyte, partial selectivity can be achieved as long as values of ΔH_{mix} differ among a set of analytes and the film. This is accomplished by using a range of coatings/interface layers that contain different functional groups (i.e. hydrogen-bond donor, hydrogen-bond acceptor, aromatic, etc.) that span the non-bonding, reversible interactions of the sorption process. These interactions have been modeled and systematically investigated using linear solvation energy relationships (LSER), in which the vapor-film interactions are characterized by the sum of all polarizability, hydrogen bond basicity and acidity, dipolarity, and dispersion interactions between the film and the vapor.[49, 59-61] By using an array of sorptive sensors, each with a different interface layer with distinct non-bonding interactions, vapor identification is possible.

Depending on the flow rate, temperature, detector cell dead volume, film thickness of the interface layer, and the vapor-film interaction, the kinetics of vapor sorption/desorption can also play an important role in the sensor response. When an interface layer is exposed to a vapor, the vapor is absorbed at the air-film interface and then diffuses into the film at a rate that is determined by the concentration gradient across the film and the diffusivity of the vapor in the film. For these types of sensors, Fickian diffusion is often observed. Fick's first law of diffusion

defines the flux, J (mass/area/time) for films of thickness h and vapors that pass perpendicularly through the film by:

$$J(x) = D\frac{\partial C}{\partial x} \quad \textbf{(6)}$$

where C(x) is the concentration in the film, x is the vertical distance from the film-substrate interface, and D is the diffusion coefficient.[62-63] Thus, the maximum flux, J_{max}, occurs when 1) the vapor concentration at the outer surface of the film ($x = h$) is in equilibrium with the atmospheric concentration which can be expressed as its partial pressure, p_i (i.e., $C(h) = C_0(p_i)$, where C_0 indicates equilibrium concentration) and 2) the concentration on the lower surface ($x = 0$) is maintained at zero. This produces the greatest concentration gradient. Therefore, under steady-state conditions, a uniform concentration profile with x (or h) would occur:

$$J_{max} = D\frac{C_o(p)}{h} \quad \textbf{(7)}$$

and the maximum flux would increase linearly with D and the solubility $C_0(p)$ and decrease with film thickness, h. For sensor applications, steady-state permeation is prohibited because films are cast onto impermeable substrates. However, the evolution of the concentration profile in the film upon vapor exposure can be determined from Fick's second law for a one-dimensional system. For a constant D, the change in concentration with time, t, is given by:

$$\frac{\partial C}{\partial t} = D\frac{\partial^2 C}{\partial x^2} \quad \textbf{(8)}$$

(Note: D will increase as a function of $(T_2/T_1)^2$,[64] such that an increase in temperature leads to a higher diffusion rate.)

Diffusion times can be estimated using the simplified one-dimensional Fick's law expression:

$$t = \frac{x^2}{4D} \quad \textbf{(9)}$$

where t is the time it takes for the vapor to diffuse a distance x, given a known value of D. The values of D will be greater for the vapor in air (D_{air}) than within the film (D_{film}). Therefore, the time it takes for the vapor to diffuse to the film surface and within the film can be estimated by using the respective values of D_{air} and D_{film}. Because values of D (usually around 10^{-7} – 10^{-9} cm^2/s for volatile organic compounds in rubbery, amorphous polymers)[65-66] are found experimentally using a gravimetric device to monitor the mass uptake of the vapor within the film under specific conditions, estimates are often used to quantify diffusion times within the film. Regardless of the actual time it takes, the diffusion time to and within the film must be far less than the residence time within the detector cell (dependent on the detector cell volume and flow rate) in order to prevent peak broadening and to ensure a complete sensor response. Rates of desorption from the film should also be considered, as these may be slow in comparison to the rates of sorption into the film. Sorbed analytes formally condense within the film, so they must also evaporate from the film. Evaporation rates are inversely proportional to the p_v.[67] Analytes with lower values of p_v would be expected to have slower desorption rates, and may result in a slow or only partially recovered sensor baseline.

1.4.1 Transducers/ Transduction Mechanisms

Several transduction mechanisms will now be described to set the context of this research. These transducers fall under three main types: (1) mass (2) resistive or (3) optical. The properties of the film that are most commonly probed include changes in mass, frequency, reflectance, absorbance, transmission, resistance/conduction, and the refractive index of the surrounding medium.

1.4.1.1 Mass-Sensitive Sensors: Surface Acoustic Wave (SAW) Sensor and Thickness Shear Mode Resonator (TSMR)/ Quartz Crystal Microbalance (QCM)

Two examples of mass-sensitive transducers are the surface acoustic wave (SAW) sensor and the thickness shear mode resonator (TSMR), also commonly referred to as a quartz crystal microbalance (QCM). These devices are examples of acoustic wave devices, and consist of a single-crystal piezoelectric substrate (often quartz) coated with an interface layer. Applying an AC electric field drives acoustic waves through the substrate, causing the device to resonate at a particular frequency.[52, 68-69] This resonant frequency will decrease by coating the substrate with an interface layer due to the increase in the overall mass of the device. Likewise, upon vapor sorption into the film, an increase in mass results in a proportional decrease in the resonant frequency allowing for quantitative analysis.

In a SAW sensor, a standing acoustic wave is generated along the surface by using two sets of interdigital electrodes (IDEs; Figure 1-4). When an alternating voltage is applied, areas of alternating strain emerge between the electrodes. Because of the piezoelectric effect, a standing wave gives rise to propagating waves.[68, 70] The waves will propagate at a synchronous, or natural, frequency, f_o. When a sorptive interface layer is coated onto the surface of a SAW sensor and exposed to a vapor, a change in mass results in a change in frequency.

Similarly, TSMR devices (Figure 1-5) consist of a circular quartz disk with thin film, circular metal electrodes on each side. When an alternating voltage is applied between the electrodes, acoustic shear waves are generated at the electrodes and propagate normal to the crystal's surface.[69-70] One main difference between TSMRs and SAW devices is that TSMRs are bulk wave oscillators, whereas, SAW devices are surface wave oscillators.[70] Though, like a SAW device, TSMRs are coated with an interface layer that responds to a change in mass at the

surface upon vapor sorption.[48, 71-72] The Sauerbrey equation relates the change in mass on the surface to the frequency response of the device:

$$\Delta F = \Delta m \frac{2F_o^2}{C\,\rho_q\,A} \quad \textbf{(10)}$$

where ΔF is the change in frequency from mass uptake at the surface, Δm is the change in mass, C is the velocity of the acoustic wave, ρ_q is the density of the piezoelectric material, A is the active crystal area, and F_o is the frequency of the uncoated device. The frequency response to VOC sorption, ΔF, is divided by the frequency change upon film coating, F_{film}, to account for the mass of the interface layer. Since all other factors are constant, $\Delta F/F_{\text{film}}$ is equal to $\Delta m_{vapor}/m_{film}$, which is related to the partition coefficient:

$$\frac{\Delta F}{F_{film}} = \frac{\Delta m}{m} = \frac{C_s K}{\rho_{film}} \quad \textbf{(11)}$$

where C_s is the concentration of the vapor in the film and ρ_{film} is the density of the sorptive film.

1.4.1.2 Resistive Sensors: Chemiresistor (CR)

An example of a resistive sensor is a CR, where a change in the analyte concentration is converted into a change in resistance (Figure 1-6). The manner in which the concentration change is converted into a change in resistance depends on the type of interface layer used. For example, metal oxides are reduced by analytes, forcing the re-injection of electrons into the bulk resistor, and decreasing the overall resistance.[73] A combination of a conducting and insulating agent, i.e. carbon-black loaded polymers[74-80] or thiolate monolayer-protected gold nanoparticles (MPNs),[47, 81-82] will swell in the presence of analytes, causing an increase in the overall resistance.

Typically, a set of IDEs is coated with the conducting or semiconducting interface layer. When a voltage is applied to the IDEs, conduction occurs, resulting in a baseline resistance that depends on the composition of the film. In the case of MPNs, the resistance changes are primarily due to swelling of the film upon vapor exposure.[47, 81-83] Upon swelling of the film, the interparticle distance (δ), or distance between nanoparticles, increases, resulting in conductance decreases and, thus, resistance increases in the film. It has been shown, however, that resistance can also decrease for cases where the permittivity of the film increased due to a polar vapor.[47, 84-85] A vapor that is more polar than the film may change the overall dielectric of the medium,[86] which is also a contributor to the response.[81] The total response is measured as a change in resistance, ΔR, and can be expressed as:

$$\frac{\Delta R}{R_b} = K(c_1\Delta\delta + c_2\Delta\varepsilon_m) \quad \textbf{(12)}$$

where R_b is the baseline resistance, K is the partition coefficient, c_1 and c_2 are constants, $\Delta\delta$ is the change in intercore distance associated with film swelling, and $\Delta\varepsilon_m$ is the change in dielectric of the medium. The measurable change in resistance is again related to K, which is related to the vapor concentration, C_v, and sensitivities can be defined as $[(\Delta R/R_b)/C_v]$.

1.4.1.3 Optical Sensors: Surface Plasmon Resonance (SPR), Localized Surface Plasmon Resonance (LSPR), and Micro Cavity Sensors

Optical sensors can be made using many platforms, e.g., fibers, cavities, etc., that respond to changes in reflectance, absorbance/transmission, fluorescence, or the refractive index of the medium. The vast majority of the literature on optical sensors focuses on liquid phase analyses (often biological),[87-91] but these sensors have also been recently utilized for the detection of vapors and gases.[92-99] Two main classes of optical sensors used for vapor detection are based on

different microcavity geometries and the phenomenon known as surface plasmon resonance (SPR). Common geometries include a microsphere, microtoroid, microring, and opto-fluidic ring resonator (OFRR; Figure 1-7).[100-103] Regardless of the geometry, the basis of the response remains the same; detection occurs when a vapor interacts with light near the boundary of the device. The microcavity consists of a thin wall, whose circular or toroidal structure serves as an optical waveguide supporting whispering gallery modes (WGMs) by total internal reflection of light within the curved boundary.[100-102] A WGM is excited at any point along the device by placing a tapered fiber-optic probe orthogonally in contact with the device. The light generated by a laser travels along the probe and couples to the device, resonating with high *Q* factors (10^6-10^9) at closely spaced wavelengths, λ_{WGM}.[100] The values of λ_{WGM} are governed by the equation:

$$\Delta\lambda_{WGM} = \frac{2\pi r \eta_{eff}}{m} \quad \textbf{(13)}$$

where *r* is the radius, η_{eff} is the effective refractive index, and *m* is an integer. The walls of the device are thin, such that an evanescent field is supported at the surface. Each device can be coated, either internally or externally, depending on the geometry, with a sorptive interface layer. Reversible sorption of VOCs results in changes in the thickness and the dielectric constant of the film. These effects change the η_{eff}, and therefore, λ_{WGM}. Shifts in λ_{WGM} can be monitored by a photodetector to determine the concentration of the vapor.

Surface plasmon resonance (SPR) sensors rely on the charge-density oscillation that can be generated between two media of different dielectric constants.[104-105] This oscillation is an electromagnetic wave that has its highest point of intensity at the interface of the two media and decays exponentially into both layers (Figure 1-8a). Because the wave is found at the boundary, the oscillations are sensitive to any change that occurs at or near the boundary, such as

adsorption onto a metallic film. Films containing metals, usually silver and gold, are used in order to produce SPR waves.[104-105]

A specific form of SPR, referred to as localized surface plasmon resonance (LSPR), occurs when light interacts with metallic particles much smaller than the incident wavelength (Figure 1-8b).[105] The plasmon oscillates locally around the particles at a specific frequency. Both the SPR and LSPR are sensitive to changes in the dielectric environment, but the wavelength of the LSPR is determined by the size, shape, material, and local dielectric environment.[92, 95-96] Upon vapor exposure, changes in the local dielectric, or refractive index, and swelling of the ligand[97, 106-107] cause a measurable shift (increase or decrease) in the wavelength. Metal nanoparticle films containing ligands that have been functionalized to interact with the vapor of interest are often used to increase vapor partitioning, and therefore, the overall optical response.

1.4.2 Interface Layers

The sensor response is dependent on the interaction between the vapor and the interface layer. Typical interface layers include graphene and carbon nanotubes, metal oxides, metalloporphyrins and metallophthalocyanines (MPc), polymers (both intrinsically conducting and composite mixtures), monolayer-protected nanoparticles (MPNs), and composite mixtures of the above for their versatility, low cost, and ease of deposition on a number of different substrates. These materials can be spin-coated, dip-coated, drop-cast, spray-coated, or grown directly onto optical, mass sensitive, or resistive transducers. The interface layer can be modified to enhance selectivity by tuning the functionalization of the material to that of the analyte (e.g. hydrogen bond donor and acceptor).

1.4.2.1 Graphene and Carbon Nanotubes

Carbon-based materials, such as graphene and carbon nanotubes (CNTs), exhibit charge-sensitive conductance/resistance and as a result, are normally coated or grown directly onto resistive based transducers, such as chemiresistors (CRs) or field effect transistors (FETs). The detection of gases or vapors using carbon-based interface layers depends on the changes in electrical properties induced by charge transfer with the analyte. Therefore, these types of interface layers are most sensitive primarily to electron-accepting or donating analytes. However, the surface of these materials can be modified to enhance selectivity to target vapors. To take advantage of their conductive properties, these interface layers are commonly combined with functionalized polymers in composite mixtures.

Graphene is a 2-dimensional sheet (single layer) of carbon and a zero bandgap semimetal. The adsorption of vapors onto the graphene sheet changes the electrical resistance. Graphene monolayers on FETs have been shown to respond to a series of vapors and provide lower noise levels than their 1-dimensional counterparts (i.e. CNTs and nanowires).[108] Even though graphene has this advantage, there is often a layer of contamination on the surface from the fabrication techniques that can greatly affect the response of this material to a given vapor. For this reason, graphene has only recently been studied as an interface layer and more extensive research has been done on the adsorption and sensing capabilities of CNTs.

CNTs were first discovered in 1991 by Iijima[109] and were later exploited for their large surface areas, high electrical conductivity, chemical stability, high mechanical strength and modulus, fast response times to low p_v analytes, and sensitivity to oxygen or oxygen-containing species.[110-111] Additionally, CNTs have been shown to be very sensitive to NO_2 and NH_3.[112] CNTs are like rolling a graphene sheet into a cylinder, where CNTs with one outer wall are

called single-walled CNTs (SWNT) and those with several concentrically nestled walls leads to a multi-walled CNT (MWNT). SWNTs are 1-dimensional conductors, whereas MWNTs have metallic or semiconducting properties. The surface of CNTs, SWNT and MWNT, can be functionalized with different types of polymers, small molecules, or even DNA at their surface to increase selectivity to specific targets. CNTs functionalized with polymers and TiO_2 have been used as interface layers on resonant frequency sensors for VOC detection.[111] Despite their advantages, CNTs typically have long recovery times, complex fabrication, little selectivity, and a very high affinity to adsorb oxygen.[110-112]

1.4.2.2 Metal Oxides (MOX)

Metal oxides can be electrically insulating (MgO, Al_2O_3), wide-band semiconductors (TiO_2, SnO_2, ZnO, Ti_2O_3), and even metal-like (V_2O_3, ReO_3, RuO_2).[110] The sensing mechanism is governed by oxidation/reduction of the analytes at the oxide surface, which leads to poor selectivity. To improve the selectivity, these materials can be doped with metals, which affects the charge transport properties through the film and the sensing characteristics.[113] Some metal oxides, however, have several stable oxidation states that govern the defects in the material and the chemisorption that takes place at the surface. Although the electron exchange between the analyte and metal oxide is typically fast, the chemisorption process can often be very slow. The electronic, and therefore, sensing properties of metal oxides can be greatly influenced by reducing the bulk material down to micrometers and even nanometers, where quantum mechanical effects start to play a role. [113] Nanocrystals (nanorods, nanowires, etc.) have shown to afford high surface areas and increased sensitivities compared to their thin film counterparts.

This is due in part to the nanowire radius being comparable to the Debye length, which makes the nanowire highly sensitive to changes at the surface.

The most common metal oxides used in nanowire chemical sensors are SnO_2, ZnO, and In_2O_3 because of their stability, sensitivity, and ease of synthesis.[114] In fact, the MOX detector array used in a μGC recently only showed a slight drift in the responses after more than three months of operation.[32] These sensors are typically fabricated as either resistors or field effect transistor (FET) devices.[115] Less commonly, metal oxide sensors are coated onto mass sensitive transducers, such as quartz crystal microbalances (QCMs).[116-118] However, a major drawback of these materials is the need to operate at elevated temperature, requiring additional power in order to achieve maximum sensitivity.[114, 119] This, in addition to limited selectivity, makes these materials less ideal for total analysis systems.

1.4.2.3 Phthalocyanines (Pc) and Metallophthalocyanines (MPc)

Phthalocyanines (Pc) were first utilized as dyes and pigments before being exploited for their chemical sensing capabilities. A large number of metallophthalocyanines (MPc) have also been synthesized and studied, in which a metal ion is coordinated within the center of the larger π-ring system of the Pc.[110, 120-123] Pc's have great thermal stability, a known redox activity, and are known to be organic p-type semiconductors.[110, 120-121] The sensitivity and selectivity of sensors coated with these materials is governed by a combination of interactions with the macrocycle, the peripheral substituents, and the metal ion center. Physisorption occurs with the macrocycle and substituents, leading to weaker responses than those caused by charge transfer with the metal ion. These materials become semiconducting upon exposure to air, where O_2 coordinates to the metal center, extracting electrons, and generating charge carriers in the bulk

film. Adsorption of analytes to metal free centers is fast, i.e. Pc's, whereas competition with O_2-bound metal centers is slower.[120-121] Other analytes that act as good π-electron acceptors will oxidize the MPc, with the ring system delocalizing the positive charge. As an effect, the conductivity is increased due to the increase in hole charge carriers. Analytes that act as good π-electron donors have the opposite effect.[110] Due to their conductivity and strong absorbance in the UV-VIS range, Pc's and MPc's are often utilized in resistive[120, 122-123] and optical[124-126] sensors, but they have served as interface layers on mass-based sensors as well.[127] However, these materials have shown significant variation in the sensitivities among different vapors.[120, 128]

1.4.2.4 Polymers

Substrates can be coated with polymers by numerous methods, including electrochemical deposition, spin-coating, drop-coating, dip-coating, layer-by-layer self-assembly, and by using a Langmuir-Blodgett technique.[129] Polymers have been used as interface layers on mass-based sensors,[22, 130] chemiresistors,[76, 131] and on optical sensors[132-134] because of their commercial availability and the ease with which the structures can be modified to include all types of functionality. The ability to functionalize the backbone and side chains, as well as to include neutral and charged particles, makes polymers a practical interface material for vapor sensing on a number of platforms. Some common functionalities that have been used are shown in Figure 1-9. Amorphous polymers are typically used in vapor sensors, with elastomers being the most commonly utilized type. Sorption is greater in elastomeric/rubbery polymers than in glassy ones, resulting in greater sensitivities. Glassy polymers suffer from many disadvantages in sensing applications, such as slow response times, complex diffusion processes, and possible partial irreversibility.

Arrays of TSMRs[130] and SAW devices[22] coated with different rubbery, amorphous polymers have been shown to provide partial selectivity to sets of organic vapors. In order to utilize polymers as interface layers on CRs, it is essential to use conducting polymers or conducting polymer composites.[76, 131] Conducting polymer composites have been made by loading an insulating polymer with a conductive filler, where the amount of conductive filler is proportional to the conductivity of the resulting film. Carbon black[76-77, 131] is a common conductive filler used in polymers that serve as chemiresistor interface layers, although metals (Pt, Pd, Au, Cu) and semi-conducting metal-oxides can also be used. A number of polymers have also been used as interface layers on optical transducers, including optical fibers,[132] photonic microharps,[133] and optofluidic ring resonators,[134] for vapor sensing.

1.4.2.5 Monolayer-Protected Gold Nanoparticles (MPN)

Substrates can be coated with MPNs by spin-coating, dip-coating, layer-by-layer self-assembly, drop-casting, and by a Langmuir-Blodgett technique. Monolayer-protected gold nanoparticles have been utilized as interface layers on chemiresistors,[13-14, 20, 38, 47, 55-57] mass-based sensors,[50, 56, 60, 84] and on numerous optical sensors[84, 93-94, 96, 97, 106-107] due to their sorptive and dispersive properties. These materials can be easily synthesized by reducing gold chloride in the presence of a surface complexing agent, where the ratio of gold to the surface agent affects the core size of the nanoparticles.[135-139] Common surface agents include amines,[140-142] charged species such as citrate,[143-145] and thiols.[135-138] Examples of thiols that have been used in the synthesis of MPNs are shown in Figure 1-10. A stronger surface complexing agent, such as a thiol, will result in smaller nanoparticles (2-5 nm),[135-138] whereas a weaker agent, such as citrate, will typically result in larger nanoparticles (10-100 nm).[143-145]

Several researchers have shown the versatility of these materials on TSMRs.[50, 56, 60, 84] Wohltjen and Snow first demonstrated the use of thiolate-capped MPN films on interdigitated electrodes (IDEs) as CR sensors for detecting vapors, referring to these materials as metal-insulator-metal ensemble (MIME) devices due to the nature of the conducting metal gold cores separated by thin insulating thiolate layer shells.[47] The reversible sorption of the vapor into the film is converted into a measurable change in resistance due to the effect of the swelling and change in the dielectric constant of the thiolate matrix (ε_{th}) on the electron tunneling through the film.[47, 61, 81]

The well-known plasmonic resonance of MPNs make them interesting coatings for optical sensors. MPNs are optically dispersive materials, meaning that their responses to VOCs are dependent on wavelength.[106-107, 146] The optical response to vapor sorption is due to changes in the film thickness (swelling) and refractive index (η), which is proportional to the square of the dielectric constant (ε). Increasing and decreasing η of the local environment surrounding the nanoparticles leads to red shifts and blue shifts in the wavelength of maximum absorbance, λ_{max}, respectively. Swelling-induced changes in the interparticle distance have been shown to lead to blue shifts in λ_{max}.[106-107] Response diversity can be achieved by functionalizing the nanoparticles with ligands of different η and different gold core sizes, which affect the position of λ_{max}, and the breadth and shape of the LSPR band.

1.4.2.6 Composite Mixtures

No one material is highly selective to a series of vapors, so composite mixtures, or admixtures, of two or more materials, have been investigated. The idea is that when materials are combined into an admixture, the performance can be enhanced compared to that of either

material alone. A composite mixture might contain one material that interacts strongly with the vapor and another material that helps to transduce the interaction. For example, composite mixtures of conductive carbon black or CNTs with insulating polymers have been extensively investigated as interface layers on chemiresistors.[74-80] This allows for some versatility, e.g. by adjusting the functionality of the polymer. Conductive fillers, like carbon black, have also been combined with dendrimers with different surface groups as composite interface layers on chemiresistors to detect butylamine vapors.[147] Polymer films have also been combined with dyes, like Nile Red (NR), that fluoresce in order to probe vapor-film interactions that may not otherwise be easily achieved.[148] A composite mixture containing MPNs has also been reported,[149] where several square planar $PtCl_2$(olefin)-(pyridine) coordination complexes were employed to enhance vapor responses of gas-phase olefins. However, as observed with these films and recommended as a precaution for other similar composite mixtures, film instability due to reactivity led to a gradual loss in selectivity. It should also be noted that precise control of the ratios of two materials in any admixture and the dispersion of one material in the other must be taken into account to ensure reproducibility in sensor responses.

1.5 Sensor Arrays

Microfabricated sensor technologies employing interface layers designed to interact with vapors through reversible, non-bonding, physisorption have been developed to an advanced level over the past 30 years.[150-151] In order to achieve any selectivity, the interaction must be specific and/or irreversible (i.e., chemical bonding). Instead, the more common approach is to use a single-transducer (ST) array that contains one transduction platform and several partially selective interface layers to increase the amount of chemical information one can obtain.

However, due to the limitations in the non-bonding energies one can achieve with a partially selective array, ST arrays often fall short when it comes to discriminating among mixtures of vapors (Figure 1-11b-d). Therefore, research has focused on developing arrays that contain the same interface layers on multiple transducers (MT arrays) with the idea that different aspects of the vapor-film interaction can be probed to enhance vapor discrimination.[23-26, 28, 152] However, only modest improvement of MT over ST arrays has been reported.[25-26] Even more recently, sensors that can be probed in multiple dimensions, also known as multi-variable (MV) sensors, have been investigated for the possibility of enhancing vapor discrimination while simplifying fabrication and data analysis.[93-94, 106-107]

1.5.1 Single-Transducer (ST) Arrays

The use of single transducer (ST) arrays that employ different partially selective interface layers on the same type of transducer are the most common approach to vapor detection.[21, 24, 38, 52, 55, 79, 153-159] Differences in the magnitude of partitioning ideally span the range of interactions associated with dispersion, dipolarity, hydrogen bond acidity, hydrogen bond basicity, and polarizability. Using the responses from complementary interface layers, the collective response pattern can be used to differentiate between vapors.[13-14, 20, 57]

ST arrays suffer from a few shortcomings. Due to the low energies of reversible vapor-interface interactions and the characteristic similarity between the patterns of a mixture and its components, recognition of individual vapors among a set of many possibilities has proven to be more manageable than discrimination of a simple mixture from its components with ST arrays (Figure 1-11).[21-23] It is generally true that standalone arrays are not capable of discriminating mixtures of more than three vapors from their components or lower-order mixtures.,[22-24]

Regardless of the transducer, adding more sensors to an array beyond ~4-6 sensors has been shown not to improve the ability of the array to differentiate one vapor from another.[24-25, 79, 160-162]

1.5.2 Multi-Transducer (MT) Arrays

Due to the shortcomings of ST arrays, MT arrays have been investigated in the hopes that combining different interface materials with devices operating on different transduction mechanisms can enhance vapor discrimination by virtue of probing different properties of the vapor-film interaction. Response diversity is enhanced if the different transducers provide complementary information on each VOC. This idea, to combine transduction principles into a hybrid, or MT, array to increase the diversity of responses is not new,[163-166] but it has only been investigated in a few additional studies.[25, 27-28, 165, 167, 168]

Although MT arrays can outperform ST arrays of similar dimension, i.e. number of sensors in the array (Figure 1-11), only a few studies have investigated this to date.[25-28, 165, 167, 169-170] Extensive research has been done by Göpel *et al.* on developing MT array technologies using different interface layers and transduction platforms that probed changes in mass (quartz crystal microbalance and surface acoustic wave sensors), dielectric (capacitance), refractive index, thickness, temperature (thermopile), resistance, and electrochemical activity (metal oxide semiconductor field effect transistor, MOSFET, sensors).[165, 167, 169-170] However, they never demonstrated advantages quantitatively. Jin *et al.* examined polymer-coated calorimeter, capacitor, and cantilever devices, and specifically examined the capability of the optimal-performing MT array to discriminate individual vapors and mixtures up to four components.[25-26] The problem of discriminating mixtures from individual components and lower-order mixture components was investigated systematically, and the 'limit of recognition' (LOR), or the

maximum recognizable mixture composition range, was coined by Zellers and used as a metric for performance.[26] More recently, Li *et al.* examined an MT array consisting of MPN-coated quartz crystal microbalances and chemiresistors. They found that the MT array outperformed ST arrays in the recognition of 15 different VOCs.[28] While these studies have shown that MT arrays generally outperform ST arrays of similar dimension, MT arrays generally fall short when it comes to discriminating mixtures of ≥ three components (Figure 1-11).[25]

1.5.3 Multivariable (MV) Sensors

The development of new interfacial materials for ST arrays is intrinsically limited by the non-bonding interaction between the vapor and interface layer. In addition, research on MT arrays has shown that MT arrays outperform ST arrays, but only marginally.[25-28] An attractive alternative is to focus on whether or not probing multiple parameters of a sensor (using the same interface layer and transducer) can enhance vapor discrimination compared to an ST or MT array. Much like the motivation behind using MT arrays, multivariable (MV) sensors may add dimensionality (i.e., more independent variables) that should increase the analyte selectivity of the system. Unlike MT arrays, which often utilize the same interface materials on a number of transducers to obtain chemically unique information, MV sensors probe multiple parameters, or variables, of one material on one transducer to obtain complementary information that will aid in vapor discrimination. Figure 1-12 illustrates this concept with a single sensing film based on a 3D network of functionalized gold nanoparticles, where vapor discrimination was achieved upon multivariate analysis of the LSPR spectra.[107]

The idea of probing multiple parameters of a single sensor is not new; the dual output (attenuation and velocity of an acoustic wave) of a polymer-coated SAW device was first

investigated over 20 years ago.[171-172] Within the last decade, MV sensing has seen renewed interest.[92-96, 106-107, 173-174] In one study, the wings of the *Morpho sulkowskyi* butterfly gave different optical responses to closely related individual vapors by virtue of the unique lamellar structure with high ridge density.[95] Using the hierarchical natural photonic structures of the iridescent scales, the authors found differences in the reflectance spectra of water, methanol, and ethanol. With the use of principal components analysis (PCA), these three vapors could be differentiated, but at very high concentration ($0.02P_o$, where P_o is the saturation vapor pressure). Traditional photonic sensors lack this degree of selectivity and require an interface layer. In additional studies, a conventional radio frequency identification (RFID) tag coated with a solid polymer electrolyte or an inductor-capacitor-resistor (LCR) resonator coated with peptide-capped gold nanoparticles were utilized to measure different parameters of the impedance.[173-174] The use of an RFID tag allowed for monitoring both the real and imaginary parts of the complex impedance, including four different frequency and magnitude parameters. Utilizing a Nafion polymer film as an interface layer, water vapor could be discriminated from acetonitrile and either ethanol or methanol, but there was no appreciable discrimination achieved between methanol and ethanol.[173]The resonance impedance spectra were measured with the LCR resonator. A total of six parameters relating to the frequency and magnitude of the resonant and antiresonant responses were measured. The sensor responses were found to be dependent on humidity, where the peptides needed to be activated to exhibit responses to the target vapors. Although methyl salicylate and dichloromethane have remarkably similar dielectric constants of 9.0 and 9.1, respectively, they could be discriminated. The authors attributed the differences of the resonance impedance to the fact that methyl salicylate is more bulky, and hence, might affect the rigidity of the linker used in this study. These unique responses by a single MV sensor

allowed for the discrimination of a total of three vapors, two of which have similar dielectric constants.[107] In a later study, Potyrailo *et al.* measured the changes in reflectance of an MPN film to discriminate among individual vapors and a binary mixture using multivariate spectral analysis and found that the MV sensor could quantify at least two to three vapors, similar to that of ST arrays.[107] The spectral analysis of MPN films had also been investigated by several other researchers previously.[92-94, 96, 106] It has been shown that LSPR spectral shifts differ for a set of VOCs due to a combination of swelling-induced increases in the interparticle distance, δ, and the change in the effective refractive index, η_{eff}, of the local environment surrounding the nanoparticles. Dalfovo *et al.* found that the nanoparticle mobility in the film induced by the individual vapors was an important factor in the LSPR sensing mechanism of these devices and in discriminating toluene from ethanol.[97] Similarly, Scholten *et al.* found that an MPN film could be used to discriminate between toluene and heptane vapors due to differences in the swelling-induced increases in δ and the effects of η_{eff}.[106] Cheng *et al.* found that immobilizing the MPNs on a substrate led to extinction and wavelength shifts of the LSPR spectra that were primarily sensitive to changes in η_{eff}.[93-94] These differences allowed for the discrimination among nine different VOCs.[94]

1.6 Chemometric Analyses for Sensor Arrays

Using the response patterns afforded by the sensor array, individual vapors can often be resolved from one another using various pattern recognition methods. Some of the most common pattern recognition methods utilized for sensor arrays are principal component analysis (PCA),[107, 175-177] linear discriminant analysis (LDA),[58, 176-177] and extended disjoint principal component regression (EDPCR) analysis.[23-26, 178-179] These are statistical methods that transform

a set of possibly correlated sensor responses into a subset of uncorrelated variables, or components, that account for the variability in the data set. These methods can be applied to stand-alone arrays, but due to the inherent limitations on the selectivity of these types of sensor arrays, an upstream chromatographic separation module is still necessary to determine the components of mixtures of three or more VOCs.[23-25]

Ideally, the chromatographic variables would be optimized to a point where perfect separation is achieved. However, fieldable μGCs are often motivated by fast analysis times, limiting the extent to which these variables can be tailored or optimized. As a result, co-elution of two or more vapors often occurs at varying degrees of severity. Partially resolved peaks make the determination and quantification of individual vapors of a complex VOC mixture difficult and sometimes even unattainable. In previous sensor array work utilizing classification models derived from EDPCR to identify components of vapor mixtures, any degree of overlapping peaks were treated as an unresolved mixture.[20, 23-25, 40, 178] This type of analysis disregards the potential value of partially resolved peaks.

One approach is to use multivariate curve resolution (MCR), which decomposes an overlapped peak into its respective constituents, in conjunction with pattern recognition methods. Without any prior knowledge of the mixture composition, MCR methods can be used to determine the number of components in the overlapped parent peak and then to extract the spectrum and elution profiles of each component. Extracted spectra can then be compared to those in a library to determine the identities and concentrations of individual vapors. Some examples of common MCR algorithms include evolving factor analysis (EFA),[180-182] alternating least squares (ALS),[181-183] and parallel factor analysis (PARAFAC).[184-185] Because the response pattern afforded by a sensor array is analogous to a spectrum, such MCR methods should be

directly applicable to microsensor arrays used as GC detectors, although this type of analysis with these systems has been extremely limited. Recently, however, the performance of an EFA-ALS technique applied to an MPN-coated CR array used as a GC detector was assessed and compared to the results obtained with EDPCR.[186] This was the first report to show additivity of MPN-coated CR sensors, which is a critical assumption with these types of chemometric analyses. This study found that EFA was able to confirm the number of components within the overlapped peaks in the vast majority of cases examined, but problems with quantitative analysis while operating EFA-ALS in blind mode (having no prior knowledge about how many components are within the overlapped peak) were apparent. This problem was a direct result of the inherent limitation of these types of sorptive ST arrays that lack sufficient diversity in responses. This study helps to illustrate the motivation for new sensor technologies, such as MV sensors, and for the continued effort in examining additional chemometric analyses to make use of the potential value of partially unresolved peaks.

1.7 Summary

As described in this introduction, numerous efforts have been made to develop new sensor technologies necessary to enhance vapor discrimination. The research in this dissertation characterized existing MPN-coated CRs as detectors in a μGC for explosive marker compounds (Chapter 2), evaluated the performance of MT arrays consisting of similarly coated CRs and TSMRs (Chapter 3), and investigated several MPN films composed of different ligand functionalities and gold core sizes as potential interface layers for MV sensors and arrays (Chapter 4). The research presented here adds to the existing literature on MPN-coated vapor sensor arrays. Chapter 2 builds upon existing literature by investigating the use of an MPN-

coated CR array as a detector in a μGC for the detection of explosive marker compounds. Chapter 3 explored different MT arrays consisting of MPN-coated CRs and TSMRs. Although the multi-variable optical responses of MPNs have been examined previously, Chapter 4 extended this knowledge by investigating eight MPN films of different ligand functionalities and gold core sizes. The role of these variables on the optical response were assessed and the results were used to determine which films would function best as interface layers in μOFFRs. This research discusses the advantages, disadvantages, and challenges associated with using MPN interface layers in ST, MT, and MV arrays for multi-vapor analysis.

1.6 References

1. MIRAN SapphIRe, Thermo Scientific, http://www.thermoscientific.com/content/tfs/en/product/miran-sapphire-portable-ambient-analyzers-1.html, accessed September 2014.
2. Gasmet DX4015, Gasmet, http://www.gasmet.com/products/portable-gas-analysers/dx4015, accessed September 2014.
3. 490 Micro GC, Agilent Technologies, http://www.chem.agilent.com/en-US/products-services/Instruments-Systems/Gas-Chromatography/490-Micro-GC/Pages/default.aspx, accessed September 2014.
4. Hapsite ER, INFICON, http://products.inficon.com/en-us/nav-products/Product/Detail/HAPSITE-ER-Identification-System?path=Products%2Fpg-ChemicalDetection%2F, accessed September 2014.
5. HazMatID 360, Smiths Detection, http://www.smithsdetection.com/chemical-identification/57-chemical-identification/hazmatid-360.html#.VBYLFvldWSo, accessed September 2014.
6. Keil, A.; Hernandez-Soto, H.; Noll, R. J.; Fico, M.; Gao, L.; Ouyang, Z.; Cooks, R. G. "Monitoring of Toxic Compounds in Air Using a Handheld Rectilinear Ion Trap Mass Spectrometer," *Anal. Chem.*, **2008**, *80*, 734-741.
7. Huang, G.; Xu, W.; Visbal-Onufrak, M. A.; Ouyang, Z.; Cooks, R. G. "Direct Analysis of Melamine in Complex Matrices Using a Handheld Mass Spectrometer," *Analyst*, **2010**, *135*, 705-711.
8. SABRE 4000, Smiths Detection, https://smiths.com/siteFiles/resources/pressReleases/attachments/SD_Sabre4000.pdf, accessed September 2014.
9. IMS Mini-200, IUT, http://www.iut-berlin.info/7.0.html?&L=1, accessed September 2014.

10. MOBILETRACE Morpho, Safran, http://www.morpho.com/detection/voir-tous-les-produits/trace-detection/mobiletrace-r/?lang=en, accessed September 2014.
11. Griffin 460, FLIR, http://gs.flir.com/detection/chemical/mass-spec/griffin-460, accessed September 2014.
12. Lu, C-J.; Jin, C.; Zellers, E. T. "Chamber Evaluation of a Portable GC with Tunable Retention and Microsensor-Array Detection for Indoor Air Quality Monitoring," *J. Environ. Mont.*, **2006**, *8*, 270-278.
13. Kim, S.K.; Burris, D.R.; Chang, H.; Bryant-Genevier, J.; Zellers, E.T. "Microfabricated gas chromatograph for on-site detection of trichloroethylene in indoor air arising from vapor intrusion. 1. Spatial/Temporal Monitoring," *Environ. Sci. Technol.*, **2012**, *46*, 6065-6072.
14. Kim, S.K.; Burris, D.R.; Bryant-Genevier, J.; Gorder, K.A.; Dettenmaier, E.M.; Zellers, E.T. "Microfabricated gas chromatograph for on-site detection of trichloroethylene in indoor air arising from vapor intrusion. 2. Field evaluation," *Environ. Sci. Technol.*, **2012**, *46*, 6073-6080.
15. CANARY-3, Defiant Technologies, http://www.defiant-tech.com/canarythree.php, accessed September 2014.
16. TRIDION-9, Torion Technologies Inc., http://www.quantanalitica.com/TRIDION%20Brochure-QA-web.pdf, accessed September 2014.
17. GUARDION, Smiths Detection, http://www.smithsdetection.com/index.php/products-solutions/chemical-agents-detection/59-chemical-agents-detection/guardion.html#.VBYRn_ldWSo, accessed September 2014.
18. PID Analyzers, HNU, http://www.hnu.com/index.php?view=%20Portable&cmd=%20102, accessed September 2014.
19. VOC-Analyzer 200, IUT, http://www.iut-berlin.info/229.0.html?&L=1, accessed September 2014.
20. Lu, C-J. ; Steinecker, W.H.; Tian, W-C.; Oborny, M.C.; Nichols, J.M.; Agah, M.; Potkay, J.A.; Chan, H.K.L.; Driscoll, J.; Sacks, R.D.; Wise, K.D.; Pang, S. W. ; Zellers, E.T. "First-generation Hybrid MEMS Gas Chromatograph," *Lab on a Chip*, **2005**, *5*, 1123-1131.
21. Senesac, L.R.; Dutta, P.; Datskos, P.G.; Sepaniak, M.J. "Analyte species and concentration identification using differentially functionalized microcantilever arrays and artificial neural networks," *Analyt. Chim. Acta*, **2006**, *558*, 94-101, 2006.
22. Zellers, E. T.; Batterman, S. A.; Han, M.; Patrash, S. J. "Optimal Coating Selection for the Analysis of Organic Vapor Mixtures with Polymer-Coated Surface Acoustic Wave Sensor Arrays," *Anal. Chem.*, **1995**, *67*, 1092-1106.
23. Hsieh, M.-D.; Zellers, E. T. "Limits of Recognition for Simple Vapor Mixtures Determined with a Microsensor Array," *Anal. Chem.* **2004**, *76(7)*, 1885-1895.
24. Park, J.; Groves, W.A.; Zellers, E.T.," Vapor Recognition with Small Arrays of Polymer-coated Microsensors -- a Comprehensive Analysis," *Anal. Chem.*, **1999**, *71*, 3877-3886.
25. Jin, J.C.; Kurzawski, P.; Hierlemann, A.; Zellers, E.T. "Evaluation of Multitransducer Arrays for the Determination of Organic Vapor Mixtures" *Anal. Chem.*, **2008**, *80*, 227-236.

26. Jin, C.; Zellers, E.T. "Limits of Recognition for Binary and Ternary Vapor Mixtures Determined with Multi-Transducer Arrays" *Anal. Chem.*, **2008**, *80,*7283-7293.
27. Pardo, M.; Kwong, L.G.; Sberveglieri, G.; Brubaker, K.; Schneider, J.F.; Penrose, W.R.; Stetter, J.R. "Data analysis for a hybrid sensor array," *Sens. Act. B*, **2005**, *106*, 136-143.
28. Li, C-L.; Chen, Y-F.; Liu, M-H.; Lu, C-J. "Utilizing Diversified Properties of Monolayer Protected Gold Nano-clusters to Construct a Hybrid Sensor Array for Organic Vapor Detection," *Sens. & Act. B*, **2012**, *169*, 349-359.
29. Cyranose 320, Sensigent Intelligent Sensing Solutions, http://www.sensigent.com/products/cyranose.html, accessed September 2014.
30. Terry, S.C.; Jermann, H.; Angel, J. "A Gas Chromatograph Air Analyzer Fabricated on a Silicon Wafer," *IEEE Trans. Electron Dev.,* **1979**, *26*, 1880-1887.
31. Manginell, R. P.; Bauer, J. M.; Moorman, M. W.; Sanchez, L. J.; Anderson, J. M.; Whiting, J. J.; Porter D. A.; Copic, D.; Achyuthan, K. E. "A Monolithically-Integrated μGC Chemical Sensor System," *Sensors*, **2011**, *11*, 6517-6532.
32. Zampolli, S.; Elmi, I.; Mancarella, F.; Betti, P.; Dalcanale, E.; Cardinali, G. C.; Severi, M. "Real-Time Monitoring of Sub-ppb Concentrations of Aromatic Volatiles with a MEMS-Enabled Miniaturized Gas-Chromatograph," *Sens. & Actuators B: Chem.*, **2009**; *141*, 322-328.
33. Lewis, P. R.; Manginell, R. P.; Adkins, D. R.; Kottenstette, R. J.; Wheeler, D. R.; Sokolowski, S. S.; Trudell, D. E.; Byrnes, J. E.; Okandan, M.; Bauer, J. M.; Manley, R. G.; Frye-Mason, G. C. "Recent Advancements in the Gas-Phase MicroChemLab," *IEEE Sens. J.*, **2006**, *6(3)*, 784-795.
34. Wapelhorst, E.; Hauschild, J-P.; Muller, J. "Complex MEMS: A Fully Integrated TOF Micro Mass Spectrometer," *Sens.& Actuators A: Phys.*, **2007**, *138*, 22-27.
35. Miller, R. A.; Nazarov, E. G.; Eiceman, G. A.; King, A. T. "A MEMS Radio-Frequency Ion Mobility Spectrometer for Chemical Vapor Detection," *Sens. & Actuators A: Phys.*, **2001**, *91*, 301-312.
36. Kim, S-S.; Young, C.; Mizaikoff, B. "Miniaturized Mid-Infrared Sensor Technologies," *Anal. Bioanal. Chem.*, **2008**, *390*, 231-237.
37. Yu, K.; Lee, D.; Krishnamoorthy, U.; Park, N.; Solgaard, O. "Micromachines Fourier Transform Spectrometer on Silicon Optical Bench Platform," *Sens. & Actuators A: Phys.*, **2006**, *130-131*, 532-530.
38. Kim, S. K.; Chang, H.; Zellers, E. T. "Microfabricated Gas Chromatograph for the Selective Determination of Trichloroethylene Vapor at Sub-Parts-Per-Billion Concentrations in Complex Mixtures," *Anal. Chem.*, **2011**, *83(18)*, 7198-7206.
39. Collin, W.; Serrano, G.; Wright, L. K.; Chang, H.; Nuñovero, N.; Zellers, E. T. "Fieldable MEMS Gas Chromatograph for Rapid Determinations of Explosive Marker Compounds in Complex Mixtures," *Proc. Transducers '13*, Barcelona, Spain, June 16-20, **2013**, pp. 2763-2766.
40. Collin, W.; Serrano, G.; Wright, L. K.; Chang, H.; Nuñovero, N.; Zellers, E. T. "Microfabricated Gas Chromatograph for Rapid, Trace-Level Determinations of Gas-Phase Explosive Marker Compounds," *Anal. Chem.*, **2013**, *86(1)*, 655-663.

41. Tian, W-C.; Pang, S. W.; Lu, C-J.; Zellers, E. T. "Microfabricated Preconcentrator-Focuser for a Microscale Gas Chromatograph," *J. Microelectromech. Sys.*, **2003**, *12(3)*, 264-272.
42. Tian, W-C.; Chan, H. K. L.; Lu, Pang, S. W.; C-J.; Zellers, E. T. "Multiple-Stage Microfabricated Preconcentator-Focuser for Micro Gas Chromatography System," *J. Microelectromech. Sys.*, **2005**, *14(3)*, 498-507.
43. Lu, C-J.; Zellers, E. T. "A Dual-Adsorbent Preconcentrator for a Portable Indoor-VOC Microsensor System," *Anal. Chem.*, **2001**, *73*, 3449-3457.
44. Serrano, G.; Reidy, S. M.; Zellers, E. T. "Assessing the Reliability of Wall-Coated Microfabricated Gas Chromatographic Separation Columns," *Sens. & Actuators B: Chem.*, **2009**, *141*, 217-226.
45. Radadia, A. D.; Masel, R. I.; Shannon, M. A.; Jerrell, J. P.; Cadwallader, K. R. "Micromachined GC Columns for Fast Separation of Organophosphonate and Organosulfur Compounds," *Anal. Chem.*, **2008**, *80*, 4087-4094.
46. Zampolli, S,; Elmi, I.; Sturmann, J.; Nicoletti, S.; Dori, L.; Cardinali, G.C.; " Selectivity Enhancement of Metal Oxide Gas Sensors Using a Micromachined Gas Chromatographic Column" *Sens. Actuators B: Chem.*, **2005**, *105*, 400-406.
47. Wohltjen, H.; Snow, A. W. "Colloidal Metal-Insulator-Metal Ensemble Chemiresistor Sensor," *Anal. Chem.*, **1998**, *70*, 2856-2859.
48. Hierlemann, A.; Ricco, A. J.; Bodenhöfer, K.; Dominik, A.; Göpel, W. "Conferring Selectivity to Chemical Sensors via Polymer Side-Chain Selection: Thermodynamics of Vapor Sorption by a Set of Polysiloxanes on Thickness-Shear Mode Resonators, *Anal. Chem.*, **2000,** *72*, 3696-3708.
49. Hierlemann, A; Zellers, E. T.; Ricco, A. J. "Use of Linear Solvation Energy Relationships for Modeling Responses from Polymer-Coated Acoustic-Wave Vapor Sensors," *Anal. Chem.* **2001**, *73*, 3458-3466.
50. Grate, J. W.; Nelson, D. A.; Skaggs, R. "Sorptive Behavior of Monolayer-Protected Gold Nanoparticle Films: Implications for Chemical Vapor Sensing," *Anal. Chem.*, **2003**, *75*, 1868-1879.
51. Patel, S. V.; Jenkins, M. W.; Hughes, R. C.; Yelton, W. G.; Ricco, A. J. "Differentiation of Chemical Components in a Binary Solvent Vapor Mixture Using Carbon/Polymer Composite-Based Chemiresistors," *Anal. Chem.* **2000**, *72(7)*, 1532-1542.
52. A Grate, J. W. "Acoustic Wave Microsensor Arrays for Vapor Sensing," *Chem. Rev.* **2000**, *100(7)*, 2627-2647.
53. Grate, J. W; Klusty, M.; Barger, W. R.; Snow, A. W. "Role of Selective Sorption in Chemiresistor Sensors for Organophosphorus Detection," *Anal. Chem.*, **1990**, *62(18)*, 1927-1934.
54. Lu, G.; Hupp, J. T. "Metal-Organic Frameworks as Sensors: A ZIF-8 Based Fabry-Pérot Device as a Selective Sensor for Chemical Vapors and Gases," *J. Am. Chem. Soc. Comm.*, **2010**, *132*, 7832-7833.

55. Han, L.; Shi, X.; Wu, W.; Kirk, F.L.; Luo, J.; Wang, L.; Mott, D.; Cousineau, L.; Lim, S.I.; Lu, S.; Zhong, C-J. "Nanoparticle-Structured Sensing Array Materials and Pattern Recognition for VOC Detection," *Sens. Actuators B: Chem.*, **2005**, *106*, 431-441.
56. Yang, C-Y.; Li, C-L.; Lu, C-J. "A Vapor Selectivity Study of Microsensor Arrays Employing Various Functionalized Ligand Protected Gold Nanoclusters," *Anal. Chim. Acta*, **2006**, *565*, 17-26.
57. Steinecker, W.H.; Kim, S.K.; Bohrer, F.I.; Farina, L.; Kurdak, Ç., Zellers, E.T. "Electron-Beam Patterned Monolayer-Protected Gold Nanoparticle Interface Layers on a Chemiresistor Vapor Sensor Array," *IEEE Sensors*, **2011**, *11*, 469-480.
58. Bohrer, F.I.; Covington, E.; Kurdak, Ç.; Zellers, E.T. "Characterization of Dense Arrays of Chemiresistor Vapor Sensors with Submicrometer Features and Patterned Nanoparticle Interface Layers," *Anal. Chem.*, **2011**, *83*, 3687-3695.
59. Grate, J.W.; Wise, B.M.; Abraham, M.H. "Method for Unknown Vapor Characterization and Classification Using a Multivariate Sorption Detector. Initial Derivation and Modeling Based on Polymer-Coated Acoustic Wave Sensor Arrays and Linear Solvation Energy Relationships," *Anal. Chem.*, **1999**, *71*, 4544-4553.
60. Li, C-L.; Lu, C-J. "Establishing Linear Solvation Energy Relationships Between VOCs and Monolayer-Protected Gold Nanoclusters Using Quartz Crystal Microbalance," *Talanta*, **2009**, *79*, 851-855.
61. Grate, J. W.; Abraham, M. H. "Solubility Interactions and the Design of Chemically Selective Sorbent Coatings for Chemical Sensors and Arrays," *Sens. & Actuators B: Chem.*, **1991**, *3*, 85-111.
62. Jaynes, D. B.; Rogowski, A. S. "Applicability of Fick's Law to Gas Diffusion," *Soil Sci. Soc. Amer.*, **1983**, *47(3)*, 425-430.
63. Compte, A.; Jou, D. "Non-Equilibrium Thermodynamics and Anomalous Diffusion," *J. Phys. A: Math. Gen.*, **1996**, *29*, 4321-4229.
64. Nelson, G. O. "Gas Mixtures: Preparation and Control," *CRC Press LLC*, Boca Raton, Florida, **1992**, ch. 5, p. 142.
65. Sun, Y-M.; Chen, J. "Sorption/Desorption Properties of Ethanol, Toluene, and Xylene in Poly (Dimethylsiloxane) Membranes," *J. Appl. Polym. Sci.*, **1994**, *51 (10)*, 1797-1804.
66. Prager, S.; Long, F. A. "Diffusion of Hydrocarbons in Polyisobutylene," *J. Am. Chem. Soc.*, **1951**, *73*, 4072-4075.
67. Caplan, K. "Evaporation Rate of Volatile Liquids," *Final Report, EPA Contract nos. 68-2-4248*, **1988**, and *68-D8-0112*, **1989**.
68. Ballantine, D. S.; White, R. M.; Martin, S. J.; Ricco, A. J.; Zellers, E. T.; Frye, G. C. Wohltjen, H. *Acoustic Wave Sensors: Theory, Design, and Physico-Chemical Applications in Applications of Modern Acoustics*; Stern, R., Ed.; Levy, M.,Ed.; Academic Press: San Diego, CA, **1997**.
69. Bodenhöfer, K.; Hierlemann, A.; Noetzel, G.; Weimar, U.; Göpel, W. "Performances of Mass-Sensitive Devices for Gas Sensing: Thickness Shear Mode and Surface Acoustic Wave Transducers," *Anal. Chem.*, **1996**, *68*, 2210-2218.

70. Grate, J. W.; Martin, S. J.; White, R.M. "Acoustic Wave Microsensors: Part I," *Anal. Chem.*, **1993**, *65 (21)*, 940-948.
71. Bodenhöfer, K.; Hierlemann, A.; Juza, M.; Schurig, V.; Göpel, W. "Chiral Discrimination of Inhalation Anesthetics and Methyl Propionates by Thickness Shear Mode Resonators: New Insights into the Mechanisms of Enantioselectivity by Cyclodextrins," *Anal. Chem.*, **1997**, *69*, 4017-4031.
72. Ying, Z.; Jiang, Y.; Du, X.; Xie, G.; Yu, J.; Wang, H. "PVDF Coated Quartz Crystal Microbalance Sensor for DMMP Vapor Detection," *Sens. & Actuators B: Chem.*, **2007**, *125*, 167-172.
73. Comini, E.; Baratoo, C.; Faglia, G.; Ferroni, M.; Vomiero, A.; Sberveglieri, G. "Quasi-One Dimensional Metal Oxide Seminconductors: Preparation, Characterization, and Application as Chemical Sensors," *Progress in Materials Science*, **2009**, *54*, 1-67.
74. Wei, C.; Dai, L.; Roy, A.; Tolle, T. B. "Multifunctional Chemical Vapor Sensors of Aligned Carbon Nanotube and Polymer Composites," *J. Am. Chem. Soc. Comm.*, **2006**, *128*, 1412-1413.
75. Philip, B.; Abraham, J. K.; Chandrasekhar, A.; Varadan, V. K. "Carbon Nanotube/PMMA Composite Thin Films for Gas-Sensing Applications," *Smart Mater. Struct.*, **2003**, *12*, 935-939.
76. Lonergan, M. C.; Severin, E. J.; Doleman, B. J.; Beaber, S. A.; Grubbs, R. H.; Lewis, N. S. "Array-Based Vapor Sensing Using Chemically Sensitive Carbon Black-Polymer Resistors," *Chem. Mater.*, **1996**, *8*, 2298-2312.
77. Severin, E. J.; Lewis, N. S. "Relationships Among Resonant Frequency Changes on a Coated Quartz Crystal Microbalance, Thickness Changes, and Resistance Responses of Polymer-Carbon Black Composite Chemiresistors," *Anal. Chem.*, **2000**, *72*, 2008-2015.
78. Severin, E. J.; Doleman, B. J.; Lewis, N. S. "An Investigation of the Concentration Dependence and Response to Analyte Mixtures of Carbon Black/Insulating Organic Polymer Composite Vapor Detectors," *Anal. Chem.*, **2000**, *72*, 658-668.
79. Doleman, B.J.; Lonergan, M.C.; Severin, E.J.; Vaid, T.P.; Lewis, N.S. "Quantitative study of the resolving power of arrays of carbon black-polymer composites in various vapor-sensing tasks," *Anal. Chem.*, **1998**, *70*, 4177-4190.
80. Lewis, N. S. "Comparisons Between Mammalian and Artificial Olfaction Based on Arrays of Carbon Black-Polymer Composite Vapor Detectors," *Acc. Chem. Res.*, **2004**, *37*, 663-672.
81. Steinecker, W.H.; Rowe, M.P.; Zeller, E.T. "Model of Vapor-Induced Resistivity Changes in Gold-Thiolate Monolayer-Protected Nanoparticle Sensor Films" *Anal. Chem.* **2007**, *79*, 4977-4986.
82. Ancona, M. G.; Snow, A. W.; Foos, E. E.; Kruppa, W.; Bass, R. "Scaling Properties of Gold Nanocluster Chemiresistor Sensors," *IEEE Sensors*, **2006**, *6(6)*, 1403-1414.
83. Maldonado, S.; García-Berríos, E.; Woodka, M. D.; Brunschwig, B. S.; Lewis, N. S. "Detection of Organic Vapors and NH_3(g) Using Thin-Film Carbon Black-Metallophthalocyanine Composite Chemiresistors," *Sens. & Actuators B: Chem.*, **2008**, *134*, 521-531.
84. Zhang, H-L.; Evans, S. D.; Henderson, J. R.; Miles, R. E.; Shen, T-H. "Vapour Sensing Using Surface Functionalized Gold Nanoparticles," *Nanotechnology*, **2002**, *13*, 439-444.
85. García-Berríos, E.; Gao, T.; Woodka, M. D.; Maldonado, S.; Brunschwig, B. S.; Ellsworth, M. W.; Lewis, N. S. "Response Versus Chain Length of Alkanethiol-Capped

Au Nanoparticle Chemiresistive Chemical Vapor Sensors," *J. Phys. Chem. C*, **2010**, *114*, 21914-21920.
86. Templeton, A. C.; Wuelfing, W. P.; Murray, R. W. "Monolayer-Protected Cluster Molecules," *Acc. Chem. Res.*, **2000**, *33*, 27-36.
87. Stewart, M. E.; Anderton, C. R.; Thompson, L. B.; Maria, J.; Gray, S. K.; Rogers, J. A.; Nuzzo, R. G. "Nanostructured Plasmonic Sensors," *Chem. Rev.*, **2008**, *108*, 494-521.
88. Nath, N.; Chilkoti, A. "A Colorimetric Gold Nanoparticle Sensor to Interrogate Biomolecular Interactions in Real Time on a Surface," *Anal. Chem.*, **2002**, *74*, 504-509.
89. Suter, J. D.; White, I. M.; Zhu, H.; Shi, H.; Caldwell, C. W.; Fan, X. "Label-Free Quantitative DNA Detection Using the Liquid Core Optical Ring Resonator," *Biosensors and Bioelectronics*, **2008**, *23*, 1003-1009.
90. Dancil, K-P. S.; Greiner, D. P.; Sailor, M. J. "A Porous Silicon Optical Biosensor: Detection of Reversible Binding of IgG to a Protein A-Modified Surface," *J. Am. Chem. Soc.*, **1999**, *121*, 7925-7930.
91. Ho, H-A.; Leclerc, M. "Optical Sensors Based on Hybrid Aptamer/Conjugated Polymer Complexes," *J. Am. Chem. Soc.*, **2004**, *126*, 1384-1387.
92. Karakouz, T.; Vaskevich, A.; Rubinstein, I. "Polymer-Coated Gold Island Films as Localized Plasmon Transducers for Gas Sensing," *J. Phys. Chem. B*, **2008**, *112*, 14530-14538.
93. Cheng, C-S.; Chen, Y-Q.; Lu, C-J. "Organic Vapour Sensing Using Localized Surface Plasmon Resonance Spectrum of Metallic Nanoparticles Self Assemble Monolayer," *Talanta*, **2007**, *73*, 358-365.
94. Chen, K-J.; Lu, C-J. "A Vapor Sensor Array Using Multiple Localized Surface Plasmon Resonance Bands in a Single UV-VIS Spectrum," *Talanta*, **2010**, *81*, 1670-1675.
95. Potyrailo, R. A.; Ghiradella, H.; Vertiatchikh, A.; Dovidenko, K.; Cournoyer, J. R.; Olson, E. "*Morpho* Butterfly Wing Scales Demonstrate Highly Selective Vapour Response," *Nature Photonics*, **2007**, *1*, 123-128.
96. Chen, B.; Liu, C.; Ota, M.; Hayashi, K. "Terpene Detection Based on Localized Surface Plasma Resonance of Thiolate-Modified Au Nanoparticles," *IEEE Sensors*, **2013**, *13(4)*, 1307-1314.
97. Dalfovo, M. C.; Salvarezza, R. C.; Ibanez, F. J. "Improved Vapor Selectivity and Stability of Localized Surface Plasmon Resonance with a Surfactant-Coated Au Nanoparticles Film," *Anal. Chem.*, **2012**, *84*, 4886-4892.
98. Sun, Y.; Shopova, S. I.; Frey-Mason, G.; Fan, X. "Rapid Chemical-Vapor Sensing Using Optofluidic Ring Resonators," *Optics Letters*, **2008**, *33(8)*, 788-790.
99. Aernecke, M. J.; Walt, D. R. "Optical-Fiber Arrays for Vapor Sensing," *Sens. & Acuators B: Chem.*, **2009**, *142*, 464-469.
100. Armani, A.M. *Single Molecule Detection Using Optical Microcavities in Photonic Microresonator Research and Application;* Chremmos, I., Ed.; Schwelb, O., Ed.; Uzunoglu, N., Ed.; Springer: US, **2010**, ch.11.
101. Yebo, N. A.; Lommens, P.; Hens, Z.; Baets, R. "An Integrated Optic Ethanol Vapor Sensor Based on a Silicon-on-Insulator Microring Resonator Coated with a Porous ZnO Film," *Optics Express*, **2010**, *18(11)*, 11859-11866.
102. Sun, Y.; Liu, J.; Frey-Mason, G.; Ja, S-J.; Thompson, A. K.; Fan, X. "Optofluidic Ring Resonator Sensors for Rapid DNT Vapor Detection," *Analyst*, **2009**, *134*, 1386-1391.

103. Stievater, T. H.; Rabinovich, W. S.; Ferraro, M. S.; Papanicolaou, N. A.; Bass, R.; Boos, J. B.; Stepnowski, J. L.; McGill, R. A. "Photonic Microharp Chemical Sensors," *Optics Express*, **2008**, *16(4)*, 2423-2430.
104. Homola, J.; Yee, S. S.; Gauglitz, G. "Surface Plasmon Resonance Sensors: Review," *Sens. & Actuators B: Chem.*, **1999**, *54*, 3-15.
105. Willets, K. A.; Duyne, R. P. V. "Localized Surface Plasmon Resonance Spectroscopy and Sensing," *Annu. Rev. Phys. Chem.*, **2007**, *58*, 267-297.
106. Scholten, K.; Reddy, K.; Fan, X.; Zellers, E. T. "Vapor Discrimination by Dual-Laser Reflectance Sensing of a Single Functionalized Nanoparticle Film," *Anal. Methods*, **2013**, *5*, 4268-4272.
107. Potyrailo, R. A.; Larsen. M.; Riccobono, O. "Detection of Individual Vapors and Their Mixtures Using a Selectivity-Tunable Three-Dimensional Network of Plasmonic Nanoparticles," *Angew. Chem. Int. Ed.*, **2013**, *52*, 1-6.
108. Dan, Y.; Lu, Y.; Kybert, N. J.; Luo, Z.; Charlie Johnson, A. T. "Intrinsic Response of Graphene Vapor Sensors," *Nano Letters*, **2009**, *9(4)*, 1472-1475.
109. Iijima, S. "Helical Microtubules of Graphitic Carbon," *Nature*, **1991**, *354*, 56-58.
110. Hatchett, D. W.; Josowicz, M. "Composites of Intrinsically Conducting Polymers as Sensing Nanomaterials," *Chem. Rev.*, **2008**, *108*, 746-769.
111. Kauffman, D. R.; Star, A. "Carbon Nanotube Gas and Vapor Sensors," *Angew. Chem. Int. Ed.*, **2008**, *47*, 6550-6570.
112. Someya, T.; Small, J.; Kim, P.; Nuckolls, C.; Yardley, J. T. "Alcohol Vapor Sensors Based on Single-Walled Carbon Nanotube Field Effect Transistors," *Nano Letters*, **2003**, *3(7)*, 877-881.
113. Lu, J. G.; Chang, P.; Fan, Z. "Quasi-One-Dimensional Metal Oxide Materials-Synthesis, Properties, and Applications," *Materials Science and Engineering R*, **2006**, *52*, 49-91.
114. Shen, G.; Chen, P-C.; Ryu, K.; Zhou, C. "Devices and Chemical Sensing Applications of Metal Oxide Nanowires," *J. Mater. Chem.*, **2009**, *19*, 828-839.
115. Comini, E. "Metal Oxide Nano-Crystals for Gas Sensing," *Anal. Chim. Acta*, **2006**, *568*, 28-40.
116. Buttry, D. A. "Measurement of Interfacial Processes at Electrode Surfaces with Electrochemical Quartz Crystal Microbalance," *Chem. Rev.*, **1992**, *92*, 1355-1379.
117. Zhang, J.; Hu, J. Q.; Zhu, F. R.; Gong, H.; O'Shea, S. J. "ITO Thin Films Coated Quartz Crystal Microbalance as Gas Sensor for NO Detection," *Sens. & Actuators B: Chem.*, **2002**, *87*, 159-167.
118. Wang, X.; Zhang, J.; Zhu, Z. "Ammonia Sensing Characteristics of ZnO Nanowires Studied by Quartz Crystal Microbalance," *Applied Surface Science*, **2006**, *252*, 2404-2411.
119. Wang, X.; Yee, S.; Carey, P. "An Integrated Array of Multiple Thin-Film Metal Oxide Sensors for Quantification of Individual Components in Organic Vapor Mixtures," *Sens. & Actuators B: Chem.*, **1993**, *13-14*, 458-461.
120. Bohrer, F. I.; Colesniuc, C. N.; Park, J. Ruidiaz, M. E.; Schuller, I. K.; Kummel, A. C.; Trogler, W. C. "Comparative Gas Sensing in Cobalt, Nickel, Copper, Zinc, and Metal-Free Phthalocyanine Chemiresistors," *J. Am. Chem. Soc.*, **2008**, *131*, 478-485.

121. Guillaud, G.; Simon, J.; Germain, J. P. "Metallophthalocyanines: Gas Sensors, Resistors, and Field Effect Transistors," *Coordination Chemistry Reviews*, **1998**, *178-180*, 1433-1484.
122. Yang, R. D.; Gredig, T.; Colesniuc, C. N.; Park, J.; Schuller, I. K.; Trogler, W. C.; Kummel, A. C. "Ultrathin Organic Transistors for Chemical Sensing," *App. Phys. Letters*, **2007**, *90*, 263506.
123. Bora, M.; Schut, D.; Baldo, M. A. "Combinatorial Detection of Volatile Organic Compounds Using Metal-Phthalocyanine Field Effect Transistors," *Anal. Chem.*, **2007**, *79*, 3298-3303.
124. Spadavecchia, J.; Ciccarella, G.; Rella, R.; Capone, S.; Siciliano, P. "Metallophthalocyanines Thin Films in Array Configuration for Electronic Optical Nose Applications," *Sens. & Actuators B: Chem.*, **2003**, *96*, 489-497.
125. Basova, T.; Kol'tsov, E.; Ray, A. K.; Hassan, A. K.; Gürek, A. G.; Ahsen, V. "Liquid Crystalline Phthalocyanine Spun Films for Organic Vapour Sensing," *Sens. & Actuators B: Chem.*, **2006**, *113*, 127-134.
126. Rella, R.; Spadavecchia, J.; Ciccarella, G.; Siciliano, P.; Vasapollo, G.; Valli, L. "Optochemical Vapour Detection Using Spin Coated Thin Films of Metal Substituted Phthalocyanines," *Sens. & Actuators B: Chem.*, **2003**, *89*, 86-91.
127. Montméat, P.; Madonia, S.; Pasquinet, E.; Hairault, L.; Gros, C. P.; Barbe, J-M.; Guilard, R. "Metalloporphyrins as Sensing Material for Quartz-Crystal Microbalance Nitroaromatics Sensors," *IEEE Sensors J.*, **2005**, *5*, 610-615.
128. Bohrer, F. I.; Colesniuc, C. N.; Park, J.; Ruidiaz, M. E.; Schuller, I. K.; Kummel, A.C.; Trogler, W. C. "Comparative Gas Sensing in Cobalt, Nickel, Copper, Zinc, and Metal-Free Phthalocyanine Chemiresistors," *J. Am. Chem. Soc.*, **2009**, *131*, 478-485.
129. Bai, H.; Shi, G. "Gas Sensors Based on Conducting Polymers," *Sensors*, **2007**, *7*, 267-307.
130. Patrick Carey, W.; Beebe, K. R.; Kowalski, B. R. "Multicomponent Analysis Using an Array of Piezoelectric Crystal Sensors," *Anal. Chem.*, **1987**, *59*, 1529-1534.
131. Swann, M. J.; Glidle, A.; Cui, L.; Barker, J. R.; Cooper, J. M. "The Determination of Gaseous Molecular Density Using a Hybrid Vapour Sensor," *Chem. Commun.*, **1998**, 2753-2754.
132. Aernecke, M. J.; Walt, D. R. "Optical-Fiber Arrays for Vapor Sensing," *Sens. & Actuators B: Chem.*, **2009**, *142*, 464-469.
133. Stievater, T. H.; Rabinovich, W. S.; Ferraro, M.S.; Papanicolaou, N.A.; Bass, R.; Boos, J. B.; Stepnowski, J. L.; McGill, R. A. "Photonic Microharp Chemical Sensors," *Optics Express*, **2008**, *16(4)*, 2423-2430.
134. Sun, Y.; Shopova, S. I.; Frye-Mason, G.; Fan, X. "Rapid Chemical-Vapor Sensing Using Optofluidic Ring Resonators," *Optics Letters*, **2008**, *33(8)*, 788-790.
135. Brust, M.; Walker, M.; Bethell, D.; Schiffrin, D.J.; Whyman, R. "Synthesis of Thiol-derivatised Gold Nanoparticles in a Two-phase Liquid-liquid System" *J. Chem. Soc., Chem. Commun.* **1994**, 801-802.
136. Brust, M.; Fink, J.; Bethell, D.; Schiffrin, D. J.; Kiely, C. "Synthesis and Reactions of Functionalised Gold Nanoparticles" *J. Chem. Soc., Chem. Commun.* **1995**, 1655-1656.

137. Yee, C.K.; Jordan, R.; Ulman, A.; White, H.; King, A.; Rafailovich, M.; Sokolov, J. "Novel One-Phase Synthesis of Thiol-Functionalized Gold, Palladium, and Iridium Nanoparticles Using Superhydride" *Langmuir* **1999**, *15*, 3486-3491.
138. Rowe, M.P.; Plass, K.E.; Kim, K.; Kurdak, Ç; Zellers, E.T.; Matzger, A.J. "Single-Phase Synthesis of Functionalized Gold Nanoparticles" *Chem. Mater.* **2004**, *16*, 3513-3517.
139. Srisombat, L-o.; Park, J-S.; Zhang, S.; Lee, T. R. "Preparation, Characterization, and Chemical Stability of Gold Nanoparticles Coated with Mono-, Bis-, and Tris-Chelating Alkanethiols," *Langmuir*, **2008**, *24*, 7750-7754.
140. Selvakannan, PR.; Mandal, S.; Pasricha, R.; Adyanthaya, S. D.; Sastry, M. "One-Step Synthesis of Hydrophobized Gold Nanoparticles of Controllable Size By the Reduction of Aqueous Chloroaurate Ions by Hexadecylaniline at the Liquid-Liquid Interface," *Chem. Comm.*, **2002**, 1334-1335.
141. Hiramatsu, H.; Osterloh, F. E. "A Simple Large-Scale Synthesis of Nearly Monodisperse Gold and Silver Nanoparticles with Adjustable Sizes and with Exchangeable Surfactants," *Chem. Mater.*, **2004**, *16(13)*, 2509-2511.
142. Liu, X.; Atwater, M.; Wang, J.; Huo, Q. "Extinction Coefficient of Gold Nanoparticles with Different Sizes and Different Capping Ligands," *Colloids and Surfaces B: Biointerfaces*, **2007**, *58*, 3-7.
143. Frens, G. "Controlled Nucleation for the Regulation of Particle Size in Monodisperse Gold Suspensions," *Nature Physics Science*, **1972**, *241*, 20-22.
144. Patungwasa, W.; Hodak, J. H. "pH Tunable Morphology of the Gold Nanoparticles Produced by Citrate Reduction," *Materials Chemistry and Physics*, **2008**, *108*, 45-54.
145. Oo, M. K. K.; Chang, C-F.; Sun, Y.; Fan, X. "Rapid, Sensitive DNT Vapor Detection with UV-Assisted Photo-Chemically Synthesized Gold Nanoparticle SERS Substrates," *Analyst*, **2011**, *136*, 2811-2817.
146. Kubo, S.; Diaz, A.; Tang, Y.; Mayer, T. S.; Khoo, I. C.; Mallouk, T. E. "Tunability of the Refractive Index of Gold Nanoparticle Dispersions," *Nano. Lett.*, **2007**, *7(11)*, 3418-3423.
147. Gao, T.; Tillman, E. S.; Lewis, N. S. "Detection and Classification of Volatile Organic Amines and Carboxylic Acids Using Arrays of Carbon Black-Dendrimer Composite Vapor Detectors," *Chem. Mater.*, **2005**, *17*, 2904-2911.
148. Levitsky, I.; Krivoshlykov, S. G. "Rational Design of a Nile Red/Polymer Composite Film for Fluorescence Sensing of Organophosphate Vapors Using Hydrogen Bond Acidic Polymers," *Anal. Chem.*, **2001**, *73*, 3441-3448.
149. Rowe, M. P.; Steinecker, W. H.; Zellers, E. T. "Exploiting Charge-Transfer Complexation for Selective Measurement of Gas-Phase Olefins with Nanoparticle-Coated Chemiresistors," *Anal. Chem.*, **2007**, *79*, 1164-1172.
150. *Chemical Reviews*, **2000**, *100*.
151. *Chemical Reviews*, **2008**, *100*.
152. Kurzawski, P.; Hegleitner, C.; Hierlemann, A. "Detection and Discrimination Capabilities of a Multitransducer Single-Chip Gas Sensor System", *Anal. Chem.*, **2006**, *78*, 6910-6920.
153. Pinnaduwage, L. A.; Hedden, D. L.; Gehl, A.; Boiadjev, V. I.; Hawk, J. E.; Farahi, R. H.; Thundat, T.; Houser, E. J.; Stepnowski, S.; McGill, R. A.; Deel, L.; Lareau,

R. T. “A sensitive, handheld vapor sensor based on microcantilevers,” *Rev. Sci. Instrum.*, **2004**, *7(5)*, 4554-4557.
154. Chapman, P. F.; Vogt, F.; Dutta, P.; Datskos, P. G.; Devault, G. L.; Sepaniak, M. J. “Facile hyphenation of gas chromatography and a microcantilever array sensor for enhanced selectivity,” *Anal. Chem.*, **2007**, *79(1)*, 364-370.
155. Patel, S. V.; Mlsna, E. T.; Fruhberger, B.; Klaassen, E.; Cemalovic, S.; Baselt, D. R. “Chemicapacitive microsensors for volatile organic compound detection,” *Sens. Act. B*, **2003**, *96*, 541-553.
156. Rock, F.; Barsan, N.; Weimar, U. “Electronic nose: current status and future trends,” *Chem. Reviews*, **2008**, *108*, 705-725.
157. Hatfield, J. V.; Neaves, P.; Hicks, P. J.; Persaud, K.; Travers, P. “Towards an integrated electronic nose using conducting polymer sensors,” *Sens. Act. B*, **1994**, *18*, 221-228.
158. Joseph, Y.; Peic, A.; Chen, S.; Michl, J.; Vossmeyer, T.; Yasuda, A. “Vapor sensitivity of networked gold nanoparticle chemiresistors: importance of flexibility and resistivity of the interlinkage,” *J. Phys. Chem.* C, **2007**, *111*, 12855-12859.
159. Dovgolevsky, E.; Tisch, U.; Haick, H. “Chemically sensitive resistors based on monolayer-capped cubic nanoparticles: towards configurable nanoporous sensors,” *Small*, **2009**, *5*, 1158-1161.
160. Ricco, A.J.; Crooks, R.M.; Osbourn, G.C. “Surface acoustic wave chemical sensor arrays: new chemically sensitive interfaces combined with novel cluster analysis to detect volatile organic compounds and mixtures,” *Acc. Chem. Res.*, **1998**, *31*, 289-296.
161. Garcia-Berrios, E.; Gao, T.; Theriot, J.C.; Woodka, M.D.; Brunschwig, B.S.; Lewis, N. S. “Response and discrimination performance of arrays of organothiol-capped Au nanoparticle chemiresistive vapor sensors,” *J. Phys. Chem. C*, **2011**, *115*, 6208-6217.
162. Evans, S. D.; Johnson, S. R.; Cheng, Y. L.; Shen, T. “Vapour Sensing Using Hybrid Organic-Inorganic Nanostructured Materials,” *J. Mater. Chem.*, **2000**, *10*, 183-188.
163. Snow, A.W.; Barger, W.R.; Klusty, M.; Wohltjen, H.; Jarvis, N.L.“Simultaneous electrical conductivity and piezoelectric mass measurements on iodine-doped phthalocyanine Langmuir-Blodgett films,” *Langmuir*, **1986**, *2*, 513-519.
164. Bott, B.; Jones, T.A. “The use of multisensor systems in monitoring hazardous atmospheres,” *Sens. Act.*, **1986**, *9*, 19-25.
165. Schierbaum, K.D.; Gerlack, A.; Haug, M.; Göpel, W. “Selective detection of organic molecules with polymers and supramolecular compounds: application of capacitance, quartz microbalance, and calorimetric transducers,” *Sens. Act. A*, **1992**, *31*, 130-137.
166. Holmberg, M.; Winquist, F.; Lundstrom, I.; Gardner, J.W.; Hines, E.L. “Identification of paper quality using a hybrid electronic nose,” *Sens. Act. B*, **1995**, *26-27*, 246-249.
167. Ulmer, H.; Mitrovics, J.; Noetzel, G.; Weimar, U.; Göpel, W. “Odours and flavours identified with hybrid modular sensor systems,” *Sens. Act. B*, **1997**, *43*, 24-33.
168. Ulmer, H.; Mitrovics, J.; Weimar, U.; Göpel, W. “Sensor arrays with only one or several transducer principles? The advantage of hybrid modular systems,” *Sens. Act. B*, **2000**, *65*, 79-81.

169. Haug, M.; Schierbaum, K.D.; Gauglitz, G.; Göpel, W. "Chemical Sensors Based Upon Polysiloxanes: Comparison Between Optical, Quartz Microbalance, Calorimetric, and Capacitance Sensors," *Sens. Act. B,* **1993**, *11*, 383-391.
170. Zhou, R.; Hierlemann, A.; Weimar, U.; Göpel, W. "Gravimetric, Dielectric and Calorimetric Methods for the Detection of Organic Solvent Vapours Using Poly(ether urethane) Coatings," *Sens. Act. B,* **1996**, *34*, 356-360.
171. Martin, S. J.; Frye, G. C.; Senturia, S. D. "Dynamics and Response of Polymer-Coated Surface Acoustic Wave Devices: Effect of Viscoelastic Properties and Film Resonance," *Anal. Chem.*, **1994**, *66*, 2201-2219.
172. Frye, G. C.; Martin, S. J. Dual Output Acoustic Wave Sensor for Molecular Identification US Patent 5,076,094 December 31, 1991.
173. Potyrailo, R.; Morris, W. "Multianalyte Chemical Identification and Quantitation Using a Single Radio Frequency Identification Sensor," *Anal. Chem*, **2007**, *79*, 45-51.
174. Nagraj, N.; Slocik, J.M.; Phillips, D.M.; Kelley-Loughanne, N.; Naik, R.R.; Potyrailo, R.A. "Selective Sensing of Vapors of Similar Dielectric Constant Using Peptide-Capped Gold Nanoparticles on Individual Multivariable Transducers," *Analyst*, **2013**, *138(15)*, 4334-4339.
175. Jolliffe, I. *Principal Component Analysis. Encyclopedia of Statistics in Behavioral Science*, Wiley: New York, **2005**.
176. Morrison, D. F. *Multivariate Statistical Methods*, 2nd Ed. McGraw Hill: New York, **1990**.
177. Woodka, M. D.; Schnee, V. P. "Fluorescent Polymer Sensor Array for Detection and Discrimination of Explosives in Water," *Anal. Chem.*, **2010**, *82(23)*, 9917-9924.
178. Zhong, Q.; Steinecker, W. H.; Zellers, E. T. "Characterization of a High-Performance Portable GC with a Chemiresistor Array Detector," *Analyst*, **2009**, *134*, 283-293.
179. Wold, S. "Pattern Recognition by Means of Disjoint Principal Components Models," *Pattern Recognition*, **1976**, *8*, 127-139.
180. Tauler, R.; Kowalski, B.; Fleming, S. "Multivariate Curve Resolution Applied to Spectral Data from Multiple Runs of an Industrial Process," *Anal. Chem.*, **1993**, *65*, 2040-2047.
181. Kuligowski, J.; Quintas, G.; Tauler, R.; Lendl, B.; Guardia, M. "Background Correction and Multivariate Curve Resolution of Online Liquid Chromatography with Infrared Spectrometric Detections," *Anal. Chem.*, **2011**, *83*, 4855-4862.
182. Pére-Trepat, E.; Lacorte, S.; Tauler, R. "Solving Liquid Chromatography Mass Spectrometry Co-Elution Problems in the Analysis of Environmental Samples by Multivariate Curve Resolution," *J. Chromatogr. A*, **2005**, *1096*, 111-122.
183. Parastar, H.; Radovic, J. R.; Bayona, J. M.; Tauler, R. "Solving Chromatographic Challenges in Comprehensive Two-Dimensional gas Chromatography-Time-of-Flight Mass Spectrometry Using Multivariate Curve Resolution-Alternating Least Squares," *Anal. Bioanal. Chem.*, **2013**, *405*, 6235-6249.
184. Parastar, H.; Tauler, R. "Multivariate Curve Resolution of Hyphenated and Multidimensional Chromatographic Measurements: A New Insight to Address Current Chromatographic Challenges," *Anal. Chem.*, **2014**, *86*, 286-297.

185. Hoggard, J. C.; Synovec, R. E. “Parallel Factor Analysis (PARAFAC) of Target Analytes in GC x GC-TOFMS Data; Automated Selection of a Model with an Appropriate Number of Factors,” *Anal. Chem.*, **2007**, *79*, 1611-1619.
186. Bryant-Genevier, J.; Scholten, K.; Kim, S. K.; Zellers, E. T. “Multivariate Curve Resolution of Co-Eluting Vapors From a Gas Chromatograph with Microsensor Array Detector,” *Sens. And Actuators B: Chem.*, **2014**, *202*, 167-176.
187. Scholten, K.; Fan, X.; Zellers, E. T. “A Microfabricated Optofluidic Ring Resonator for Sensitive, High-Speed Detection of Volatile Organic Compounds,” *Lab Chip*, **2014**, *14*, 3873-3880.

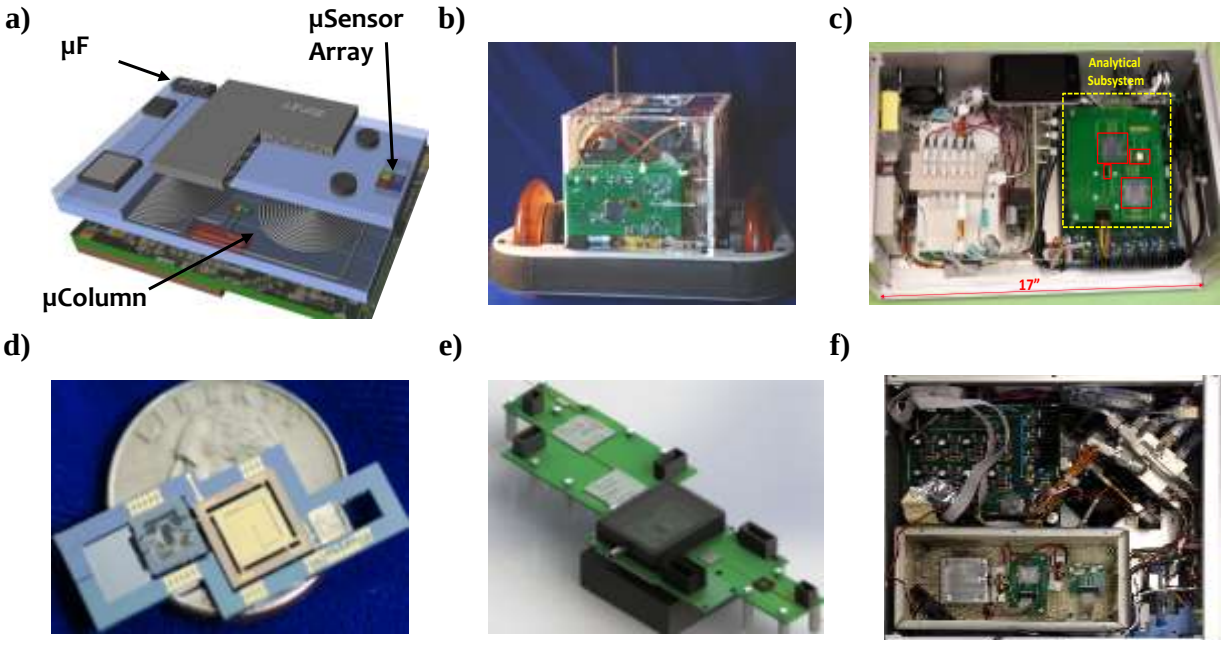

Figure 1-1. (a) Concept diagram of a WIMS^2 μGC, illustrating the three main components, and WIMS^2 μGC prototypes: (b) MERCURY, designed for robot-mounted routine surveillance (c) SPIRON, designed for vapor intrusion of TCE at ppt-levels (d) ORION, ultra small, low power GC (e) MARS, 2-dimensional GC (μGC x μGC) and (f) INTREPID, designed for explosive markers detection.

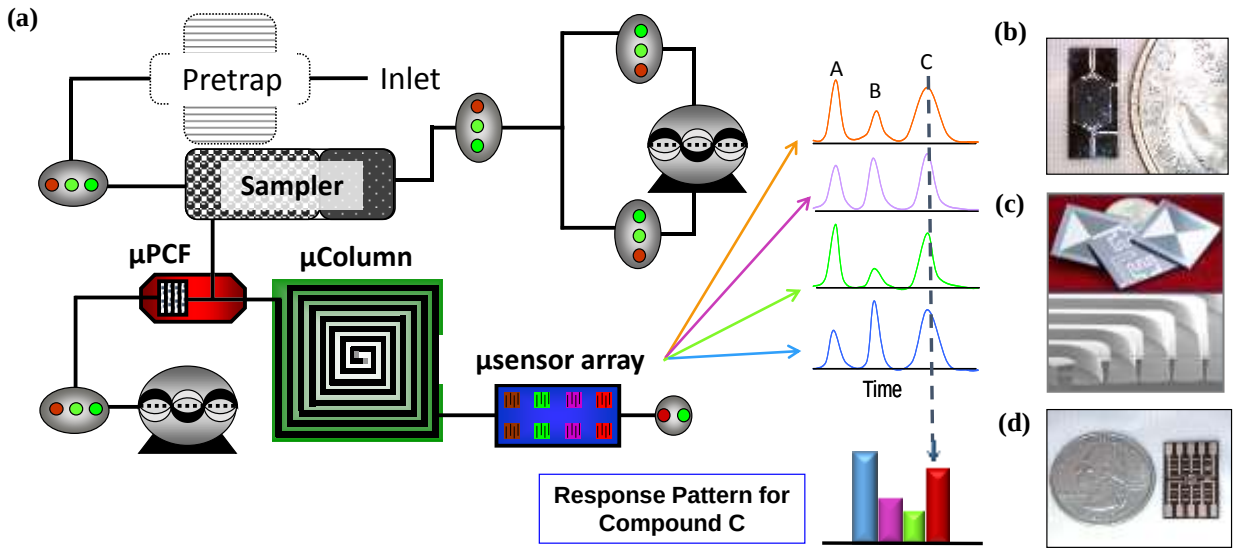

Figure 1-2. (a) General schematic of a WIMS^2 µGC, illustrating the main components of the analytical system: photographs of (b) µPCF that provides a sharp injection, (c) µcolumn that separates the components of the vapor mixture, (d) µsensor array that affords a response pattern (crude spectrum) that is used to identify the components of the mixture.

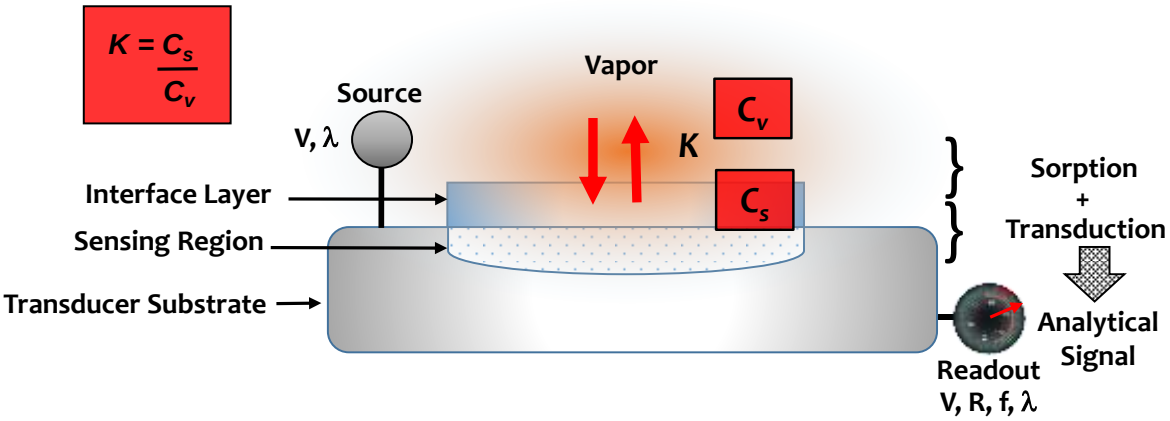

Figure 1-3. General depiction and operation of a sorption-based sensor where an electrical/optical input is converted to an analytical signal.

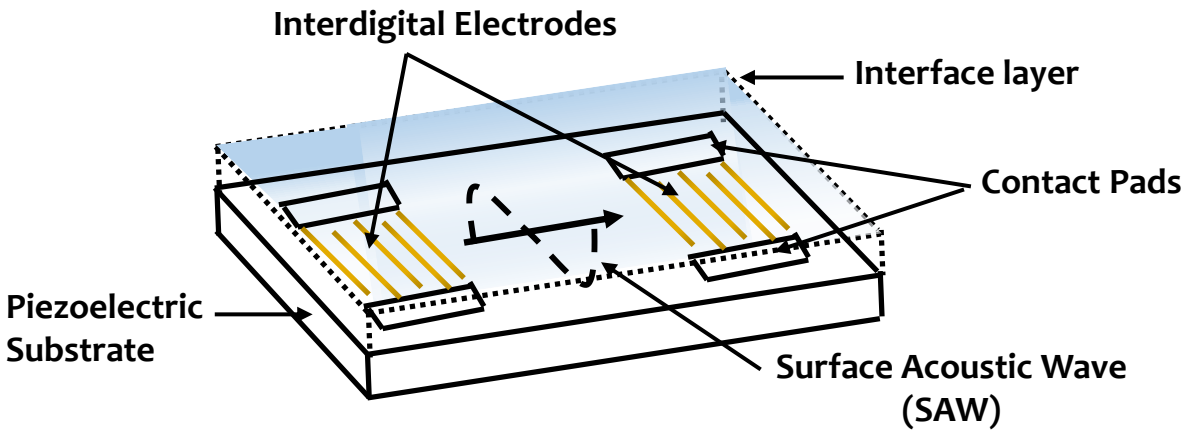

Figure 1-4. Schematic of a SAW device coated with an interface layer, showing the direction of wave propagation.

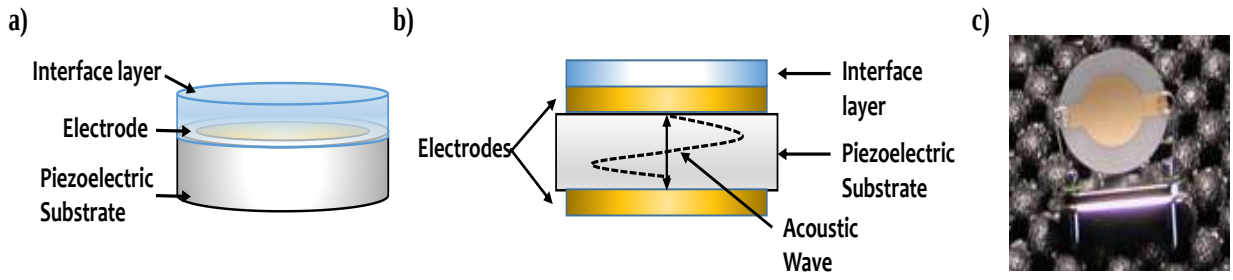

Figure 1-5. Schematic of a TSMR device coated with an interface layer: (a) side view and (b) cross-sectional view, illustrating direction of wave propagation. (c) Photograph of an uncoated TSMR device.

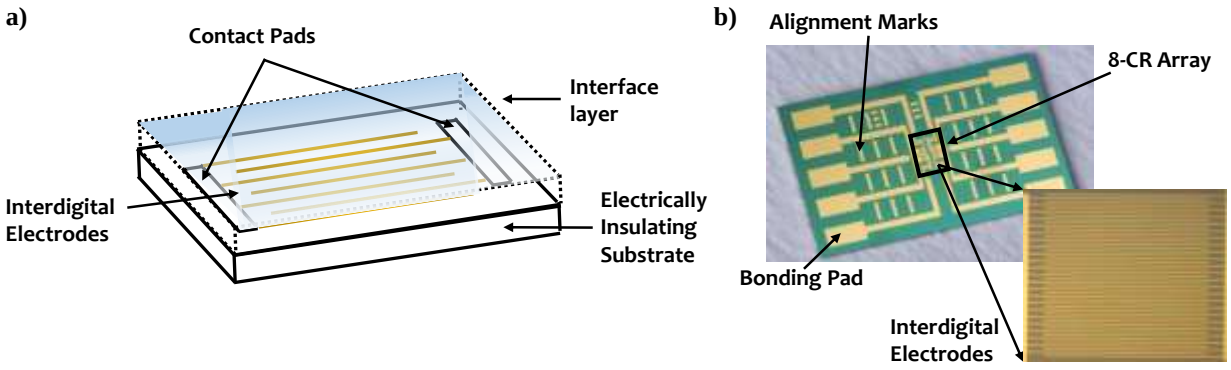

Figure 1-6. (a) Schematic of a CR device coated with an interface layer and (b) photograph of an uncoated 8-CR array.

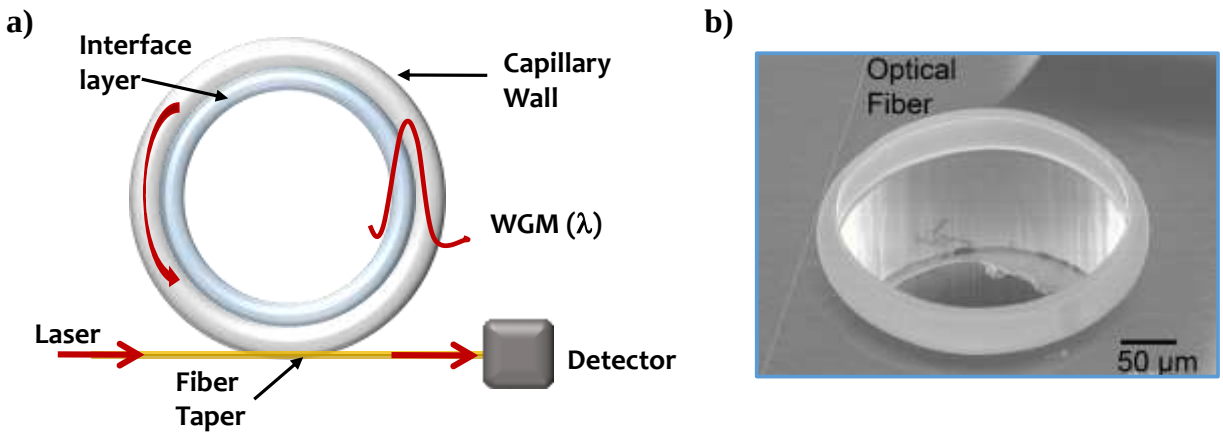

Figure 1-7. (a) Schematic of an OFRR device coated with an interface layer and (b) SEM image of a microfabricated OFRR device used for vapor sensing.[187]

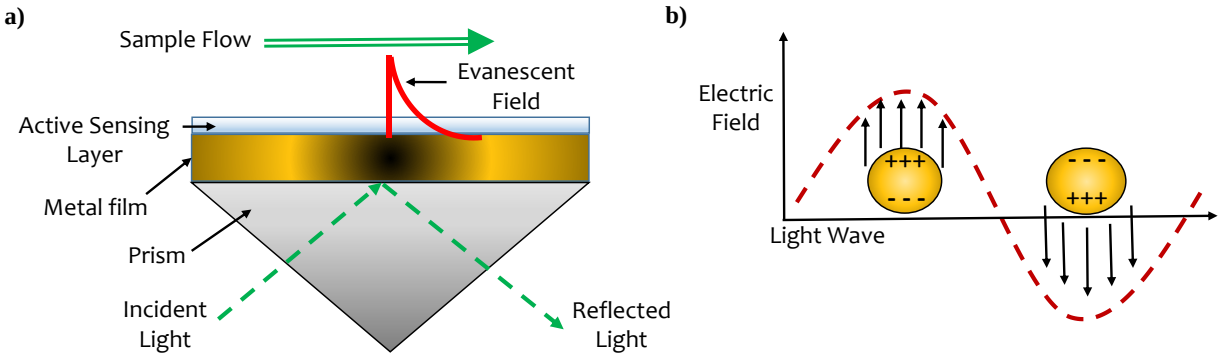

Figure 1-8. (a) Typical configuration to induce surface plasmon resonance and (b) depiction of the collective oscillation of free electrons due to an applied electric field, leading to localized surface plasmon resonance of small nanoparticles.

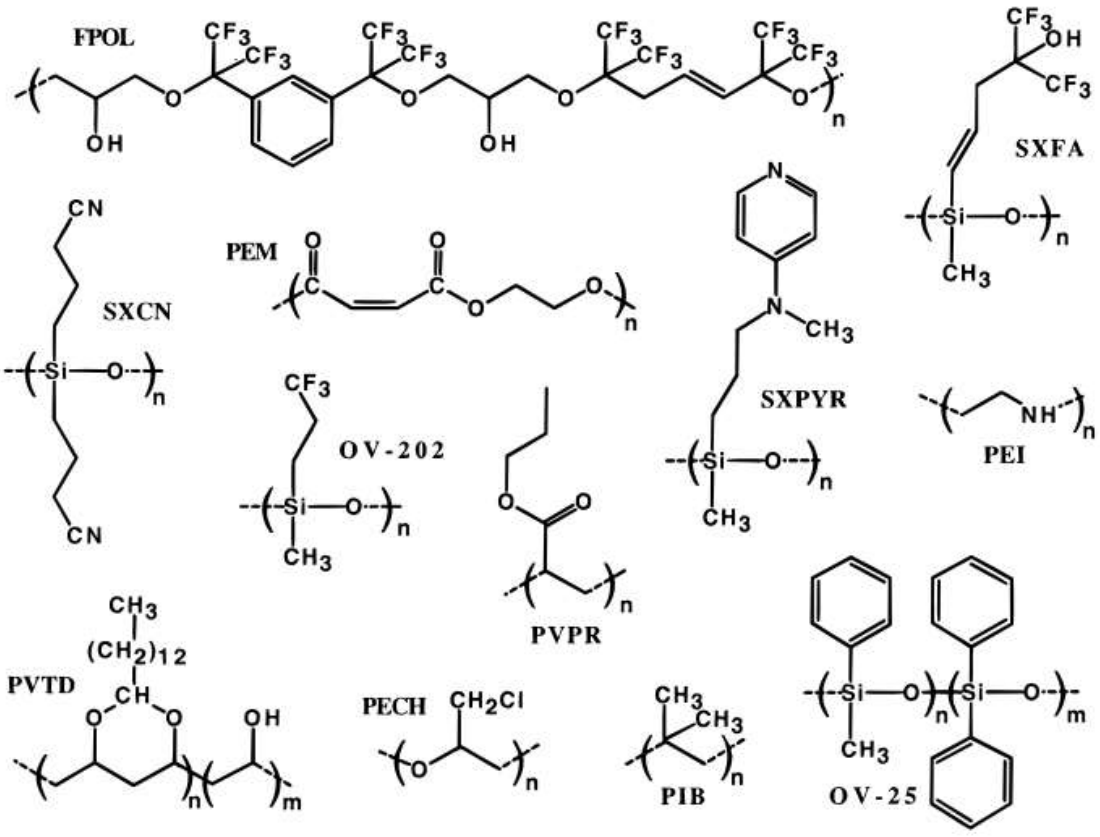

Figure 1-9. Common repeat units of polymer interface layers used in vapor sensing.[52]

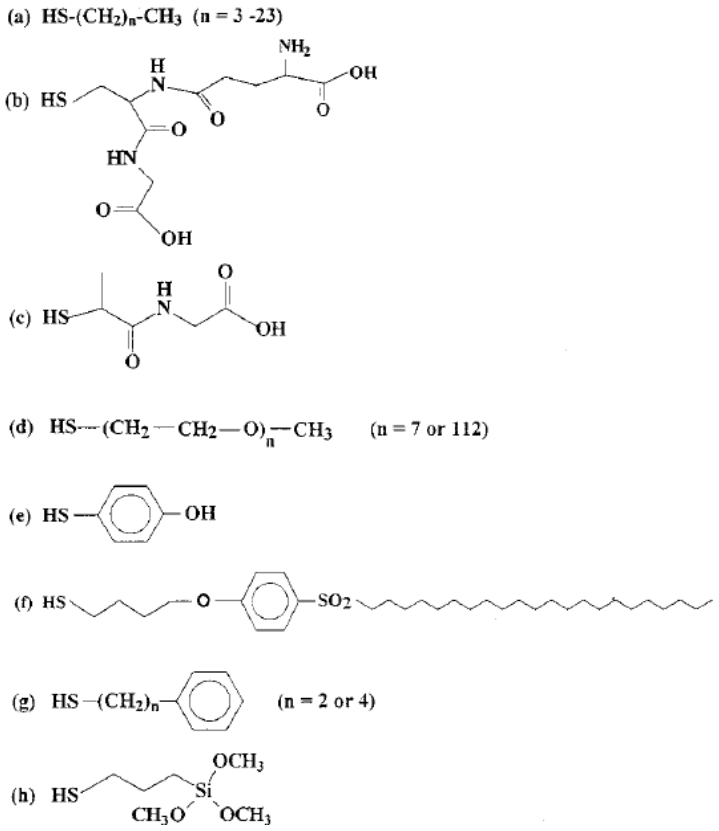

Figure 1-10. Examples of thiols used to synthesize MPNs.[86]

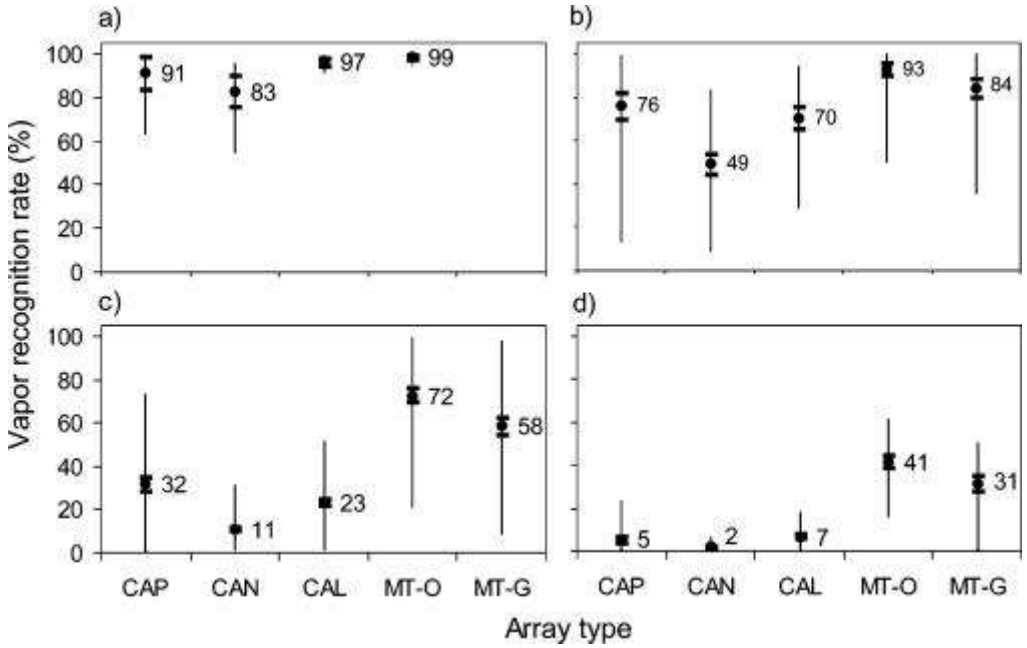

Figure 1-11. Comparison of 5-sensor ST arrays to 5-sensor global and optimal MT arrays (MT-G and MT-O, respectively; see text for explanation) for the recognition of (a) 11 individual vapors, (b) 55 binary mixtures, (c) 165 ternary mixtures, and (d) 330 quaternary mixtures. Confidence interval (95%) around mean recognition rate is shown for each array type, along with the range (minimum to maximum) of recognition rates calculated for each array type. Reprinted from *Anal. Chem.*, **2008**, *80(1)*, 227-236.[25]

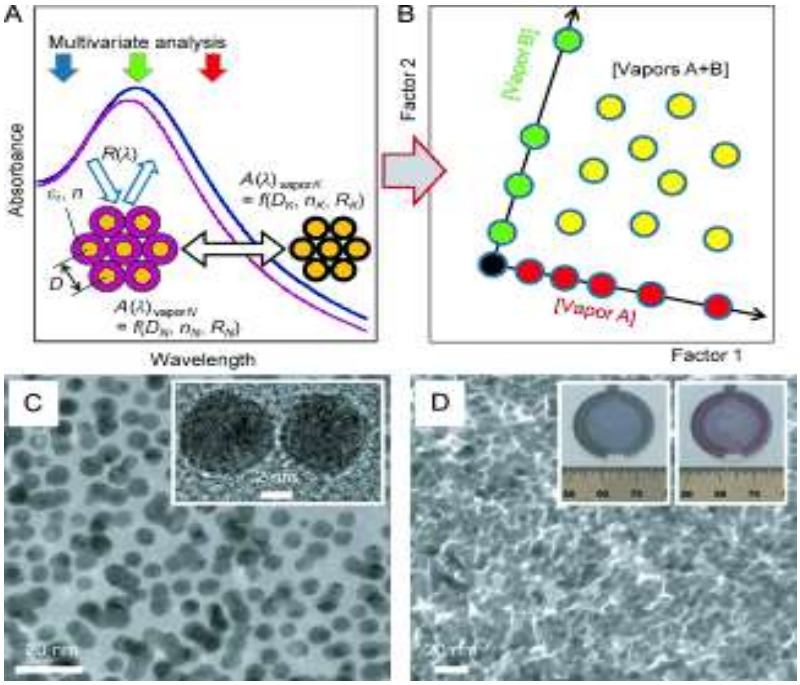

Figure 1-12. Selective detection of vapors using a single sensing film based on a 3D network of organothiol-functionalized plasmonic nanoparticles: A) Mechanisms facilitating vapor response selectivity involve vapor-induced modulation of interparticle spacing D, dielectric constant ε_r, and refractive index *n* of the ligand shell, and film reflectivity *R*. B) Concept of spectral discrimination of vapors A and B and their mixtures A+B upon multivariate analysis of resulting LSPR spectra. C) TEM image of 1-mercapto-(triethylene glycol) methyl ether functionalized gold nanoparticles. Inset, high-resolution TEM of two nanoparticles. D) TEM image of a sensing film formed from nanoparticles. Insets, color change of the spin-cast sensing film before (left) and during (right) water vapor exposure. Reprinted from *Angew. Chem. Int. Ed.*., **2013**, *52 (39)*, 10360-10364.[107]

CHAPTER II

NANOPARTICLE-COATED CHEMIRESISTOR ARRAY AS A MICROSCALE GAS CHROMATOGRAPH DETECTOR FOR EXPLOSIVE MARKER COMPOUNDS: FLOW RATE AND TEMPERATURE EFFECTS

PUBLISHED IN *ANALYST*, 2013, *138*, 6860.

2.1 Introduction

The use of thiolate-monolayer-protected gold nanoparticles (MPNs) as interface films on arrays of chemiresistor (CR) sensors for analyzing volatile organic compounds (VOC) has been studied extensively over the past 15 years.[1-9] Reversible vapor sorption leads to changes in the electron tunneling resistance of the film by virtue of swelling induced changes in the volume and dielectric constant.[1,8] The partially selective responses from an array of CRs coated with films of MPNs having different thiolate structures collectively yield a pattern that can be used to differentiate one analyte from another.[3,5,9] However, as with all sorption-based vapor sensor arrays, the diversity of response patterns achievable is quite limited, and the components of VOC mixtures cannot generally be quantitatively determined.[10-13] This has led to the use of MPN-coated CR arrays as detectors in meso-scale and micro-scale gas chromatographic (GC) instrumentation,[14-20] which has proven to be quite effective. The small size, low power consumption, simple fabrication and supporting electronics, as well as favorable scaling laws favor the use of these devices as μGC detectors.

This study is part of an effort to develop μGC instrumentation for monitoring vapor-phase markers of the explosive 2,4,6-trinitrotoluene (TNT), ultimately for screening personnel and baggage in transportation terminals. Although numerous technologies are currently used for such security screening,[21-26] and reports on newer sensing approaches have appeared recently,[27-31] relatively few commercial systems have been adapted to the direct determination of explosives or their marker compounds in the gas phase.[23,26,32] Toward that end, the portable instrument prototype we are developing for determinations of selected TNT marker compounds combines a high-volume preconcentration module of conventional design with a μGC analysis module comprising a Si-micromachined focuser (μF) and separation column (μcolumn), and a microfabricated MPN-coated CR array detector.[33]

Here we explore the dynamic responses of an MPN-coated CR array used as a (μ)GC detector for the analysis of the following three gas-phase markers of TNT: 2,4-dinitrotoluene (2,4-DNT), 2,6-dinitrotoluene (2,6-DNT), and the taggant 2,3-dimethyl-2,3-dinitrobutane (DMNB), the vapor pressures, p_v, of which are 5.3×10^{-5}, 1.2×10^{-4}, and 2.7×10^{-4} kPa, respectively.[34] Given the low volatility of the target analytes, it is necessary to operate the array at elevated temperature to avoid excessive broadening of response profiles. Although the flow rate employed is constrained by considerations of chromatographic efficiency and focuser injection band width, the effect of this variable on the responses of the sorption-based CR sensors in a closed-cell detector must also be considered.

Increasing the operating temperature of an MPN-coated CR-array detector could have several effects on eluting peaks. Since vapor pressures increase, the extent of sorption at a given vapor concentration should decrease because of the reduction in the thermodynamic partition coefficient, *K*. The absolute concentration will also decrease by the ideal gas law. These factors

should decrease the peak area, *A*. The effect on the resolution of two closely eluting peaks will depend on the peak widths, which are conveniently represented by the full-width at half maximum ($W_{½}$), and are affected by mass transport rates in and out of the MPN films. Since vapor diffusion rates in the headspace and MPN films will increase, peaks should be narrower due to enhanced mass transport. The effect on detectability (i.e., limit of detection, LOD) is hard to predict because peak height, *H*, may increase or decrease depending on whether the kinetics or thermodynamics dominate the vapor-MPN interaction.

A few studies have explored the effects of flow rate and/or temperature on the responses of MPN-coated CR arrays as GC or μGC detectors for common VOCs.[14,17,35] For flow rates of a few mL/min, compatible with GC separations, reports suggest that mass transport to the MPN film and in/out of the film is fast compared to detector cell residence times.[14,17] Consistent with this, relative response patterns did not change with flow rate, but sensitivities decreased with increasing flow rate, which led to an increase in chromatographic resolution, R_s.[17] One study showed that the *H* value for *n*-octane passed through a maximum with increasing flow rate, which was rationalized as reflecting initial peak sharpening at lower flow rates followed by dilution-induced reductions in *H* (and *A*) at higher flow rates.[14] As a result, LODs were not highly dependent on flow rate. Over the modest temperature ranges spanned in previous studies (i.e., 25-45°C), increases in sensor temperature led to the expected decreases in *A*, *H*, and $W_{½}$ and increases in R_s.[14,35] Thus, the optimization of flow rate and temperature entails tradeoffs among sensitivity, detectability, and chromatographic resolution.

In this study, we examine the stability of MPN-coated sensors at elevated temperature and the effects of flow rate and temperature on the responses of an MPN-coated CR array to the TNT marker compounds mentioned above. Because of the low p_v values of the markers, the

range of operating temperatures tested (i.e., 50-80°C) was higher than those studied previously. The range of flow rates tested (i.e., ~1-4 mL/min) is typical of those used in (μ)GC.[14,17,18,33] The dependent variables examined are *A*, *H*, $W_{½}$, retention time (t_R), asymmetry factor (*A*F) and the pairwise $R_s = 1.18(t_{R2} - t_{R1})/(W_{½-1} + W_{½-2})$.[36] Tests were performed with the CR array in a large exposure chamber and then in a low-dead-volume detector cell downstream from a conventional capillary GC column. These were followed by tests with upstream μF and μcolumn devices.

2.2 Experimental

2.2.1 Materials and Devices

All markers and other test compounds were purchased from Sigma-Aldrich/Fluka (Milwaulkee, WI) or Acros/Fisher (Pittsburgh, PA) in > 97% purity and were used as received. The adsorbent used in the μF was the graphitized carbon Carbopack B (C-B, specific surface area = 100 m^2/g, Supelco, Bellefonte, PA). The PDMS stationary phase used in the μcolumn was acquired from Ohio Valley (OV-1, Marietta, OH). The MPNs contained thiolate monolayers derived from *n*-octanethiol (C8), 4-(phenylethynyl)-benzenethiol (DPA), 6-phenoxyhexane-1-thiol (OPH), and methyl-6-mercaptohexanoate (HME) and were taken from existing supplies synthesized by the method reported by Rowe *et al*..[37] Average Au core diameters ranged from 3.4 (C8) to 4.7 nm (HME), with relative standard deviations (RSD) of 5-23% for any given type of MPN.

The CR array chip (2.0 × 1.2 cm) has been described previously.[18] It has eight Au/Cr interdigital electrodes (IDEs) arranged in a 4 × 2 pattern on a thermal-SiO_x/Si substrate. The thickness of the Au/Cr metal film is 2000/300 Å. Each IDE has 24 finger pairs with 5 μm widths/spaces, 450 μm length, and 410 μm overlap. The array was cleaned by sequential

sonication in acetone and 2-propanol, followed by drying in a stream of scrubbed air. MPNs were dissolved in suitable solvents (toluene for C8, DPA, and OPH, dichloromethane for HME) at concentrations of ~5 mg/mL. Adjacent sensors were coated with the same type of MPN by drop casting with a 0.5 μL syringe to create multilayer films with baseline resistances between 1-10MΩ. The array was capped with a Macor lid and sealed using a VHB-tape gasket (3M, St. Paul, MN), which created a detector cell volume of 1.6 μL (0.3*w* × 0.4*l* × 0.013*h* cm). Inlet/outlet ports drilled into the lid were fitted with deactivated fused-silica capillaries and sealed with epoxy. The array was enclosed in a Faraday cage fashioned from aluminum to eliminate noise from ambient electromagnetic sources during testing.

The μF and the μcolumn used in this study have been described elsewhere.[38-40] Briefly, the 0.41-cm^2 μF chip has a 4.3-mm^3 deep-reactive-ion-etched (DRIE) Si cavity, a side port for filling with adsorbent (~2 mg of sieved C-B), inlet and outlet flow channels, and an additional etched flow channel that forms a tee connection with the main inlet channel, which facilitates capturing and backflushing of the vapor samples. A Pyrex cap was anodically bonded over the chip to seal the cavity and all channels. Evaporated Au-on-Cr heater contact pads and a Ti/Pt resistance temperature device (RTD) are used for thermal desorption/injection (the μF can be heated from 25 to 225 °C in ~0.6 sec).

The 3.2-cm^2 DRIE-Si/Pyrex μcolumn chip has a 1-m long square-spiral channel with a cross section of 150 × 240 μm and integrated heaters and temperature sensors for temperature programming. Short segments of deactivated fused silica capillary were inserted into the inlet and outlet ports at the edge of chip and sealed with epoxy (Hysol Epoxy Patch 1C, Rocky Hill, CT). A PDMS stationary phase (avg. thickness = 0.15 μm) was deposited on the internal channel walls by a static method and cross-linked *in situ*.[39]

2.2.2 Test Apparatus and Methods

For initial testing at elevated temperature, an un-lidded CR array was mounted in a 0.5-L temperature-regulated stainless-steel chamber equipped with electrical feedthroughs and fluidic ports. Test atmospheres of each vapor were generated by passing scrubbed air through a fritted bubbler containing the liquid analyte, followed by dilution in a dry, scrubbed air stream maintained at ~14 L/min. After passing through the chamber, a small portion of the test atmosphere could be directed to 6-port valve with a sampling loop to a pre-calibrated flame ionization detector (FID) to verify VOC concentrations.

Additional testing at elevated temperature was performed with the CR array connected to an upstream conventional capillary column (9-m long, 250-μm i.d., 0.25-μm thick PDMS phase, Supelco) inside the oven of a bench-scale GC (Model HP6890, Agilent Technologies, Palo Alto, Ca). Tank air was used as the carrier gas and toluene was used as the test compound. Samples were drawn from static test atmospheres of toluene in Tedlar® bags through a 25-μL gas sampling loop and injected via a 6-port valve. Injected masses ranged from 40-150 ng and were confirmed by a pre-calibrated FID connected downstream from the CR array. The array was maintained at 70°C (via GC oven) for several hours per day over an 11-day period, and toluene calibrations were performed each day.

In the final series of tests on the effects of the sensor operating temperature, a μF was placed inside the GC oven and connected to the downstream side of the GC injection port. The μF outlet was connected to the CR array, which was also mounted in the oven. All connections were made with 250-μm i.d. deactivated fused-silica capillaries via press-fit connectors. An autosampler mounted on the GC was used to inject standard solutions of the marker compounds in acetone (~20-30 ng injected) to the front end of the μF, which was held at a baseline

temperature of 80 °C with its integrated heater. N_2 was used as the carrier gas. The solvent was purged from the μF via a vent line that bypassed the CR array. The μF was then rapidly heated to 225°C and the sample was backflushed to the downstream CR array. Samples of the marker compounds were tested individually. The oven (CR array) temperature was adjusted to several values in the range of 50-80°C and allowed to stabilize for at least 20 min prior to collecting measurements. The flow rate was held constant and measured with a downstream bubble buret.

For testing the effect of flow rate on sensor responses, the μcolumn was installed between the μF and CR array in the GC oven and the entire subsystem was heated to a baseline temperature of 70°C. Samples were introduced to the μF, the solvent was purged, and the samples injected as described above. The μcolumn was heated to 120°C with the onboard heaters. Flow rates ranged from 1.1 – 3.7 mL/min.

2.2.3 Mixture analysis with microsystem

The μF and μcolumn were connected upstream of a CR array inside the GC oven and held at 70°C. Samples of the marker compounds and four n-alkane interferences in CS_2 solution were loaded onto the μF by syringe using the autosampler, the solvent was purged, and then the samples were thermally desorbed/injected with backflushing at 3 mL/min. The μcolumn was held at 70°C for 20 sec and then ramped to 130°C at 300°C/min with the onboard heaters.[41] The masses injected were 4, 20, and 50 ng for 2,4-DNT, DMNB, and the n-alkanes, respectively (note: 2,6-DNT was not included in these tests; see below). Single-point sensitivity estimates were derived from the baseline-normalized resistance changes (peak heights, $\Delta R/R_b$) per unit mass injected. Estimated limits of detection (LOD) were taken as three times the standard deviation of the noise of the baseline divided by the sensitivity value derived from peak heights.

2.2.4 Data collection and analysis

For the chamber tests, each CR in the array was connected in series with a reference resistor (R_{ref}) and biased with a dc voltage from a battery (V_A = 1.59 V). The voltage drop across the CR (V_S) was measured by a digital voltmeter with multiplexer card (model 34970A/34902A, Agilent Technologies, Santa Clara, CA) and recorded with Agilent software on a PC. The sensor resistance (R_{sen}) was calculated via $R_{sen} = (V_S \cdot R_{ref})/(V_A - V_S)$.[8] For later tests, each CR in the array was again connected in series with an R_{ref} that was closely matched to the baseline resistance of the CR (R_b) and biased with a 1.5 V dc voltage from a battery (V_A). The voltage drop across the CR was collected and converted to relative resistance change ($\Delta R/R_b$) via the expression $\Delta R/R_b = V_S/(150V_B(1-(V_B/V_A)))$, where V_B = the baseline voltage of the CR. A DAQ card installed in a laptop computer was used to record the voltage change from each CR at 20 Hz after signal amplification. Data were logged and then exported to GRAMS (32/AI 6.00a, Galactic Industries, Salem, NH) for subsequent processing.

2.3 Results and discussion

2.3.1 Stability of MPN-coated CR arrays

In a series of preliminary tests, a CR array was repeatedly exposed to test atmospheres of five individual VOCs (i.e., toluene, *n*-propanol, 2-butanone, *n*-octane, and nitromethane) in dry air at 25.0 ± 0.1 °C in the test chamber over a 90-day period. Between exposures, the array was stored in a plastic box in the dark at room temperature. Results are summarized in Table A.1 and Figure A.1 in Appendix A accompanying this article. Under these conditions, the sensors exhibited stable, reproducible responses to the VOCs: sensitivities increased by less than 16% for four of the VOCs and by 35% for the fifth VOC (i.e., *n*-propanol), and normalized response

patterns did not change significantly. These results suggest that no significant oxidation or loss of thiolate ligands occurred over the test period.[42]

In a second series of preliminary tests, an array with a single C8-coated sensor was installed as the detector downstream from a 30-m capillary column and calibrations were performed with isopropylbenzene at discrete sensor temperatures ranging from 25-75°C. Results (Figure A.2, Appendix A) show that there was a steady reduction in peak area with increasing temperature but that the calibration curves remained linear. Re-calibration at 25°C gave the same sensitivity as found at the outset, indicating that the C8 MPNs are stable up to at least 75°C. A subsequent test in which a CR array was calibrated with 2,6- and 2,4-DNT at 70°C, heated to 95°C for 30 min, and re-calibrated at 70°C showed a significant decrease in sensitivity. These results are consistent with a report showing that thiolate ligands are prone to desorption from the gold core of MPNs at temperatures above 90°C.[43] Therefore, in subsequent testing the maximum temperature was limited to 80°C. Furthermore, due to the excessively broad responses to the marker compounds at low temperatures, the minimum test temperature was set at 50°C.

The medium-term stability of a CR array (as a GC detector) at elevated temperature was then assessed using toluene as the analyte. Duplicate films of each type of MPN were coated on adjacent sensors and, with the exception of one HME-coated sensor that showed excessive noise, the baseline resistances and toluene sensitivities within each pair coated with the same MPN were similar (i.e., RSD < 8%). Therefore, data from only one of each pair coated with a given type of MPN are presented. The array was held at 70°C in air for 15 hr prior to exposure, and was then held at 70°C for 6-10 hr per day over 11 days (total = 80 hrs at 70°C). Overnight it was allowed to cool to room temperature under a flow of clean air. Toluene sensitivity ($\Delta R/R_b$/ng)

was checked every day (~50-150 ng injected) at both 70°C and 30°C. Baseline resistances at 70°C were stable (RSD ≤ 10% for C8 and HME, and ≤ 2% for DPA and OPH). Response patterns constructed from the absolute *H*-value sensitivities at 70°C are presented in Figure 2-1. Patterns derived from *A*-value sensitivities were nearly identical to these ($r \geq 0.98$). Furthermore, the response patterns at 30°C derived from *H* values or *A* values were highly correlated with those at 70°C ($r \geq 0.98$ in both cases). Thus, the temperature dependence of the responses is similar for all sensors, as also reported for a polymer-coated surface-acoustic-wave sensor array.[44]

As shown, the average sensitivity values derived from all four sensors showed a net increase of only 21% over the entire test period, corresponding to ~2% drift per day on average. Although the net increase in individual-sensor sensitivities varied from 17-27%, the collective response pattern for toluene remained highly correlated with that from the first day ($r \geq 0.97$). On the basis of these results the elevated-temperature stability of absolute and relative responses from the array sensors was deemed satisfactory.

2.3.2 Effect of temperature on responses to the marker compounds

A representative set of responses from the OPH-coated sensor to 30-ng samples of 2,4-DNT desorbed directly from the μF to the array at each of several temperatures at a flow rate of 3 mL/min are shown in Figure 2-2. A similar series of tests was then performed at 1.2 mL/min with all three marker compounds at five discrete temperatures ranging from 55°C to 80°C. Table 2-1 presents the ratios of *A*, *H*, $W_{1/2}$, LOD, t_R, and *AF* values at the lowest and highest temperature. As shown, the values of all of these variables decreased with increasing temperature. The ratios are similar among the sensors for a given marker, with the exception of

the OPH-coated sensor, for which the *H* ratios are consistently lower and the $W_{1/2}$ and t_R ratios are consistently higher than those of the other sensors, despite the ratio of *A* values being similar to those of the other sensors. Normalized response patterns for a given marker derived from the *A* values at the two temperature extremes were nearly identical ($r \geq 0.99$). The corresponding patterns derived from the corresponding *H* values, however, were somewhat more variable for two of the markers: r = 0.91, 0.95, 0.99 for DMNB, 2,6-DNT, and 2,4-DNT, respectively.

Average reductions in apparent t_R values (i.e., time from injection to appearance of peak maximum) over this temperature range were in the order DMNB < 2,6-DNT < 2,4-DNT (Table 2-1). Note that, although the flow rate measured downstream of the array at room temperature was held constant, mass balance constraints would cause an increase in local flow rate at elevated temperature, but only by about 7% between 55 and 80°C. As shown, the DMNB t_R value was almost unaffected, whereas the 2,6- and 2,4-DNT t_R values decreased by several fold. Similar trends are apparent in the values of $W_{1/2}$. For all sensors the temperature sensitivity of t_R (and $W_{1/2}$) increases as the marker volatility decreases, and for all markers the OPH sensor stands out as having somewhat greater sensitivity than the other sensors. The degree of tailing with the OPH sensor was greater at the lower temperature than with the other sensors, as shown in the traces in Figure 2-2 and also by the *AF* ratios (Table 2-1) and *AF* values (Table A.2). In addition to differences in the *temperature dependencies* of t_R, there were differences in the t_R *values* at a given temperature for the OPH sensor. For example, even at 80°C the t_R values for 2,4-DNT were 9, 11, 23, and 10 sec for C8, DPA, OPH, HME, respectively.

Changes in diffusion rates in the headspace of the detector cell should be similar for all markers (see below), and although non-uniform mixing within the detector cell could be contributory, it seems more likely that these trends arise from differences in the rates of sorption

and/or desorption in the MPN films, particularly for the DNT isomers. The most likely explanation for the OPH behavior is that the thickness of the OPH film was greater than that of the other MPNs. The film casting method employed is not very precise and film thicknesses were not measured. Since baseline resistances as well as vapor sensitivities in MPN-CR sensors are independent of film thickness (above a minimum value),[8] a thicker OPH film may have gone undetected. Thus, despite the fact that the HME sensor was more sensitive to all three markers than was the OPH sensor, mass transfer in and out of the thicker OPH film could have been slower.

Since R_s varies inversely with the average of the $W_{½}$ values of adjacent peaks, all other factors notwithstanding, substantial increases in R_s would be expected by increasing the array temperature from 55 to 80 °C. That is, if Δt_R were constant, R_s would hypothetically increase by as much as ~3-fold for the DMNB/2,6-DNT pair and ~4-fold for 2,6-DNT/2,4-DNT pair. However, since the rates at which t_R decreases with temperature are only slightly lower than those of $W_{1/2}$ (Table 2-1), increases in R_s are likely to be quite modest.

Since LODs are estimated from values of H, and baseline noise levels were remarkably stable among all sensors in the CR array, differing by < 5% between 55 and 80°C, decreases in H values would translate into commensurate increases in LODs. The average decreases in H over this temperature range were 4.5-, 1.6-, and 1.3-fold for DMNB, 2,6-DNT, and 2,4-DNT, respectively. The higher ratio for DMNB is consistent with its film sorption/desorption kinetics being faster than those of the less volatile DNT isomers, such that the decrease in H is dictated primarily by thermodynamic factors. This is unfortunate, because the LOD of DMNB is the highest of the markers, due to its higher p_v value (see below).

In light of these results, as well as additional data collected on the performance of the μF and μcolumn in parallel studies,[33,38] an operating temperature of 70°C was chosen for the CR array. In fact, for practical reasons, a decision was made to house all of the microfabricated components of the μGC analysis module within one mini-oven to establish a common baseline temperature. Therefore, all subsequent testing described below was performed with the CR array maintained at 70°C.

2.3.3 Effect of flow rate on responses to the marker compounds

Since tests of flow rate were performed with an upstream μF and μcolumn, the effects of changes in flow rate must take these additional components into account. At higher flow rates, the injection band emanating from the μF would be narrower and, since the markers spend less time in the separation column, the on-column band broadening would be less as well. Any dispersion associated with mixing in the detector cell would also decrease with increasing flow rate. All of these factors should lead to an increase in H and a decrease in $W_{1/2}$ with increasing flow rate. None of these factors should affect A. However, the concentration of the analyte in the flow stream may decrease with increasing flow rate because of dilution in the carrier gas, and since the partitioning into the MPN films is concentration dependent, this factor would tend to decrease A (and H). The rates of sorption and desorption of the markers into and out of the MPN films may also be important (*vida supra*). Although the MPN films sorb only a small fraction of the mass of vapor in the headspace above the sensor, if the time required to diffuse into or out of the films as the vapor passes through the detector cell were comparable to, or longer than, the cell residence time, then $W_{1/2}$ would increase, and both A and H would decrease. Thus, values of

A are predicted to decrease with increasing flow rate and the net effects on $W_{1/2}$ and *H* would depend on which factors mentioned above dominate.[14]

For a detector cell volume of 1.6 μL, flow rates ranging from 1.1 to 3.7 mL/min correspond to cell residence times ranging from 87 to 26 ms, respectively. The published diffusion coefficient, *D*, of 2,6-DNT at 20°C is 0.03 cm^2/s, and that for 2,4-DNT is 0.20 cm^2/s.[46-47] No value could be found for DMNB. The *D* value for 2,4-DNT appears to be erroneous, as it is higher than that of methanol, which is unrealistic. Using the value for 2,6-DNT as a benchmark, and assuming it would increase as $(T_2/T_1)^2$,[48] the estimated *D* value in air at 70°C would be 0.04 cm^2/sec. Diffusion times can be estimated using the one-dimensional Fick's law expression $t = x^2/4D$, where *x* = distance traveled (i.e., cell height or film thickness) and *t* = time. Given the detector cell dimensions, it would take ~1 ms to traverse the height of the cell and reach the MPN film surface. Assuming a *D* value of 10^{-8} cm^2/s for the markers in the MPN film, which is a rough, conservative estimate of D for the diffusion of a vapor within an amorphous rubbery polymer (no D values of vapors in MPN films could be found),[49-50] and an estimated average film thickness of ~240 nm obtained from our AFM measurements of similarly deposited MPN films,[51] it would require ~14 ms for the marker compounds to traverse the MPN film. Thus, on the basis of these rough estimates, mass transport in the headspace above the array would be fast relative to transport through the film, and the latter would be of the same order as the cell residence times.

Figure 2-3 shows some representative responses to each individual marker compound at flow rates of 1.1 to 3.7 mL/min from the DPA sensor, and Table 2-2 presents ratios of the peak parameters (i.e., *A*, *H*, $W_{1/2}$, LOD, t_R, and *AF*) for all sensors and markers over this flow rate range (i.e., lowest:highest). As shown, and as also reflected in the *AF* values in Table A.3

(Appendix A), the extent of peak tailing is generally greater for 2,4-DNT. A portion of this can be attributed to desorption from the μF and elution through the μcolumn, [38,41] but the dynamics of the detection process apparently also contribute (*vida infra*).

Figures A.3-5 in Appendix A show plots of flow rate versus *A*, *H*, $W_{1/2}$, as well as the relative response patterns for the three marker compounds. Increasing the flow rate from 1.1 to 3.7 mL/min led to decreases in *A* for all three markers, with the magnitude of the change in the order 2,4-DNT < 2,6-DNT < DMNB, which follows the order of volatility (and elution). For a given marker, the ratio of *A* values was in the order C8 > DPA > OPH~HME. To the extent that sensor responses are dictated by thermodynamics (i.e., partitioning), *A* should decrease in proportion to the headspace concentration and no differences among the sensors should be observed. Dilution from the increased flow rate would be counteracted by any chromatographic factors that result in sharpening of the eluting band such that, if the bandwidth were to decrease in proportion to the flow rate increase, then the mass per unit air volume would not change and no reduction in *A* should occur. Otherwise, both the mass per unit volume and the mass uptake by the film would decrease, leading to a decrease in *A*. If the kinetics of mass uptake or release by the MPN films were slow compared to the transport of vapor through the detector cell, then this would superimpose a nulling effect on the trends expected on the basis of thermodynamic factors.

As shown in Table 2-2, the average ratios of *A* values (highest:lowest) over the 3.4-fold flow rate range tested were 2.8, 2.1, and 1.4 for DMNB, 2,6-DNT, and 2,4-DNT, respectively, and the ratios for the C8 and DPA sensors were consistently larger than those for the OPH and HME sensors. In contrast, the average ratios of $W_{½}$ values were 1.2, 3.0, and 3.3 for DMNB, 2,6-DNT, and 2,4-DNT, respectively. The DMNB $W_{½}$ values pass through a minimum at ~2

mL/min, whereas the values for the other two markers decreased monotonically (see Appendix A). The *H* values for DMNB passed through a *maximum* at 2 mL/min but then decreased with further increases in flow rate, while those for 2,6- and 2,4-DNT increased roughly linearly with flow rate, yielding average ratios of ~0.8 and ~0.5, respectively, over the entire range. As with the ratios of *A* values, the *H* ratios are generally larger for the C8 and DPA sensors, while this trend was less apparent for the ratios of $W_{½}$ values.

Collectively, these data indicate that multiple factors affect the dynamics of the responses; mass transport within the MPN films is clearly important, and vapor-specific and film-specific differences in behavior occur. We surmise that dilution of the air concentrations of the markers with increasing flow rate is an important determining factor, but that the evaporation rate of the sorbed markers, which is expected to vary in inverse proportion to the analyte vapor pressure,[52] is an important co-factor.

For DMNB, the ~2.8-fold net decrease in *A* is consistent with what would be expected from dilution, given that the net decrease in $W_{1/2}$ was only ~20%. However, the fact that $W_{1/2}$ passed through a minimum (and *H* passed through a maximum) indicates that there was an additional factor at play. At low flow rates the DMNB sorption/desorption kinetics are apparently fast enough for mass transport in the film to keep pace with the gradual decrease in elution bandwidth and cell residence time, such that the peaks got narrower and (slightly) taller, as expected. The observed peak broadening and shortening above 2 mL/min, however, suggests that mass transport in the film began to lag behind that in the headspace of the cell.

For 2,6-DNT and 2-4-DNT, mass transport in the film was apparently slow relative to the cell residence time over the entire range of flow rates, as reflected in the $W_{1/2}$ values, which were from 2-20 times larger than those for DMNB (see Figures A3-A5, Appendix A). The $W_{1/2}$ values

for 2,4-DNT were consistently larger than those for 2,6-DNT, as well. Although the peaks for the DNT isomers grew narrower and taller with increasing flow rate, as expected from the decrease in the column band widths, the decrease in *A* values was less than expected. This is indicative of a lag in mass transport in the film. That the extent of attenuation (lag) varies inversely with the vapor pressure of the marker suggests that desorption out of the films is likely to be more important than sorption into the films; the latter should not depend on vapor pressure, whereas sorbed analytes, which formally condense within the MPN film, must then evaporate from the films, and evaporation rates are inversely proportional to vapor pressure.[52] The consistently larger spread in t_R values among the sensors for the less volatile markers supports this notion (Figure A.6). The larger ratios of *A*, $W_{1/2}$, and *H* for the non-polar C8 and DPA films are consistent with their weaker intermolecular interactions with the sorbed marker molecules and lower apparent mass uptake. On the basis of the individual values of $W_{1/2}$ and t_R, increases in R_s of up to 1.2-fold for the 2,6-DNT/2,4-DNT pair and up to 1.7-fold for the DMNB/2,6-DNT pair would be expected.

Despite the differences in the ratios of *A* values among the sensors (Table 2-2), the changes in normalized response patterns derived from the *A* values were relatively modest (see Figures A3-A5, Appendix A) and for all three markers r values among the patterns remained ≥ 0.97 over the flow rate range examined. Patterns derived from *H* values for DMNB were relatively unaffected (r > 0.99), whereas those for 2,6-DNT and 2,4-DNT changed significantly over the range of flow rates examined (r = 0.66 and 0.57, respectively).

The matter of deciding on an optimal flow rate required consideration of the tradeoffs among the μF injection bandwidth, chromatographic resolution, overall analysis time, and LODs. The analysis time is dictated by the t_R value of 2,4-DNT, which was 64 s at 3.0 mL/min and 56 s

at 3.7 mL/min (i.e., a difference of 12%). A marginal decrease in injection bandwidth and a marginal increase in R_s were observed above 3 mL/min, as well.[41] Although H values for 2,4-DNT and 2,6-DNT continued to increase for all sensors above 3.0 mL/min, those for DMNB continued to decrease, with commensurate changes in the LODs. Since DMNB had the highest LOD among the markers, a decision was made to operate at 3 mL/min to avoid the additional reduction in the DMNB LOD at the higher flow rate.

2.3.4 Mixture analysis with microsystem components

Figure 2-4 shows chromatograms from each sensor in the array for a mixture of DMNB, 2,4-DNT, and four *n*-alkanes (C_{10}, C_{12}, C_{13}, and C_{14}), which are representative of jet fuel. The 2,6-DNT was removed from the set of marker compounds at this point, in recognition of its concentration in the headspace of TNT being nearly 10 times lower than that of 2,4-DNT (note: 2,4-DNT is reported to comprise 35% of the mass of vapors in the headspace above TNT).[34,53] The chromatograms were generated with the all three microsystem components (i.e., μF, μcolumn, and sensor array) maintained at a baseline temperature of 70°C. The μcolumn was temperature programmed as described in the Experimental Section and the flow rate was 3.0 mL/min.

Despite the fact that the injected masses of the 2,4-DNT and DMNB were only 4 and 20 ng, respectively, while those for the *n*-alkanes were 50 mg each, responses to the markers from the DPA, OPH, and HME sensors were significantly larger than responses to the alkanes. Even for the C8 sensor, responses to the markers were comparable to the alkane responses, owing to the lower vapor pressures of the markers (note: p_v values for the alkanes range from roughly 0.002 to 0.2 kPa;[54] which are from 1-2 orders of magnitude higher than those of the markers).

The peaks for the *n*-alkanes exhibited some tailing ($AF \leq 1.9$), but were more symmetric than those for the markers. DMNB was chromatographically resolved from the closest eluting alkane (C_{12}), but the R_s values differed among the sensors in the array, ranging from 1.4 (C8) to 0.57 (HME). Regardless, since there are substantial differences in the array response patterns between C_{12} and DMNB, simple deconvolution could be used to recover the response pattern and to quantify this marker.[15] The 2,4-DNT peaks were fully resolved from those of the closest eluting alkane (C_{14}), however, the extremely large $W_{1/2}$ values of the 2,4-DNT peaks and the differences in $W_{1/2}$ and t_R values among the sensors resulted in a net analysis time of 115 sec for full recovery of the baseline. On the basis of the least sensitive sensor in the array (i.e., DPA), the estimated LODs are 4 ng for DMNB, 2 ng for 2,4-DNT, and 20-50 ng for the interferences.

2.4 Conclusions

We conclude that the MPN-coated CR arrays studied here are sufficiently stable in air up to 70°C to provide reliable detector performance in μGC field applications using air as the carrier gas. Observed decreases in *A*, *H*, $W_{1/2}$, *AF*, and effective t_R with increased temperature for the explosive marker compounds were qualitatively consistent with expected temperature induced decreases in the partition coefficients and increases in diffusion rates, and with results reported by other investigators for common VOCs studied at lower temperatures with similar sensor arrays.[14,17,35] Observed changes in these response parameters with flow rate, however, reflected the influence of multiple factors and led to flow rate dependencies that were sensor- and vapor-specific. Differences in the vapor pressures of the markers, and consequent differences in desorption rates from the MPN films, are apparently responsible for observed differences in optimal flow rates even at the elevated operating temperatures employed. Since responses to

such semi-volatile analytes from any type of microsensor employing sorptive interface layers would be affected similarly, these findings may have broad implications, i.e., the dynamics of the responses must be considered carefully in the design and operation of μGC systems using such detectors, and tight controls on flow rate would be required for reliable analyte recognition and quantification.

Taking account of these results, as well as factors related to the performance of upstream μGC components, a flow rate of 3 mL/min and an array operating temperature of 70 °C were selected. Under these conditions, the temperature-programmed separation of the two primary marker compounds, DMNB and 2,4-DNT, from four *n*-alkanes of similar volatility was achieved in < 2 min, with LODs of ≤ 4 ng from all microsensors in the array. A fieldable prototype incorporating a μGC module similar to that studied here has been constructed, and results of performance evaluations of this instrument will be reported in the near future.[41]

2.5 References

1. Wohltjen, H.; Snow, A.W. "Colloidal Metal-Insulator-Metal Ensemble Chemiresistor Sensor," *Anal. Chem.*, **1998**, *70*, 2856-2859.
2. Joseph, Y.; Krasteva, N.; Besnard, I.; Guse, B.; Rosenberger, M.; Wild, U.; Knop-Gericke, A.; Schlogl, R.; Krustev, R.; Yasuda, A.; Vossmeyer, T. "Gold-Nanoparticle/Organic Linker Films: Self-Assembly, Electronic and Structural Characterisation, Composition and Vapour Sensitivity," *Faraday Discuss.*, **2004**, *125*, 77-97.
3. Han, L.; Shi, X.; Wu, W.; Kirk, F.L.; Luo, J.; Wang, L.; Mott, D.; Cousineau, L.; Lim, S. I.; Lu, S.; Zhong, CJ. "Nanoparticle-Structured Sensing Array Materials and Pattern Recognition for VOC Detection," *Sens. Actuators B: Chem.*, **2005**, *106*, 431-441.
4. Ibanez, F.J.; Gowrishetty, U.; Crain, M.M.; Walsh, K.M.; Zamborini, F.P. "Chemiresistive Vapor Sensing with Microscale Films of Gold Monolayer Protected Clusters," *Anal. Chem.*, **2006**, *78*, 753-761.
5. Yang, C-Y.; Li, C-L.; Lu, C-J. "A Vapor Selectivity Study of Microsensor Arrays Employing Various Functionalized Ligand Protected Gold Nanoclusters," *Analytica Chimica Acta*, **2006**, *565*, 17-26.
6. Wang, L.; Shi, X.; Kariuki, N.N.; Schadt, M.; Wang, G.R.; Rendeng, Q.; Choi, J.; Luo, J.; Lu, S.; Zhong, CJ. "Array of Molecularly Mediated Thin Film Assemblies of

Nanoparticles: Correlation of Vapor Sensing with Interparticle Spatial Properties," *J. Am. Chem. Soc.*, **2007**, *129*, 2161-2170.
7. Joseph, Y.; Peic, A.; Chen, X.; Michl, J.; Vossmeyer, T.; Yasuda, A. "Vapor Sensitivity of Networked Gold Nanoparticle Chemiresistors: Importance of Flexibility and Resistivity of the Interlinkage," *J. Phys. Chem. C*, **2007**, *111*, 12855-12859.
8. Steinecker, W.H.; Rowe, M.P.; Zellers, E.T. "Model of Vapor-Induced Resistivity Changes in Gold-Thiolate Monolayer-Protected Nanoparticle Sensor Films," *Anal. Chem.*, **2007**, *79*, 4977-4986.
9. Bohrer, F.I.; Covington, E.; Kurdak, C.; Zellers, E.T. "Characterization of Dense Arrays of Chemiresistor Vapor Sensors with Submicrometer Features and Patterned Nanoparticle Interface Layers," *Anal. Chem.*, **2011**, *83*, 3687-3695.
10. Park, J.; Groves, W. A.; Zellers, E.T. "Vapor Recognition with Small Arrays of Polymer-Coated Microsensors. A Comprehensive Analysis," *Anal. Chem.*, **1999**, *71*, 3877-3886.
11. Jin, C.; Zellers, E. T. "Limits of Recognition for Binary and Ternary Vapor Mixtures Determined with Multitransducer Arrays," *Anal. Chem.*, **2008**, *80*, 7283−7293.
12. Hsieh, M-D.; Zellers, E.T. "Limits of Recognition for Simple Vapor Mixtures Determined with a Microsensor Array," *Anal. Chem.*, **2004**, *76*, 1885-1895.
13. Scholten, K.; Wright, L. K.; Zellers, E. T. "Vapor Discrimination with Single- and Multi-Transducer Arrays of Nanoparticle-Coated Chemiresistors and Resonators," *IEEE Sensors*, **2013**, *13*, 2146-2154.
14. Zhong, Q.; Steinecker, W.H.; Zellers, E.T. "Characterization of a High-Performance Portable GC with a Chemiresistor Array Detector," *Analyst*, **2008**, *134*, 283-293.
15. Jin, C.; Zellers, E.T. "Chemometric Analysis of Gas Chromatographic Peaks Measured with a Microsensor Array: Methodology and Performance Assessment," *Sens. Actuators B: Chem.*, **2009**, *139*, 548-556.
16. Cai, QY.; Zellers, E.T. "Dual-Chemiresistor GC Detector Employing Monolayer-Protected Metal Nanocluster Interfaces," *Anal. Chem.*, **2002**, *74*, 3533-3539.
17. Lu, C-J. ; Steinecker, W.H.; Tian, W-C.; Oborny, M.C.; Nichols, J.; Agah, M.; Potkay, J.; Chan, H.K.L.; Driscoll, J.; Sacks, R.D.; Wise, K.D.; Pang, S. W. ; Zellers, E.T. "First-generation Hybrid MEMS Gas Chromatograph," *Lab on a Chip*, **2005**, *5*, 1123-1131.
18. Kim, S.K.; Chang, H.; Zellers, E.T. "Microfabricated Gas Chromatograph for the Selective Determination of Trichloroethylene Vapor at Sub-Parts-Per-Billion Concentrations in Complex Mixtures," *Anal. Chem.*, **2011**, *83* (18), 7198-7206.
19. Kim, S.K.; Burris, D.R.; Chang, H.; Bryant-Genevier, J.; Zellers, E.T. "Microfabricated Gas Chromatograph for On-Site Detection of Trichloroethylene in Indoor Air Arising from Vapor Intrusion. 1. Field Evaluation," *Environ. Sci. Technol.*, **2012**, *46*, 6065-6072.
20. Kim, S.K.; Burris, D.R.; Chang, H.; Bryant-Genevier, J.; Zellers, E.T. "Microfabricated Gas Chromatograph for On-Site Detection of Trichloroethylene in Indoor Air Arising from Vapor Intrusion. 2. Spatial/Temporal Monitoring," *Environ. Sci. Technol.*, **2012**, *46*, 6073-6080.
21. HazMatID ranger, Smith Detection, http://www.smithsdetection.com/hazmatid_ranger.php, accessed January 2013.
22. RespondeR RCI, Smith Detection, http://www.smithsdetection.com/responder_RCI.php, accessed January 2013.
23. Sabre 5000, Smith Detection, http://www.smithsdetection.com/sabre5000.php, accessed January 2013.

24. Tridion-9, Torion, http://www.torion.com/products/24, accessed January 2013.
25. MobileTrace, Morpho, http://www.morpho.com/detection/see-all-products/trace-detection/mobiletrace-r/?lang=en, accessed January 2013.
26. Fido XT, ICx, http://www.icxt.com/uploads/file/products/brochures/Fido_XT.pdf, accessed January 2013.
27. Forzani, E.S.; Lu, D.; Leright, M.J.; Aguilar, A.D.; Tsow, F.; Iglesias, R.A.; Zhang, Q.; Lu, J.; Li, J.; Tao, N. "A Hybrid Electrochemical-Colorimetric Sensing Platform for Detection of Explosives," *JACS Comm.*, **2009**, *131*, 1390-1391.
28. Xin, Y.; He, G.; Wang, Q.; Fang, Y. "A Portable Fluorescence Detector for Fast Ultra Trace Detection of Explosive Vapors," *Rev. Sci. Instrumm.*, **2011**, *82*, 103102.
29. Caron, T.; Guillemot, M.; Montméat, P.; Veignal, F.; Perraut, F.; Prené, P.; Serein-Spirau, F. "Ultra-Trace Detection of Explosives in Air: Development of a Portable Fluorescent Detector," *Talanta*, **2010**, *81*, 543-548.
30. Clavaguera, S.; Montméat, P.; Parret, F.; Pasquinet, E.; Lère-Porte, J-P.; Hairault, L. "Comparison of Fluorescence and QCM Technologies: Example of Explosives Detection with a π-Conjugated Thin Film," *Talanta*, **2010**, *82*, 1397-1402.
31. Simoens, F.; Arnaud, A.; Castelein, P.; Goudon, V.; Imperinetti, P.; Lalanne Dera, J.; Meilhan, J.; Ouvier Buffet, J. L.; Pocas, S.; Maillou, T.; Hairault, L.; Gellie, P.; Barbieri, S.; Sirtori, C. "Millimetre Wave and Terahertz Sensors and Technology III," *Proceedings SPIE 7837*, Toulouse, France, **2010**, p. 78370B-1.
32. Hapsite GC/MS, http://www.inficonemergencyresponse.com/en/hapsite_er//index.html, accessed January 2013.
33. Collin, W. R.; Serrano, G.; Wright, L. K.; Chang, H.; Nuñovero, N.; Zellers, E. T. "Fieldable MEMS Gas Chromatograph for Rapid Determinations of Explosive Marker Compounds in Complex Mixtures," *Proceedings 17th International Conf. on Solid-State Sensors, Actuators and Microsystems*, *Transducers '13*, Barcelona, Spain, **2013**, p. 2763.
34. R. P. Murmman, T. F. Jenkins and D. C. Leggett, CREEL, *Special Report 158*, **1971**, available at http://www.dtic.mil/cgi-bin/GetTRDoc?AD=ADA040632, accessed October 2012.
35. Jian, R-S.; Huang, R-X.; Lu, C-J. "A Micro GC Detector Array Based on Chemiresistors Employing Various Surface Functionalized Monolayer-protected Gold Nanoparticles,"*Talanta*, **2012**, *88*, 160-167.
36. *Modern Practice of Gas Chromatography*, ed. R.L. Grob, John Wiley & Sons, Inc., New York, 3rd edn., **1995**, ch. 2, p. 115.
37. Rowe, M.P.; Plass, K.E.; Kim, K.; Kurdak, C.; Zellers, E.T.; Matzger, A.J. "Single Phase Synthesis of Functionalized Gold Nanoparticles," *Chem. Mat.*, **2004**, *16*, 3513-3517.
38. Serrano, G.; Sukaew, T.; Zellers, E.T. "Hybrid Preconcentrator/Focuser Module for Determinations of Explosive Marker Compounds with a Micro-scale Gas Chromatograph," *J. Chromatogr. A*, **2013**, *1279*, 76-85.
39. Serrano, G.; Reidy, S.M.; Zellers, E.T. "Assessing the Reliability of Wall-Coated Microfabricated Gas Chromatographic Separation Columns," *Sens. Actuators B: Chem.*, **2009**, *141*, 217-226.
40. Sukaew, T.; Zellers, E. T. "Evaluating the Dynamic Retention Capacities of Microfabricated Vapor Preconcentrators as a Function of Flow Rate," *Sens. Actuators B: Chem.*, **2013**, *183*, 163-171.

41. Collin, W. R.; Serrano, G.; Wright, L. K.; Chang, H.; Nuñovero, N.; Zellers, E. T. "Microfabricated Gas Chromatograph for Rapid, Trace-Level Determinations of Gas-Phase Explosive Marker Compounds," *Anal. Chem.*, **2013**, *86 (1)*, 655-663.
42. Joseph, Y.; Guse, B.; Nelles, G. "Aging of 1,ω-Alkyldithiol Interlinked Au Nanoparticle Networks," *Chem. Mater.*, **2009**, *21*, 1670-1676.
43. Büttner, M.; Belser, T.; Oelhafen, P. "Stability of Thiol-Passivated Gold Particles at Elevated Temperatures Studied by X-ray Photoelectron Spectroscopy," *J. Phys. Chem.B*, **2005**, *109*, 5464-5467.
44. Zellers, E. T.; Han, M. "Effects of Temperature and Humidity on the Performance of Polymer-Coated Surface Acoustic Wave Vapor Sensor Arrays," *Anal. Chem.*, **1996**, *68*, 2409-2418.
45. Dolan, J. W. "Peak Tailing and Resolution." LC Resources, http://www.chromatographyonline.com/lcgc/data/articlestandard/lcgceurope/202002/19199/article.pdf, accessed March 2013.
46. GSI Chemical Database. GSI Environmental, http://www.gsi-net.com/en/publications/gsi-chemical-database.html, accessed March 2012.
47. EPA. Part 5: Chemical-specific parameters, http://www.epa.gov/superfund/health/conmedia/soil/pdfs/part_5.pdf, accessed August 2012.
48. Nelson, G. O. "Gas Mixtures: Preparation and Control," CRC Press LLC, Boca Raton, Florida, **1992**, ch. 5, p. 142.
49. Sun, Y-M.; Chen, J. "Sorption/Desorption Properties of Ethanol, Toluene, and Xylene in Poly (Dimethylsiloxane) Membranes," *J. Appl. Polym. Sci.*, **1994**, *51 (10)*, 1797-1804.
50. Prager, S.; Long, F. A. "Diffusion of Hydrocarbons in Polyisobutylene," *J. Am.Chem. Soc.*, **1951**, *73*, 4072-4075.
51. Covington, E.; Bohrer, F. I.; Xu, C.; Zellers, E. T.; Kurdak, Ç. "Densely Integrated Array of Chemiresistor Vapor Sensors with Electron-Beam Patterned Monolayer-Protected Gold Nanoparticle Interface Films," *Lab Chip*, **2010**, *10*, 3058-3060.
52. K. Caplan, *Evaporation Rate of Volatile Liquids*, Final Report, EPA Contract Nos. 68-2-4248, 1988 and 68-D8-0112, 1989.
53. Jenkins, T.F.; Leggett, D.C.; Miyares, P.H.; Walsh, M.E.; Ranney, T.A.; Cragin, J.H.; George, V. "Chemical Signatures of TNT-filled Land Mines," *Talanta*, **2001**, *54*, 501-513.
54. C. L. Yaws, in Chemical Properties Handbook, McGraw-Hill, New York, 1999.

Table 2-1. Ratios of peak parameters as a function of temperature for each marker compound with each of the four sensors in the CR array.

Parameter[a]	DMNB					2,6-DNT					2,4-DNT				
	C8	DPA	OPH	HME	Avg.	C8	DPA	OPH	HME	Avg.	C8	DPA	OPH	HME	Avg.
A_1/A_2	6.6	5.9	6.1	6.6	6.3	4.0	3.6	3.8	4.0	3.9	5.7	5.5	5.1	5.9	5.6
H_1/H_2	4.7	4.6	3.4	5.1	4.5	1.8	1.7	1.3	1.6	1.6	1.2	1.5	1.2	1.3	1.3
$W_{½-1}/W_{½-2}$	1.2	1.2	1.5	1.3	1.3	2.0	2.4	3.2	2.5	2.5	4.5	4.9	5.1	4.7	4.8
t_{R1}/t_{R2}	1.0	1.2	1.2	1.1	1.1	1.8	1.8	2.8	2.1	2.1	4.4	5.1	5.3	4.4	4.8
LOD_1/LOD_2	0.21	0.22	0.29	0.20	0.23	0.56	0.59	0.77	0.63	0.64	0.83	0.67	0.83	0.77	0.78
AF_1/AF_2[b]	1.1	1.1	1.2	1.2	1.1	1.1	1.1	1.2	1.1	1.1	1.2	1.3	1.5	1.3	1.3

[a] *A*, peak area; *H*, peak height; $W_{1/2}$, full width at half maximum; *AF*, asymmetry factor; T_1 = 55°C, T_2 = 80°C; flow rate = 1.2 mL/min. Injected masses were between 20 and 30 ng.
[b] *AF* is the ratio of the 2nd half of the peak width to the 1st half of the peak width at10% of H.[45]

Table 2-2. Ratios of peak parameters and LODs as a function of flow rate (1.1:3.7 mL/min) with the CR array installed as the detector downstream from the μF and μcolumn at 70°C.

Parameter[a]	DMNB					2,6-DNT					2,4-DNT				
	C8	DPA	OPH	HME	Avg.	C8	DPA	OPH	HME	Avg.	C8	DPA	OPH	HME	Avg.
A_1/A_2	3.3	2.8	2.5	2.5	2.8	2.6	2.1	1.8	1.7	2.1	1.8	1.4	1.1	1.1	1.4
H_1/H_2	2.7	2.6	1.9	1.7	2.2	0.84	0.95	0.66	0.69	0.79	0.53	0.56	0.37	0.44	0.48
$W_{1/2\text{-}1}/W_{1/2\text{-}2}$	1.2	1.1	1.2	1.3	1.2	3.5	2.8	3.0	2.8	3.0	3.9	3.2	3.3	2.7	3.3
t_{R1}/t_{R2}	1.7	1.7	1.7	1.7	1.7	1.7	1.6	1.7	1.7	1.7	1.9	1.8	1.9	2.0	1.9
LOD_1/LOD_2	0.36	0.38	0.52	0.58	0.46	1.2	1.1	1.5	1.4	1.3	1.9	1.8	2.7	2.3	2.2
AF_1/AF_2	1.1	1.1	1.2	1.1	1.1	1.3	1.2	1.4	1.2	1.3	1.2	1.2	1.4	1.2	1.3

[a] Flow rate$_1$ = 1.1 mL/min; Flow rate$_2$ = 3.7 mL/min.

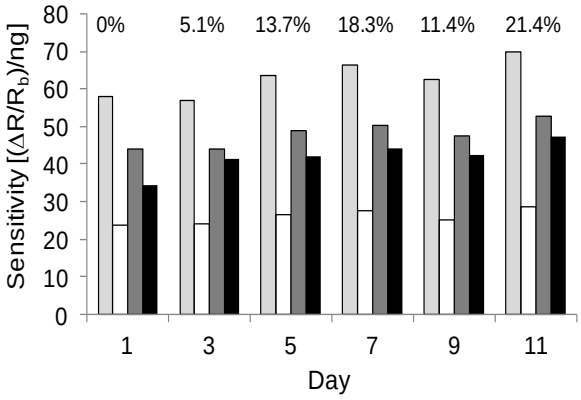

Figure 2-1. Response patterns for toluene derived from peak-height sensitivities at 70°C over time. Absolute sensitivities are shown and the fractional drift in average sensitivity, relative to Day 1, is presented above each pattern; pair-wise correlation coefficients of the normalized response patterns between any two days were ≥ 0.97. Sensors, in order from left to right, are C8 (light grey), DPA (white), OPH (dark grey), and HME (black).

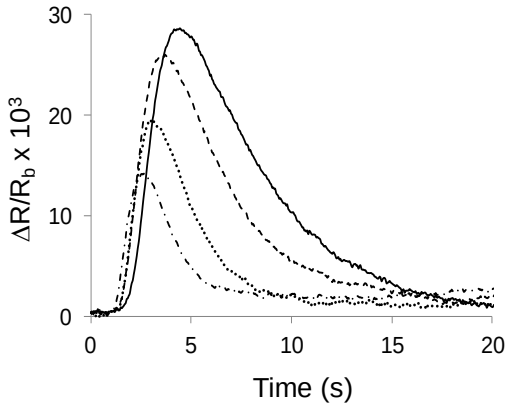

Figure 2-2. Representative responses from an OPH sensor at different temperatures to injections of 2,4-DNT (solid line, 50°C; dashed line, 60°C; dotted line, 70°C; dotted-dashed line, 80°C) at 3 mL/min. Note: peaks were re-aligned to facilitate comparisons.

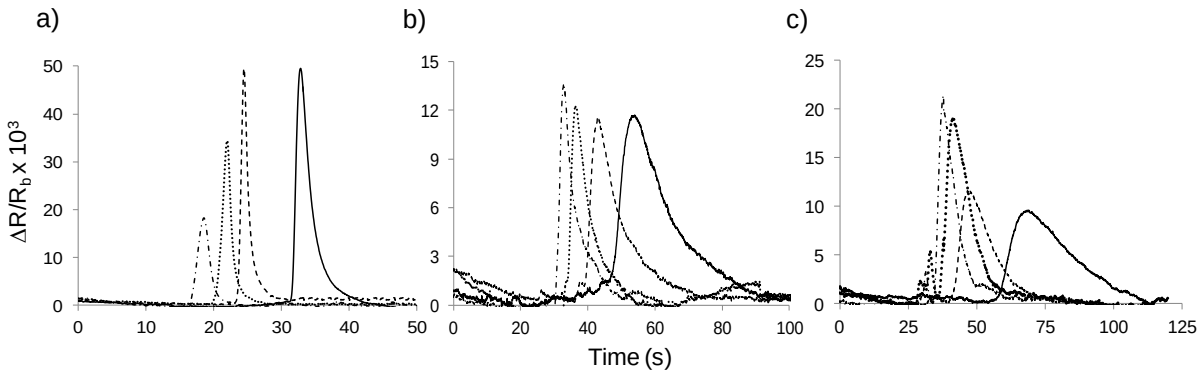

Figure 2-3. Representative responses from a DPA sensor to a) DMNB (25 ng); b) 2,6-DNT (2.5ng); and c) 2,4-DNT (2.5 ng) at 70°C as a function of flow rate: solid line, 1.1 mL/min; dashed line, 2.0 mL/min; dotted line, 3.0 mL/min; dotted-dashed line, 3.7 mL/min.

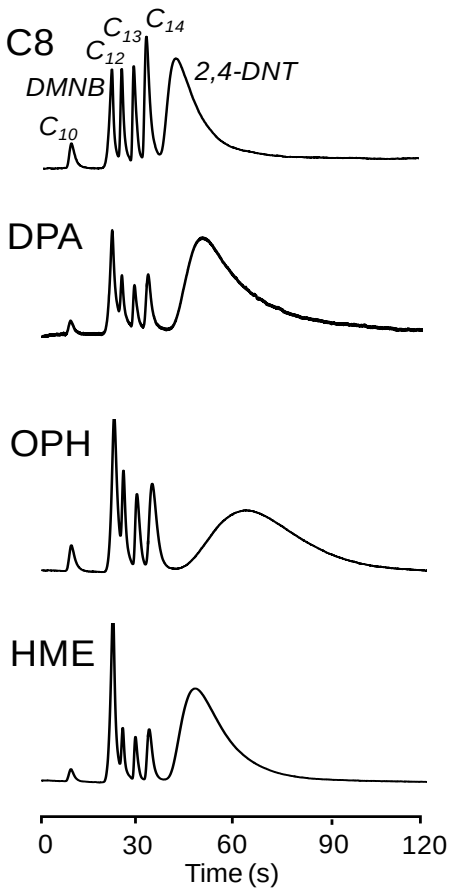

Figure 2-4. Chromatograms obtained with the μF, μcolumn, and sensor array; flow rate: 3.0 mL/min; oven temperature: 70°C; μfocuser injection temperature: 225°C; μcolumn temperature program: 70°C (0-20 sec), 130°C (21-120 sec). The y-axis for the DPA trace has been expanded to improve visibility.

CHAPTER III

VAPOR DISCRIMINTATION WITH SINGLE- AND MULTI-TRANSDUCER ARRAYS OF NANOPARTICLE-COATED CHEMIRESISTORS AND RESONATORS

PUBLISHED IN *IEEE Sensors*, 2013, *13(6)*, 2146.

3.1 Introduction

Microsensor arrays for the quantitative analysis of airborne volatile organic compounds (VOC) typically comprise a small set of transducers coated with interface layers that interact reversibly and differentially with a wide range of VOCs. Examples include arrays of polymer-coated surface acoustic wave resonators,[1, 2] cantilevers,[3-6] and capacitors,[7] as well as chemiresistors (CR) coated with metal-oxide semiconductors,[8] conducting polymers,[9] carbon-loaded insulating polymers,[10] or monolayer-protected nanoparticles (MPN).[11-14] By comparing the collective response patterns generated by the array to calibrated patterns in a reference library it is possible to differentiate one vapor from another.

Previous reports have shown that the recognition of individual vapors among a set of, say, 10 or more possibilities is often more facile than the discrimination of even a simple mixture from its components due to the low energies of reversible vapor-interface interactions involved and the inherent similarity of the patterns of a mixture and its components.[3, 15, 16] The discrimination of mixtures of more than three vapors from their components or lower-order mixtures is generally not possible with standalone arrays.[2, 15, 16] Furthermore, several reports

have shown that the capability of an optimally selected set of sensors to differentiate one vapor from another does not improve beyond ~4-6 sensors in the array, regardless of the transducer.[2, 10, 17-19] Combining sensors that operate on different transduction principles into hybrid, or multi-transducer (MT), arrays as a means of increasing the diversity of responses was first reported over 25 years ago[20, 21] and has been explored in a few subsequent studies.[18, 22-27] Although the performance of MT arrays can be superior to that of single-transducer (ST) arrays of similar dimension (i.e., number of sensors), only a few studies have explored this topic systematically.[18, 23, 26, 27]

Two popular transducers are the TSMR and the CR. TSMRs, also known as quartz crystal microbalances, are bulk-wave mechanical oscillators. When coated with a sorptive interface layer and exposed to a vapor, mass uptake in the film due to vapor partitioning causes a measurable shift in resonant frequency.[28] Typical CRs are interdigital electrodes that measure changes in resistance (directly or indirectly) of a conductive or semiconductive interface film accompanying vapor sorption. Previous studies have explored the VOC responses of TSMRs and CRs coated with films of the same carbon-loaded insulating polymers and noted that the correlation varied with the VOC density.[29, 30] Han, *et al.*[31] and Yang *et al.*[32] compared responses from TSMRs and CRs with matching films of MPNs and found transducer-dependent differences in the sign and/or magnitude of responses. More recently, Steinecker *et al.* showed correlations between MPN-coated TSMR and CR responses that depended on the VOC density and dielectric constant,[33] suggesting that the pooled responses might provide more information than either alone. Subsequently, Bohrer *et al.* compared responses collected from four TSMRs and four ultra-small CRs with matching films of MPNs with four different thiolate moieties.[34] None of these studies examined CRs and TSMRs in MT arrays as a means for enhancing VOC

discrimination. Very recently, Li et al. reported that an 8-sensor MT array composed of TSMRs and CRs with the same four MPN coatings could discriminate among 15 individual vapors better, on average, than either 4-sensor ST array, as expected, but noted that some 4-sensor MT arrays did not perform as well as the 4-sensor ST arrays.[27]

In this article, we report on a study of the diversity of response patterns of MT and ST arrays of MPN-coated TSMR and CR sensors. Using the data set of vapor sensitivities reported by Bohrer *et al.*,[34] we derived response patterns from every possible array of 2-8 sensors that could be constructed from the set of four TSMR and four CR sensors for each of the five vapors tested. Monte Carlo simulations were used to iteratively generate synthetic responses with different levels of random error superimposed on the calibrated sensitivities, and then principal component regression analysis was used to estimate the rates of recognition (RR) achievable among the different possible arrays. The performance was evaluated as a function of the array dimension, transducer type, and the thiolate functionalities on the MPNs. Analyses of binary mixtures were performed similarly by assuming linear additivity of responses.

3.2 Data Set and Analytical Methods

3.2.1 Sensor Fabrication, Coating, and Vapor Exposures

Detailed descriptions of the devices, interface films, and exposure tests are provided in the original study[34] and are only summarized here. The dielectric constants and (liquid) densities of the five VOCs are as follows: 2.00 ε_o, 0.703 g/ml (n-octane); 2.40 ε_o, 0.865 g/ml (toluene), 20.10 ε_o, 0.804 g/ml (n-propanol), 18.50 ε_o, 0.805 g/ml (2-butanone); 39.40 ε_o, 1.13 g/ml (nitromethane), where ε_o is the permittivity of free space.

Each CR chip had a set of four closely spaced interdigital electrodes (IDE) with active

areas of 150 μm^2. All four CR devices on a given chip were coated simultaneously with a continuous film of the same MPN by drop casting from a suitable solvent. The average thickness of the multilayer films was ~240 nm on the basis of AFM images of a representative film.[34] Four such CR chips were coated; one with each of the MPNs listed below. The average sensitivity from the sensors coated with a given MPN was used as the basis for the data analyses performed here.

Each of the four TSMRs consisted of a circular quartz crystal 1.4-cm diameter with 0.8-cm diameter gold electrode and a resonant frequency of 10 MHz. TSMR devices were coated by airbrushing a solution of MPNs with pressurized air as the propellant. Film masses of 24–28 μg were derived from the frequency shifts via the Sauerbrey equation, and gave average thicknesses of 116-136 nm, presumed to be in the acoustically thin regime.[35] MPNs with thiolate monolayers derived from n-octanethiol (C8), 4-(phenylethynyl)-benzenethiol (DPA), 6-phenoxyhexane-1-thiol (OPH), and methyl-6-mercaptohexanoate (HME) and ranging in Au core diameters from 3.4-4.7 nm were used.

CRs were mounted on custom PC boards and biased with the DC voltage from a battery (V=1.59 V) and connected in series with a reference resistor (R_{ref} = 3.0 MΩ). The voltage drop was measured by a multiplexer card (model 34970A/34902A, Agilent Technologies, Santa Clara, CA) and subsequently converted to resistance. All four CR array chips were installed in sockets on the floor of a 0.5-L stainless steel exposure chamber. TSMRs were mounted between Viton O-rings in a custom-made holder threaded into the lid of the chamber, and frequency was monitored by a phase-lock oscillator (Maxtek, Beaverton, OR).

3.2.2 Data Analysis

The performance of every possible MT and ST array of 2-8 sensors permutable from the four MPN-CRs and four MPN-TSMRs was assessed by use of Monte Carlo simulations and extended disjoint principal component regression (EDPCR) classification models. Synthetic responses were generated by randomly selecting a vapor concentration within the range of 5-15×LOD (where the LOD was dictated by the least sensitive sensor in the array) and then multiplying by the experimental sensitivity (i.e., slope of the calibration curve). Error was introduced by multiplying that response value by a factor derived from randomly sampling a Gaussian distribution with a mean of one and a standard deviation of 0.05, 0.075, or 0.10, corresponding to random sensitivity errors, ε, of 5, 7.5, or 10% of the response, respectively. This range of fractional sensitivity errors is consistent with experimental observations for the sensors used in this data set[34] and in others we have studied.[2, 13, 16]

The error enhanced responses from all sensors in the array under consideration were combined and the location of the resulting response vector was projected sequentially onto the principal component corresponding to the original calibrations for each vapor via EDPCR. The identity of the vapor assigned to this synthetic response (test) vector was that for which the Euclidean distance between test and calibration vector was the shortest. This procedure was performed iteratively (i.e., 500 samples) to obtain a precise statistical estimate of recognition rate (RR; the fraction of correct assignments out of the total) for each array at each level of ε. Details of this methodology and its rationale as applied to sensor array evaluations can be found elsewhere.[2, 13, 15, 16]

Assessment of binary mixture recognition was performed similarly by assuming that the composite response to a binary mixture was equivalent to the sum of the responses of the two components at their respective concentrations.[36] Thus, sensor responses were computed for an

independent, randomly selected concentration of each vapor alone (within the range of 5-15×LOD, as defined above) and then combined. Using EDPCR, the composite response vector was assigned to the mixture or to one of the component vapors (i.e., each binary mixture was considered separately). Iteration, again, yielded a precise statistical estimate of the RR for the mixture. All 10 possible binary mixtures were considered in succession.

EDPCR modeling and Monte Carlo simulations were performed on a desktop computer using routines written in Visual Basic (version 7.0, Microsoft Corp.) and linked to spreadsheets in Excel (version 7.0, Microsoft Corp.). Principal components (PC) plots were generated using R statistical software (version 2.13.1, R Foundation).

3.3 Results and Discussion

3.3.1 Individual Vapor Recognition

For reference, the 10 vapor-wise 4-ST_{tsmr} and 4-ST_{cr} array response patterns, normalized to the highest-sensitivity sensor for a given vapor, are presented in Figure 3-1. As noted in the original article,[34] the DPA-coated TSMR sensor (DPA_{tsmr}) exhibits the highest of all TSMR sensitivities for all vapors, due to the higher fractional mass of organic material in the DPA film, while the DPA-coated CR sensor (DPA_{cr}) exhibits the lowest of all CR sensitivities for all vapors, due to the lower swelling efficiency of the rigid conjugated structure of the DPA moiety. Among the CRs, the OPH_{cr} has the highest sensitivity to all VOCs except OCT for which the $C8_{cr}$ is the most sensitive. The latter can be attributed to a combination of vapor affinity and the flexibility and swelling efficiency of the highly intercalated C8 chains on adjacent MPN cores.[34] Among the CRs the range of relative sensitivities between any two sensors is as high as 35-fold (typically < 15-fold), whereas among the TSMRs the range is about 5-fold or less.

Figure 3-2a plots the average RR value (ε = 5%) of all five individual vapors for the best performing 2-, 3-, and 4-ST and MT arrays. Among all possible 2-ST_{tsmr} and 2-ST_{cr} arrays, the average RR values for recognition of the individual vapors span from 46.4–97.1% for the former and from 65.6–88.1% for the latter. For the 2-MT arrays the range is 58.4–90.6 % (Table 3-1). This emphasizes the importance of being judicious in selecting sensors to include in an array.[15] Surprisingly, the best 2-ST_{tsmr} array ($C8_{tsmr}$+OPH_{tsmr}, RR = 97.1%) outperforms the best 2-ST_{cr} array ($C8_{cr}$+DPA_{cr}, RR = 88.1%) and the best MT array (HME_{cr}+DPA_{tsmr}, RR = 90.6%). The differences in average RR values reflect 'real' differences in expected performance, but are not statistically significant because the range of individual-vapor RR values is quite broad, as shown in Table 3-1. That an array of just two sensors effectively recognizes and discriminates among five vapors is consistent with results reported previously for arrays of polymer-coated SAW sensors and MPN-coated CRs.[2, 13, 15, 16] That a 2-ST_{tsmr} array affords a higher degree of diversity is surprising because of its dependence only on mass uptake; the dependence of the CRs on changes in volume and dielectric constant might have been expected to yield greater diversity, given the range of densities and dielectric constants among the test vapors.

Increasing the number of sensors in the array leads to a significant increase in the RR of the best-performing ST_{cr} arrays, but little or no change in RR for the best ST_{tsmr} arrays; the 4-ST_{tsmr} and 4-ST_{cr} arrays perform equally well (RR ≅ 97%). Although this level of performance is quite good, as shown, the best 3- and 4-MT arrays perform slightly better on average (RR = 99.7%). These results suggest that only two of the four TSMR sensors contribute a significant amount of uncorrelated (i.e., independent) information about the vapors to the ST_{tsmr} arrays, and that combining certain TSMR and CR transducers results in a modest increase in uncorrelated information relative to either ST array.

The plateau in the RR value for mid-range array dimensions is followed by a decline at higher dimensions (Figure 3-2b), which is a general feature of vapor sensor arrays;[2, 18, 19] additional sensors contribute little or no independent information about the vapors, despite having interface films of MPNs with different thiolate functionalities, while they contribute an increasing amount of dispersion to all response patterns. As expected, the average RR value decreases as the degree of superimposed variation in sensitivity increases for the optimal MT arrays of 2-8 sensors (Figure 3-2b). If a minimum threshold RR of 95% is adopted,[2] then no more than 7.5% random variation in sensitivity among the sensors is tolerable without a significant loss in average performance for this data set. Although maintaining this level of control in sensitivity drift is apparently achievable in practice,[37] this constraint on performance must be kept in mind.

The correlation matrix in Table 3-2 presents the pair-wise correlation coefficients, r, derived from the linear regressions of the sensitivities to all five test vapors of one sensor onto those of another. Among the TSMR sensor pairs, Table 3-2 shows that the $C8_{tsmr}$, DPA_{tsmr} and HME_{tsmr} responses are highly correlated (i.e., r = 0.99 in all cases) and the RR values for the corresponding 2-ST_{tsmr} arrays are low (i.e., < 65%). The other three pairs of TSMR sensors have r values $\leq$ 0.83 and the RR values for these 2-ST_{tsmr} arrays are higher. A similar analysis of the 2-CR and 2-MT arrays, however, reveals several instances where a low r value between a pair of sensors does not produce a high RR, such as for $C8_{cr}$+OPH_{cr} and $C8_{cr}$+HME_{cr}. This is due to OCT, for which the relative sensitivities of the sensors differ markedly from those for the other four vapors, while the relative sensitivities to the other vapors are more highly correlated.

The representative linear regressions shown in Figure 3-4 for the $C8_{cr}$+OPH_{cr} array reveal that the high correlation among the other four vapors is masked by the OCT data point when the

r value is derived from the entire set of vapor sensitivities. Although OCT is easily discriminated from the other vapors, none of the other vapors is easily discriminated from one another, and the average RR value is therefore quite low. Even a relatively high r value does not necessarily result in a low RR value: if the regression line does not pass near or through the origin, then the r value inflates the degree of correlation among the sensor responses to the different vapors. This highlights the shortcomings of using pair-wise correlation metrics to select sensors and/or interface materials. Interestingly, three of the four cross-transducer pairs with a common MPN coating give high r values and correspondingly low RR values. The HME coated pair is the exception, with a relatively low r value of 0.65 and a relatively high RR value of ~78%. Accordingly, the HME_{cr} and HME_{tsmr} sensors are included in the best-performing 4-MT array (see below).

Figure 3-3 shows principal component projections for each 4-ST array and the best-performing 4-MT array ($C8_{tsmr}$+OPH_{tsmr}+HME_{tsmr}+HME_{cr}). The central cluster corresponding to each vapor is the result of using synthetic responses with ε =1% and the corresponding elliptical boundary is the 95% confidence interval (CI_{95}) calculated from the synthetic responses generated with ε =5%. As shown, the CI_{95} boundaries for POH, TOL and NME overlap in the 4-ST_{cr} plot and those for POH and TOL overlap in the 4-ST_{tsmr} plot. There is only a slight overlap for the NME+MEK and TOL+POH pairs in the 4-MT plot. Consistent with this, confusion matrices derived from EDPCR analyses indicate that TOL and POH are confused for each other at rates of 3-7% for the 4-ST_{cr} and 4-ST_{tsmr} arrays and only 0.8% for the 4-MT array. For all arrays, OCT is well separated and easily discriminated from all other vapors.

Table 3-1 presents the compositions of the best-performing 2-, 3-, and 4-ST and MT arrays along with the average and range of RRs for individual-vapor recognition. As the array

dimension increases, the number of MT arrays providing acceptable performance increases: there are 11 3-MT arrays and 18 4-MT arrays with average RR values ≥ 95%. Among these there are six 3-MT arrays that outperform the best 3-ST array and 13 4-MT arrays that outperform the best 4-ST array. Table 3-1 also shows the arrays of each dimension that provide the lowest RR values; the worst-performing 2-, 3-, and 4-MT arrays give RR values much lower than those of the best-performing ST arrays of the same dimension, demonstrating, again, the importance of careful sensor selection. Notably, C8, OPH, and HME all appear in the best-performing 3- and 4-sensor arrays, regardless of transducer type, indicating that the extent of vapor-interface interaction is perhaps a more important determinant of array diversity than is the transducer.

3.3.2 Binary Mixture Analyses

With 2- and 3-sensor arrays, the only binary mixtures that could be discriminated from their components with RR values >95% are those containing OCT. Among these arrays, the best 2-ST_{cr} array performs slightly better than the best 2-MT array, but the best 3-ST_{cr} array and the best 3-MT array perform equally well. The 2- and 3-ST_{tsmr} arrays do not perform as well. None of the 2- or 3-sensor arrays could discriminate any of the other six binary mixtures from their components with RR values > 90%.

With arrays of 4 sensors, the performance generally follows what would be expected on the basis of the cluster separation distances in the PCA plots of Figure 3-3. For the 4-ST_{cr} array, mixtures containing OCT are easily discriminated from their components, whereas mixtures of other vapors give much lower RR values (Table 3-3). For the 4-ST_{tsmr} arrays only one mixture could be analyzed effectively (i.e., NME+OCT, RR = 96.4%), consistent with these two vapors having the greatest separation in Figure 3-3b. In general, the RR values for the mixtures depend

strongly on their separation distances in Figs. 3-3a-c, as expected.

Two approaches were taken to further assess the performance of the 4-MT arrays. First, the two 4-MT arrays yielding the highest average RR values on the basis of individual-vapor recognition were considered. These also give the highest average RR values among all 10 binary mixture analyses: 74.7% for both arrays. This value exceeds the average RR values for the 4-ST_{cr} and 4-ST_{tsmr} arrays by a small margin (71.3 and 69.7%, respectively). However, neither top MT array provides an RR >95% for any specific mixture.

In the second approach to MT array assessment, the 4-MT array giving the highest mixture-specific RR value was selected successively for each of the 10 mixtures. In those cases where the array composition differed from the two selected on the basis of the highest overall average RR, the array is listed in Table 3-3. As shown, there are eight different 4-MT arrays required to achieve the highest possible RR values for all mixtures, and each of the eight possible sensors is represented at least once among these 4-MT arrays. In all cases, the highest RR value for a specific mixture is always provided by a 4-MT array, but the best performance for one or two specific mixtures by one 4-MT array is invariably coupled with significantly poorer performance than a different 4-MT array for several of the other mixtures. Furthermore, none of the 4-MT arrays consistently outperforms either 4-ST array for all mixtures.

This prompted the question of whether a single MT array of higher dimension might provide better overall performance. To answer this, again two approaches were taken. First, the best 5-, 6-, 7-, and 8-MT arrays were identified on the basis of overall average performance. The average RR values for these arrays range from 71.6 to 68.6 %, which are lower than the RR values for the best performing 4-MT arrays (overall average) shown in Table 3-3. Second, starting with the best 4-MT array for each mixture in Table 3-3, the best-performing MT arrays

of higher dimension were identified for that specific mixture. Figure 3-5 shows some representative data.

For mixtures containing OCT, performance peaks at n = 4 or 5 sensors and stays constant or declines very slightly out to n = 8, as shown for the TOL+OCT case. For mixtures with components separated by a somewhat shorter Euclidean distance than those between OCT and the other components (on the basis of Figure 3-3c), the performance declines gradually but steadily as each additional sensor is added to the optimal MT array, as shown in Figure 3-5 for TOL+MEK. Where the Euclidean distance between mixture components is quite short (Figure 3-3c), there is a dramatic decrease in RR value as the array dimension increases to n = 8, as shown in Figure 3-5 for POH+NME. These trends re-affirm that adding highly correlated sensors to an array merely increases the dispersion of the patterns used for discrimination, and show further that performance degrades more rapidly for mixtures of components with more similar patterns.

These results suggest the possibility of deploying an array of all eight sensors and then down-selecting the subset of sensors providing the best performance for a given analysis as needed. Since the problems posed in the binary analyses assumed that the range of possible analytes was limited to the mixture or either of its two components, it is feasible to exercise such an option. If the components of the mixture were not known and constrained in this way, however, this option would not be feasible. Such constraints would apply when using an MT array as the detector for (micro) gas chromatographic (GC) analysis,[37, 38] where the identities of co-eluting or partially co-eluting analytes could be determined *apriori* by calibration. In this case, post-measurement down-selection of a different optimal subset of sensors for each set of overlapping peaks eluting in specific retention time windows would be possible.

Note that the average RR of the optimal mixture-specific 4-MT arrays that could be down-selected is 86.9%, with only four mixtures giving RR values > 95%. Thus, although this average RR exceeds that for the 4-MT array selected on the basis of overall average RR value (74.7%), such performance is still not acceptable. Taking advantage of partial chromatographic resolution by use of multivariate curve resolutions methods should enhance the discrimination, though for co-eluting vapors with similar patterns the chromatographic resolution may need to be fairly high.[39]

3.4 Conclusions

Distinct differences were observed in the vapor discrimination capabilities of ST arrays of low dimension (i.e., $n \leq 4$) assembled from the MPN-coated CR and TSMR vapor sensors considered here, consistent with the results reported by Li, et al.[27] Although the best MT arrays generally outperformed the best ST arrays, differences were often marginal and exceptions occurred. The specific sensors included in the MT array were critical, and both the interface material and transducer were important factors. Correlation analysis was of limited use in assessing the extent to which two sensors complement each other in effecting the discrimination of multiple vapors. PCA and comparisons of Euclidean distances were much better tools for predicting recognition rates, particularly for binary mixtures.

The relatively facile problem of discriminating among a set of individual vapors could be solved adequately with both types of 4-ST arrays and with numerous 4-MT arrays. Importantly, performance was not improved by adding more sensors to the MT array. This finding is consistent with those from other studies of this topic with vapor sensor arrays employing sorptive interfaces, and argues strongly for moving the research agenda beyond such problems to the

more challenging problems of quantitatively analyzing mixtures of vapors.[2, 16, 18]

No single array of any type provided universally optimal performance for the 10 binary mixtures considered here, despite each mixture being tested separately and the problem being constrained to a determination of whether one or both components was present. Furthermore, six of the mixtures could not be determined with sufficiently high RR values to be effective with any array. Increasing the number of sensors in the array from four to eight invariably led to a decline in performance, which was often dramatic, and serves as yet another reminder to limit the number of sensors used for a given analysis.[16, 18, 26]

This study lends support to arguments that the only feasible way to take advantage of the vapor recognition capabilities of ST or MT arrays in performing quantitative analyses of vapor mixtures is to couple them with an upstream chromatographic separation module.[2, 16, 18, 26, 36-39] Although the 4-MT array providing the highest average RR value among the individual vapors also provided the highest average RR value for the 10 binary mixtures, if each mixture was considered separately, then the best-performing 4-MT array differed in all but one case. Using a large MT array as a GC detector and down-selecting subsets of sensors to analyze different overlapping peaks in specific retention-time windows, as proposed here, shows promise and could be pre-programmed into the chemometric software routines used in such (micro)systems.

3.5 References

1. Grate, J. W. "Acoustic wave microsensor arrays for vapor sensing," *Chem. Rev.*, **2000**, *100*, 2627-2648.
2. Park, J.; Groves, W. A.; Zellers, E. T. "Vapor recognition with small arrays of polymer-coated microsensors. A Comprehensive Analysis," *Anal. Chem.*, 1999, *71*, 3877-3886.
3. Senesac, L. R.; Dutta, P.; Datskos, P. G.; Sepaniak, M. J. "Analyte species and concentration identification using differentially functionalized microcantilever arrays and artificial neural networks," *Analyt. Chim. Acta*, **2006**, *558*, 94-101.

4. Pinnaduwage, L. A.; Hedden, D. L.; Gehl, A.; Boiadjev, V. I.; Hawk, J. E.; Farahi, R. H.; Thundat, T.; Houser, E. J.; Stepnowski, S.; McGill, R. A.; Deel, L.; Lareau, R. T. "A sensitive, handheld vapor sensor based on microcantilevers," *Rev. Sci. Instrum.*, **2004**, *7(5)*, 4554-4557.
5. Chapman, P. J.; Vogt, F.; Dutta, P.; Datskos, P. G.; Devault, G. L.; Sepaniak, M. J. "Facile hyphenation of gas chromatography and a microcantilever array sensor for enhanced selectivity," *Anal. Chem.*, **2007**, *79(1)*, 364-370.
6. Li, M.; Myers, E.; Tang, H. X.; Aldridge, S. J.; McCaig, H. C.; Whiting, J. J.; Simonson, R. J.; Lewis, N. S.; Roukes, M. L. "Nanoelectromechanical resonator arrays for ultrafast, gas-phase chromatographic chemical analysis," *Nano Lett.*, **2010**, *10*, 3899-3903.
7. Patel, S. V.; Mlsna, E. T.; Fruhberger, B.; Klaassen, E.; Cemalovic, S.; Baselt, D. R. "Chemicapacitive microsensors for volatile organic compound detection," *Sens. Act. B*, **2003**, *96*, 541-553.
8. Rock, F.; Barsan, N.; Weimar, U. "Electronic nose: current status and future trends," *Chem. Reviews*, **2008**, *108*, 705-725.
9. Hatfield, J. V.; Neaves, P.; Hicks, P. J.; Persaud, K.; Travers, P. "Towards an integrated electronic nose using conducting polymer sensors," *Sens. Actuators B: Chem.*, **1994**, *18*, 221-228.
10. Doleman, B. J.; Lonergan, M. C.; Severin, E. J.; Vaid, T. P.; Lewis, N. S. "Quantitative study of the resolving power of arrays of carbon black-polymer composites in various vapor-sensing tasks," *Anal. Chem.*, **1998**, *70*, 4177-4190.
11. Han, L.; Shi, X.; Wu, W.; Kirk, F. L.; Luo, J.; Wang, L.; Mott, D.; Cousineau, L.; Lim, S. I-I.; Lu, S.; Zhong, C-J. "Nanoparticle-structured sensing array materials and pattern recognition for VOC detection," *Sens. Actuators B: Chem.*, **2005**, *106*, 431-441.
12. Joseph, Y.; Peic, A.; Chen, X.; Michl, J.; Vossmeyer, T.; Yasuda, A. "Vapor sensitivity of networked gold nanoparticle chemiresistors: importance of flexibility and resistivity of the interlinkage," *J. Phys. Chem. C*, **2007**, *111*, 12855-12859.
13. Zhong, Q.; Steinecker, W. H.; Zellers, E. T. "Characterization of a high-performance portable GC with a chemiresistor array detector," *Analyst*, **2008**, *134*, 283-293.
14. Dovgolevsky, E.; Tisch, U.; Haick, H. "Chemically sensitive resistors based on monolayer-capped cubic nanoparticles: towards configurable nanoporous sensors," *Small*, **2009**, *5*, 1158-1161.
15. Zellers, E. T.; Batterman, S. T.; Han, M.; Patrash, S. J. "Optimal coating selection for the analysis of organic vapor mixtures with polymer-coated surface acoustic wave sensor arrays," *Anal. Chem.*, **1995**, *67*, 1092-1106.
16. Hsieh, M-D.; Zellers, E. T. "Limits of recognition for simple vapor mixtures determined with a microsensor array," *Anal. Chem.*, **2004**, *76*, 1885-1895.
17. Ricco, A. J.; Crooks, R. M.; Osbourn, G. C. "Surface acoustic wave chemical sensor arrays: new chemically sensitive interfaces combined with novel cluster analysis to detect volatile organic compounds and mixtures," *Acc. Chem. Res.*, **1998**, *31*, 289-296.
18. Jin, C.; Kurzawski, P.; Hierlemann, A.; Zellers, E. T. "Evaluation of multitransducer arrays for the determination of organic vapor mixtures," *Anal. Chem.*, **2008**, *80*, 227-236.
19. Garcia-Berrios, E.; Gao, T.; Theriot, J.; Woodka, M. D.; Brunschwig, B. S.; Lewis, N. S. "Response and discrimination performance of arrays of organothiol-capped Au nanoparticle chemiresistive vapor sensors," *J. Phys. Chem. C*, **2011**, *115*, 6208-6217.

20. Snow, A. W.; Barger, W. R.; Klusty, M.; Wohltjen, H.; Jarvis, N. L. "Simultaneous electrical conductivity and piezoelectric mass measurements on iodine-doped phthalocyanine Langmuir-Blodgett films," *Langmuir*, **1986**, *2*, 513-519.
21. Bott, B.; Jones, T. A. "The use of multisensor systems in monitoring hazardous atmospheres," *Sens. Act.*, **1986**, *9*, 19-25.
22. Schierbaum, K. D.; Gerlack, A.; Haug, M.; Göpel, W. "Selective detection of organic molecules with polymers and supramolecular compounds: application of capacitance, quartz microbalance, and calorimetric transducers," *Sens. Actuators A*, **1992**, *31*, 130-137.
23. Pardo, M.; Kwong, L. G.; Sberveglieri, G.; Brubaker, K.; Schneider, J. F.; Penrose, W. R.; Stetter, J. R. "Data analysis for a hybrid sensor array," *Sens. Actuators B: Chem.*, **2005**, *106*, 136-143.
24. Holmberg, M.; Winquist, F.; Lundstrom, I.; Gardner, J. W.; Hines, E. L."Identification of paper quality using a hybrid electronic nose," *Sens. Actuators B: Chem.*, **1995**, *26-27*, 246-249.
25. Ulmer, H.; Mitrovics, J.; Weimar, U.; Göpel, W. "Sensor arrays with only one or several transducer principles? The advantage of hybrid modular systems," *Sens. Actuators B: Chem.*, **2000**, *65*, 79-81.
26. Jin, C.; Zellers, E. T. "Limits of recognition for binary and ternary vapor mixtures determined with multitransducer arrays," *Anal. Chem.*, **2008**, *80*, 7283-7293.
27. Li, C-L.; Chen, Y.; Liu, M-H.; Lu, C-J. "Utilizing diversified properties of monolayer protected gold nanoclusters to construct a hybrid sensor array for organic vapor detection," *Sens. Actuators B: Chem.*, **2012**, *169*, 349-359.
28. Janghorbani, M.; Freund, H. "Application of a piezoelectric quartz crystal as a partition detector," *Anal. Chem.*, **1973**, *45*, 325-332.
29. Severin, E.; Lewis, N. S. "Relationships among resonant frequency changes on a coated quartz crystal microbalance, thickness changes, and resistance responses of polymer-carbon black composite chemiresistors," *Anal. Chem.*, **2000**, *72*, 2008-2015.
30. Mills, C.; Beeley, J.; Wyse, C.; Cumming, D.; Glidle, A.; Cooper, J. "Polymer-based micro-sensor paired arrays for the determination of primary alcohol vapors," *Sens. Actuators B: Chem.*, **2007**, *125*, 85-91.
31. Han, L.; Daniel, D. R.; Maye, M. M.; Zhong, C-J. "Core-shell nanostructured nanoparticle films as chemically sensitive interfaces," *Anal. Chem.*, **2001**, *73*, 4441-4449.
32. Yang, C-Y.; Li, C-L.; Lu, C-J. "A vapor selectivity study of microsensor arrays employing various functionalized ligand protected gold nanoparticles," *Analyt. Chim. Acta*, **2006**, *565*, 17-26.
33. Steinecker, W. H.; Rowe, M. P.; Zellers, E. T. "Model of vapor-induced resistivity changes in gold-thiolate monolayer-protected nanoparticle sensor films," *Anal. Chem.*, **2007**, *79*, 4977-4986.
34. Bohrer, F. I.; Covington, E.; Kurdak, Ç.; Zellers, E. T. "Characterization of dense arrays of chemiresistor vapor sensors with submicrometer features and patterned nanoparticle interface layers," *Anal. Chem.*, **2011**, *83*, 3687-3695.
35. Grate, J. W.; Nelson, D. A.; Skaggs, R. "Sorptive behavior of monolayer-protected gold nanoparticle films: implications for chemical vapor sensing," *Anal. Chem.*, **2003**, *75*, 1868-1879.
36. Cai, Q. Y.; Zellers, E. T. Dual-chemiresistor GC detector employing monolayer-encapsulated metal nanocluster interfaces," *Anal. Chem.*, **2002**, *74*, 3533-3539.

37. Kim, S. K.; Chang, H.; Zellers, E. T. "Microfabricated gas chromatograph for the selective determination of trichloroethylene vapor at sub-parts-per-billion concentrations in complex mixtures," *Anal. Chem.*, **2011**, *83*, 7198-7206.
38. Lu, C-J.; Steinecker, W. H.; Tian, W-C.; Oborny, M. C.; Nichols, J. M.; Agah, M.; Potkay, J. A.; Chan, H. K. L.; Driscoll, J.; Sacks, R. D.; Wise, K. D.; Pang, S. W.; Zellers, E. T. "First-generation hybrid MEMS gas chromatograph," *Lab Chip*, **2005**, *5*, 1123-1131.
39. Jin, C.; Zellers, E. T. "Chemometric analysis of gas chromatographic peaks measured with a microsensor array: methodology and performance assessment," *Sens. Actuators B: Chem.*, **2009**, *139*, 548-556.

Table 3-1. Average and range of recognition rates (RR) among the 5 individual vapors for the best- and worst-performing arrays consisting of 2, 3, and 4 sensors (ε = 5%).

Array Dimension and Type	Composition	RR (%) Avg.	Range
n = 2 sensors			
Best-performing			
ST_{cr}	$C8_{cr}$ + DPA_{cr}	88.1	77.9–98.2
ST_{cr}	OPH + HME_{cr}	79.7	62.1–97.3
ST_{cr}	DPA_{cr} + OPH_{cr}	79.6	60.4–98.8
ST_{tsmr}	$C8_{tsmr}$ + OPH_{tsmr}	97.1	93.7–100.0
ST_{tsmr}	DPA_{tsmr} + OPH_{tsmr}	84.7	70.8–98.6
ST_{tsmr}	OPH_{tsmr} + HME_{tsmr}	70.7	55.6–85.9
MT	HME_{cr} + DPA_{tsmr}	90.6	83.5–97.7
MT	$C8_{cr}$ + OPH_{tsmr}	82.5	68.6–96.4
MT	OPH_{cr} + HME_{tsmr}	80.4	68.2–92.5
Worst-performing			
ST_{cr}	$C8_{cr}$ + HME_{cr}	65.6	37.5–93.6
ST_{tsmr}	DPA_{tsmr} + HME_{tsmr}	46.4	31.7–61.2
MT	OPH_{cr} + DPA_{tsmr}	58.4	37.0–79.8
3 sensors			
Best-performing			
ST_{cr}	HME_{cr} + $C8_{cr}$ + OPH_{cr}	94.6	90.0–99.2
ST_{cr}	DPA_{cr} + OPH_{cr} + HME_{cr}	92.5	86.7–98.3
ST_{cr}	$C8_{cr}$ + DPA_{cr} + HME_{cr}	86.3	75.5–97.0
ST_{tsmr}	HME_{tsmr} + $C8_{tsmr}$ + OPH_{tsmr}	97.7	94.8–100.0
ST_{tsmr}	$C8_{tsmr}$ + DPA_{tsmr} + OPH_{tsmr}	97.0	93.8–100.0
ST_{tsmr}	DPA_{tsmr} + OPH_{tsmr} + HME_{tsmr}	86.7	73.5–100.0
MT	HME_{cr} + $C8_{tsmr}$ + OPH_{tsmr}	99.7	99.3–100.0
MT	DPA_{cr} + $C8_{tsmr}$ + OPH_{tsmr}	99.2	98.3–100.0
MT	DPA_{cr} + OPH_{tsmr} + HME_{tsmr}	99.0	97.9–100.0
Worst-performing			
ST_{cr}	$C8_{cr}$ + DPA_{cr} + OPH_{cr}	85.6	72.5–98.8
ST_{tsmr}	$C8_{tsmr}$ + DPA_{tsmr} + HME_{tsmr}	83.2	71.9–94.4
MT	C8 + HME_{cr} + HME_{tsmr}	69.2	43.4–95.0
4 sensors			
Best-performing			
ST_{cr}	DPA_{cr} + HME_{cr} + $C8_{cr}$ + OPH_{cr}	96.7	93.9–99.5
ST_{tsmr}	DPA_{tsmr} + HME_{tsmr} + $C8_{tsmr}$ + OPH_{tsmr}	96.5	92.3–100.0
MT	HME_{cr} + HME_{tsmr} + $C8_{tsmr}$ + OPH_{tsmr}	99.7	99.4–99.9
MT	DPA_{cr} + HME_{tsmr} + $C8_{tsmr}$ + OPH_{tsmr}	99.1	98.2–100.0
MT	DPA_{cr} + HME_{cr} + DPA_{tsmr} + OPH_{tsmr}	98.6	96.9–100.0
Worst-performing			
MT	$C8_{cr}$ + HME_{cr} + $C8_{tsmr}$ + HME_{tsmr}	70.0	45.3–94.8

Table 3-2. Matrix of pair-wise correlation coefficients, r, derived from the linear regression of sensitivities between each pair of sensors, and the average RR values (%, in parentheses) of the corresponding 2-sensor arrays derived from Monte Carlo/EDPCR analyses (ε =5%) for the five individual test vapors.

	$C8_{cr}$	DPA_{cr}	OPH_{cr}	HME_{cr}	$C8_{tsmr}$	DPA_{tsmr}	OPH_{tsmr}	HME_{tsmr}
$C8_{cr}$	1							
DPA_{cr}	0.59 (88.1)	1						
OPH_{cr}	0.22 (79.0)	0.87 (79.6)	1					
HME_{cr}	0.38 (65.6)	0.93 (67.6)	0.99 (79.7)	1				
$C8_{tsmr}$	0.94 (62.9)	0.83 (79.1)	0.53 (79.1)	0.65 (78.6)	1			
DPA_{tsmr}	0.90 (69.6)	0.87 (65.8)	0.62 (58.4)	0.74 (90.6)	0.99 (65.0)	1		
OPH_{tsmr}	0.53 (82.5)	0.89 (78.7)	0.91 (59.8)	0.95 (77.1)	0.76 (97.1)	0.83 (84.7)	1	
HME_{tsmr}	0.94 (69.6)	0.80 (70.7)	0.52 (80.4)	0.65 (77.8)	0.99 (63.3)	0.99 (46.4)	0.78 (70.7)	1

Table 3-3. Recognition rates (RR, %) of binary vapor mixtures for the 4-ST arrays, the two 4-MT arrays giving the highest overall average RR values, and the 4-MT arrays giving the highest mixture-specific RR values as determined by Monte Carlo/EDPCR analyses (ε =5%).

Array Composition				RR (%)										
				POH OCT	TOL OCT	MEK OCT	NME OCT	TOL NME	MEK NME	POH NME	TOL POH	MEK POH	MEK TOL	Average
4-ST arrays														
$C8_{cr}$	OPH_{cr}	DPA_{cr}	HME_{cr}	96.2	97.8	97.8	98	36.8	47.8	31.8	31.8	68.4	72.8	71.3
$C8_{tsmr}$	OPH_{tsmr}	DPA_{tsmr}	HME_{tsmr}	67.8	78.8	90.0	96.4	72.4	52.0	77.6	27.8	66.6	47.6	69.7
Best 4-MT arrays: overall average														
$C8_{tsmr}$	OPH_{tsmr}	HME_{cr}	HME_{tsmr}	81.8	90.6	81.0	90.6	79.2	58.6	71.8	49.2	66.6	**78.0**	74.7
$C8_{tsmr}$	OPH_{tsmr}	DPA_{cr}	HME_{tsmr}	85.2	78.4	86.4	93.2	84.6	**84.0**	**89.8**	44.0	58.8	42.8	74.7
Best 4-MT arrays: mixture specific														
OPH_{tsmr}	DPA_{cr}	DPA_{tsmr}	HME_{cr}	81.2	77.4	50.0	70.6	83.0	78.2	75.0	**62.4**	41.6	75.2	69.5
$C8_{cr}$	$C8_{tsmr}$	OPH_{cr}	HME_{cr}	96.6	98.2	**98.4**	97.8	36.2	52.0	29.0	25.8	70.6	72.0	67.7
$C8_{cr}$	OPH_{cr}	HME_{cr}	DPA_{tsmr}	**97.4**	97.4	97.2	98.0	35.4	47.4	31.8	24.8	**71.6**	74.2	67.5
OPH_{tsmr}	DPA_{cr}	HME_{cr}	HME_{tsmr}	85.2	65.8	46.2	73.8	**89.6**	78.2	68.0	56.0	36.2	75.6	67.5
$C8_{cr}$	OPH_{cr}	HME_{cr}	HME_{tsmr}	96.0	**99.6**	98.2	97.4	37.2	53.0	24.2	24.2	69.6	71.6	67.1
$C8_{cr}$	$C8_{tsmr}$	OPH_{cr}	HME_{tsmr}	94.2	95.8	97.8	**98.4**	6.6	35.4	24.0	16.0	58.0	45.0	57.1

[a] Dashed boxes indicate the highest RR value for a given mixture among all 4-MT arrays.

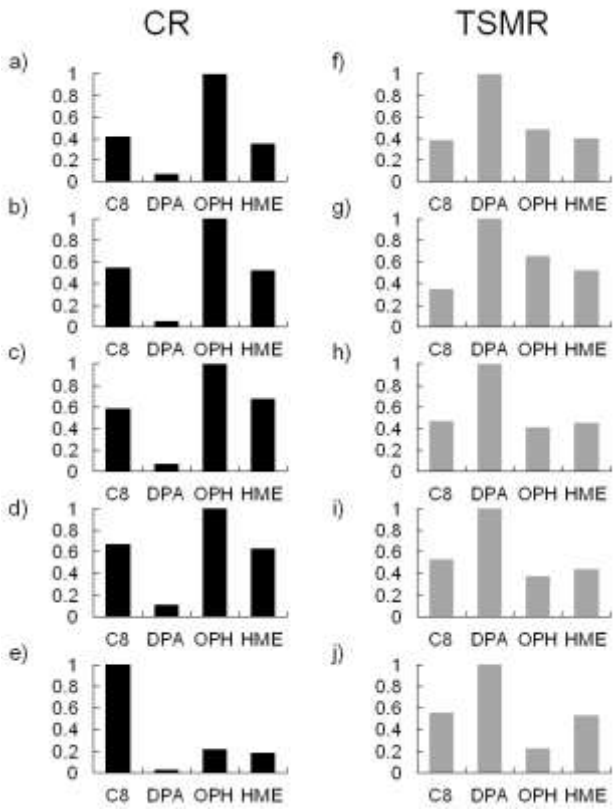

Figure 3-1. Normalized sensitivities from the 4-ST_{cr} (a-e) and 4-ST_{tsmr} (e-h) arrays for the five test vapors: a,f) 2-butanone; b,g) nitromethane; c,h) toluene; d,i) n-propanol; and e,j) n-octane. Sensitivities are normalized to the sensor giving rise to the largest response.

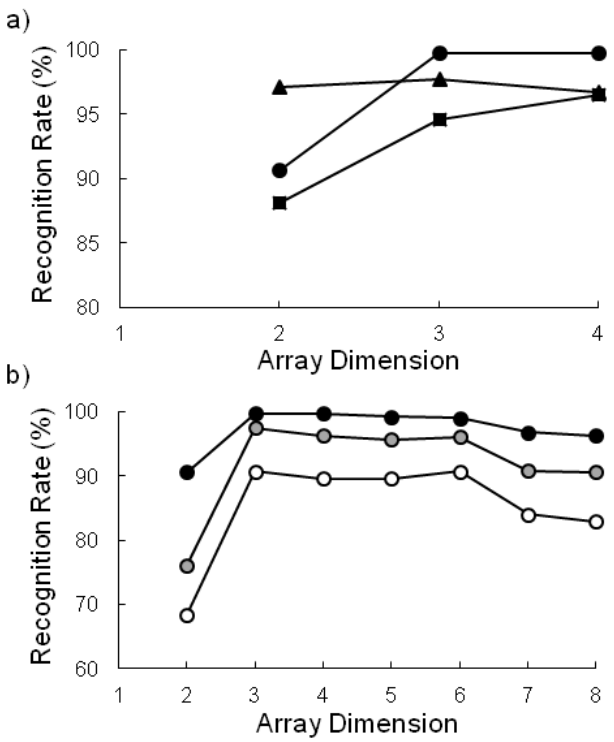

Figure 3-2. Recognition rates for individual-vapor discriminations from the best-performing arrays of each dimension: a) ST_{cr} arrays (filled squares), ST_{tsmr} arrays (filled triangles), and MT arrays (filled circles) (ε=5%); b) MT arrays for ε=5% (filled circles), 7.5% (shaded circles), and 10% (unfilled circles).

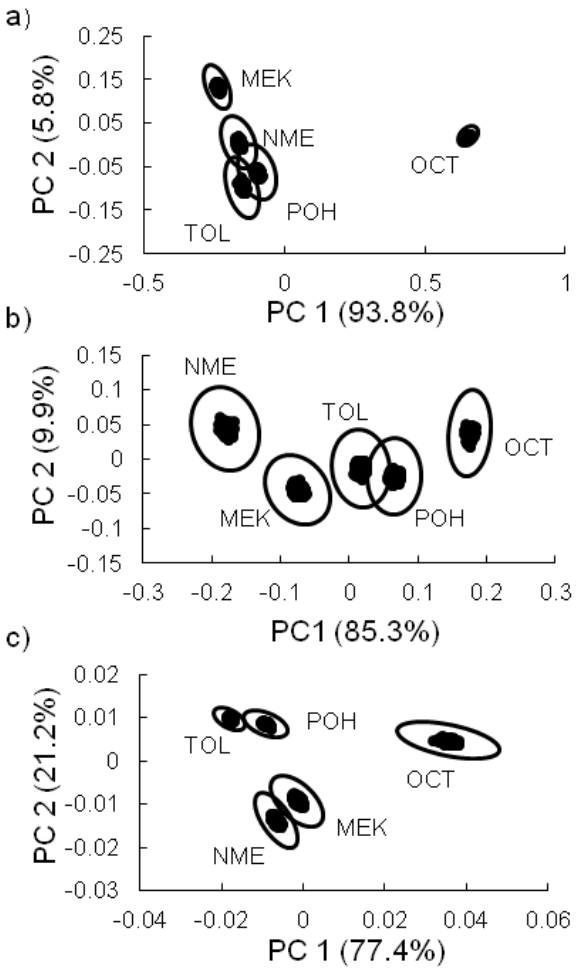

Figure 3-3. Principal components projections from the (a) 4-ST_{cr}, array (b) 4-ST_{tsmr} array, and (c) best-performing 4-MT array (i.e., $C8_{tsmr}$+OPH_{tsmr}+HME_{tsmr}+HME_{cr}), derived from responses to the five test vapors. Data points are Monte-Carlo generated synthetic responses with ε=1% and ellipses represent the boundary of the 95% confidence interval with ε=5%.

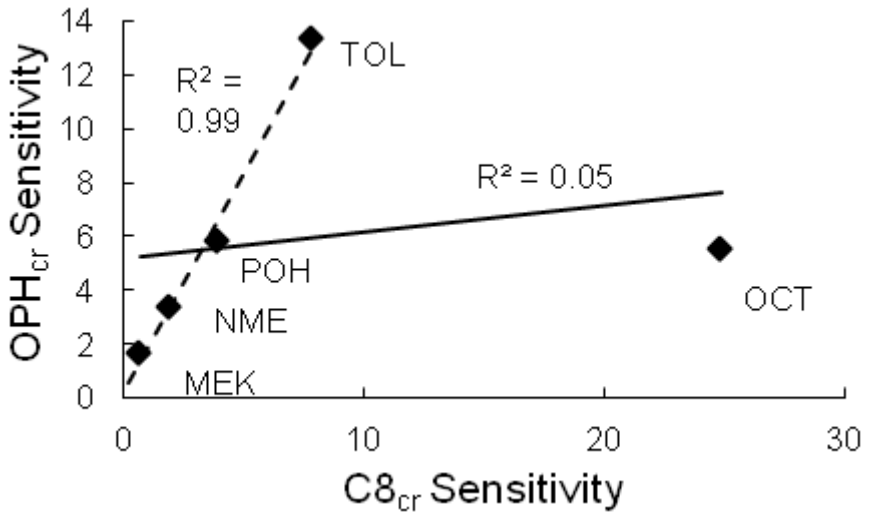

Figure 3-4. Plot of $C8_{cr}$ sensitivities vs. OPH_{cr} sensitivities ($\Delta R/R_b/mg \cdot m^{-3}$) for the five test vapors. Solid line shows the best-fit line from linear regression for all five vapors with corresponding R^2 value. Dashed line shows best-fit line from linear regression excluding the n-octane data point with corresponding R^2 value.

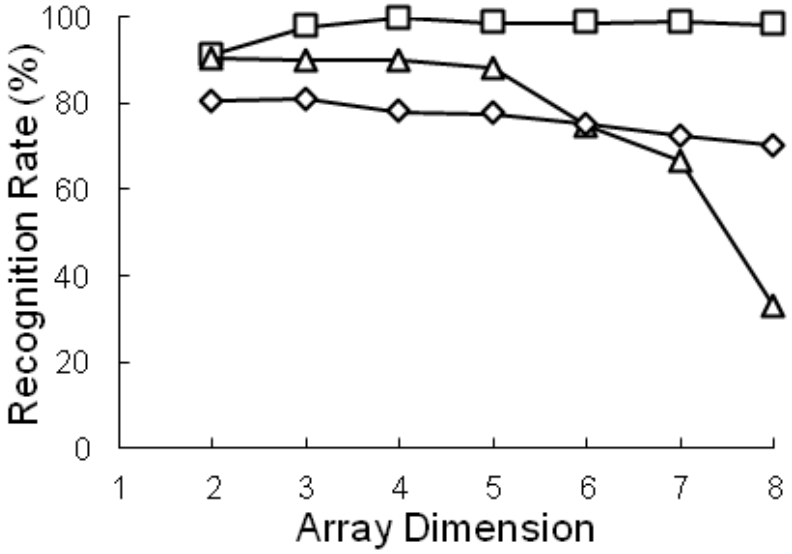

Figure 3-5. Recognition rates for a representative subset of three different binary vapor mixtures from the best-performing MT arrays of a given dimension (n = 2-8, ε=5%); TOL+OCT (unfilled squares); TOL+MEK (unfilled diamonds); NME+POH (unfilled triangles).

CHAPTER IV

VAPOR DISCRIMINATION WITH INDIVIDUAL PLASMONIC GOLD NANOPARTICLE FILMS

4.1 Introduction

The selectivity of (micro)sensor arrays employing interface films that interact with analyte vapors by reversible physisorption is inherently limited by the narrow range of energies spanned by such interactions.[1-3] Although the response patterns generated from an array can permit the discrimination of numerous vapors presented to that array individually, if more than two vapors are presented simultaneously, then the capability for quantitative analysis of the vapor mixture is greatly diminished. Thus, numerous types of single-transducer (ST) arrays are capable of recognizing and differentiating individual vapors and determining the components of many binary mixtures; but the quantitative analysis of ternary or higher mixtures is not usually possible, regardless of the number of sensors included in the array.[1-11] Combining sensors that operate on different transduction principles into hybrid or multi-transducer (MT) arrays has been explored in a limited number of studies as a means of enhancing diversity.[3, 12-17] MT arrays consisting of judiciously selected gravimetric, capacitive, and/or calorimetric sensors, for example, have been shown to outperform their single-transducer (ST) analogues, affording accurate determinations of the components of most binary mixtures and even some of the ternary

vapor mixtures tested.[3, 18] However, the capability for reliably analyzing ternary or higher order mixtures has not been demonstrated, to date, with any type of sensor array.[3, 16]

Another promising approach to increasing diversity and improving vapor discrimination entails so-called multi-variable (MV) sensing, in which several ostensibly independent (or at least partially independent) parameters are measured from each sensor.[19-20] An early example of MV sensing was reported by Frye et al.; measuring both the frequency shift and attenuation of surface acoustic waves (SAW) in a polymer-coated SAW sensor allowed for multi-vapor discrimination at high concentrations.[21-22] A more recent reported example entailed measuring various components of the complex impedance of a single polymer- or nanoparticle-coated inductor-capacitor-resistor (LCR) resonator, which also yielded a set of different responses for different vapors.[19-20]

Yet another example of what might be considered MV sensing entails measuring shifts in the optical absorbance or reflectance of plasmonic nanoparticle films at several wavelengths.[23-25] The sensitivity of the localized surface plasmon resonance (LSPR) of multi-layer and monolayer metal nanoparticle films to vapor sorption is exploited. Investigations reported to date have included gold, silver, and core-shell silver nanoparticles either anchored to a substrate as a monolayer or deposited as a multilayer film with either a polymer add layer or thiolate- or citrate-monolayer functionalization to enhance sensitivity or to impart partial selectivity to a set of vapors.[23-30] Spectral shifts arise from changes in the effective refractive index, RI_{eff}, of the local environment surrounding the nanoparticles and, for films in which the nanoparticles are free to expand, also from changes in interparticle distance, δ. Of course, the extent to which a given vapor sorbs into the film affects both of these variables.

Theoretically,[30-34] if the *RI* of the sorbed vapor is lower than that of the MPN matrix it will reduce RI_{eff} and cause a blue shift in the wavelength of maximum absorbance, λ_{max}. If the vapor *RI* is higher, then it will cause a red shift in λ_{max}. The change in RI_{eff} has also been shown to create shifts in the total absorbance.[30] If the nanoparticles are not anchored to the substrate, then sorption-induced swelling of the surrounding ligand or polymer matrix will increase δ and the ensuing decoupling of the resonant frequency of the LSPR results in a decrease in the magnitude of the absorbance.[31-34] Previous reports also suggest that increases in δ are accompanied by a blue shift in λ_{max}.[28, 30]

The combined effects of changes in RI_{eff} and δ upon vapor sorption may enhance or diminish the change in the amplitude and wavelength shift attributable to one factor or another, and the net response would depend on which factor dominates. Prevailing evidence suggests that increases in δ are more important than changes in *RI* on the overall response of multi-layer MPN films.[25, 28, 30]

Karakouz *et al.* related the magnitude of the shift in λ_{max} of polymer-functionalized gold nano-islands to the polarity of the vapors and consequent affinity for the polymer[24] and Chen *et al.* utilized the shift in λ_{max} of gold nano-islands functionalized with thiolate monolayers for the detection of terpene.[27] Cheng *et al.* used self-assembled monolayers (SAM) of silver and gold nanoparticles immobilized on glass substrates to detect several VOCs by measuring changes in the total absorbance and shifts in λ_{max}.[23] In their follow-up study, they modified their immobilized nanoparticles with decanethiol, naphthalenethiol, and 2-mercaptobenzothiazole to impart chemical selectivity, and they showed that absorbance changes near λ_{max} permitted VOC discrimination.[26] The same group subsequently demonstrated a make-shift gas chromatographic

detector that relied on reflectance measurements of immobilized gold-citrate nanoparticles coated on a glass capillary probed with a simple green light-emitting diode.[29]

Scholten *et al.* used a single thiolate-monolayer protected gold nanoparticle (MPN) film probed at two wavelengths to measure changes in reflectance upon vapor exposure and used this to discriminate between toluene and heptane.[28] Accounting for differences in swelling efficiency between the two VOCs, they asserted that swelling-induced increases in δ dominated over the changes in *RI*. More recently, Potyrailo *et al.* also used changes in reflectance at several wavelengths of an MPN film to discriminate among several individual vapors and between two selected vapors and their binary mixture.[25]

This approach to enhancing the diversity of responses from an array of vapor sensors shows considerable promise because of the sensitivity of the LSPR to multiple variables. Studies to date have been limited in scope and have not explored many of the variables of interest. None of these studies has examined the impact of ligand functionality and core size on the ability of the MPN film to discriminate among vapors. Additionally, none of these studies has systematically compared the diversity of responses achievable with optically probed MPN films to that achievable with ST arrays that probe changes in mass or resistance of similar films.

In this study, we investigate optical MV vapor sensing with multi-layer films of plasmonic MPNs as a function of probing wavelength and ligand functionality for a small set of VOCs. We also investigate the influence of gold core size on responses. Initial attempts to use reflectance measurements gave way to transmission measurements at three wavelengths. MPN films (core size ~4-5 nm) containing six different thiolate ligand functionalities were examined. This is the first study that explores the effects of ligand functionality and the gold core size (5-40 nm) on sensor responses of mobile nanoparticle films containing the same ligand. To

accomplish this and prevent aggregation of the larger core sizes, a dithiane ligand of a longer chain length was utilized. Discrimination of individual vapors was achieved by measuring the changes in absorbance at three different wavelengths. The vapor discrimination capabilities of single and dual MPN films probed optically are compared to the performance of similarly coated chemiresistor (CR) and thickness shear mode resonator (TSMR) arrays of similar dimension, i.e. number of sensors/parameters measured.

4. 2 Experimental

4.2.1 Materials

The following VOCs were used as test vapors: tetrachloroethylene (PCE), toluene (TOL), *n*-octane (OCT), butyl acetate (BAC), 2-butanone (MEK), and 2-propanol (IPA). They were purchased from Sigma-Aldrich/Fluka (Milwaulkee, WI) or Acros/Fisher (Pittsburgh, PA) in > 99% purity and were used as received. Citrate-stabilized gold nanoparticles of 5 and 40 nm diameters and hexamethyldisilazane (HMDS, 99.9%) were obtained from Sigma Aldrich (Milwaulkee, WI) and used as received. MPNs containing thiolate monolayers derived from 1-mercapto-(triethylene glycol) methyl ether (TEG) were purchased from Nanoprobes (Yaphank, NY) and had a reported diameter of 5.16 ± 0.89 nm.

Figure 4-1 shows the structures of the thiols and dithiane of the MPNs studied here. All but the TEG were synthesized in house (Figure 4-1). Most MPNs had core diameters of 4 or 5 nm. For the DTE, a batch with an average core size of 40 nm was made. MPNs with 4-nm core sizes had thiolate monolayers derived from *n*-octanethiol (C8), 4-(phenylethynyl)-benzenethiol (DPA), 6-phenoxyhexane-1-thiol (OPH), and methyl-6-mercaptohexanoate (HME) and were taken from existing supplies synthesized by a known method.[35] Average Au core diameters

ranged from 3.4 (C8) to 4.7 nm (HME), with relative standard deviations (RSD) of 5-23% for any given type of MPN.

Initial attempts to synthesize larger MPNs with octane thiolate or dodecane thiolate monolayers by a simple phase transfer method[36] failed and resulted in extensive aggregation. To obtain larger MPNs that were soluble in organic solvents and stable against aggregation, a larger ligand containing a dithiane was employed. These MPNs contained a thiolate monolayer derived from (Z)-octadec-9-en-1-yl-5-(1,2-dithiolan-3-yl)pentanoate) (DTE) and were synthesized by a previously reported method,[37] in which a place exchange reaction between the organic ligand and citrate stabilized nanoparticles of varying sizes occurred. The MPN core sizes will be denoted as a subscript hereafter, i.e. DTE_5 and DTE_{40}. Briefly, the dithiane was first derived from (±)-*α*-lipoic acid and oleyl alcohol as previously described[37] and confirmed by ^{1}H and ^{13}C NMR spectroscopy. To complete the phase transfer, a surfactant, CTAB or Tween 80 depending on the core size,[37] was added to the stabilized nanoparticles in a citrate buffer and allowed to sit for 20 min. A drop of concentrated HCl was added before adding a solution of the ligand in $CHCl_3$. The mixture was shaken until the phase transfer was complete, as noted by the color change in both the aqueous and organic fractions. The organic fraction was collected and washed with EtOH to remove any excess surfactant. This phase transfer procedure was repeated for nanoparticles with core sizes of 5 and 40 nm. TEM images of DTE_5 and DTE_{40} are shown in the Appendix B (Figure B.1).

Of the thiols used to create the MPNs in this study, the only one with a published *RI* value was C8. Estimates of the *RI* values for DPA, OPH, and HME were generated using Percepta Platform -PhysChem Module from ACD/Labs[38] available online.[39] As a check on the modeled *RI* values, those for both octanethiol and decanethiol differed by < 0.5% from their

reported literature values, which raised confidence in the *RI* values estimated for DPA, OPH, and HME. The *RI* values for TEG and DTE could not be determined by this method. On the basis of an empirical comparison of *RI* values among a set of seven thiols and their hydrocarbon analogues with ≥ 6 carbons, an average difference of ~0.05 *RI* units was found. Therefore, a factor of 0.05 was added onto the values of *RI* for triethylene glycol monomethyl ether and hexadecane, structural analogues of TEG and DTE, respectively, to obtain estimated *RI* values for these monolayers. The estimated RI values are listed in Table 4-1.

4.2.2 Devices

For the reflectance measurements, a 4" wafer of anti-reflective coated glass (Edmunds Optics, Barrington, NJ) was diced into 1 cm × 2 cm chips with a dicing saw, cleaned with piranha solution (3:1 H_2O_2: H_2SO_4), and then exposed to vapors of HMDS to promote adhesion of the MPN films to the surface of the substrate. For the transmission measurements, standard glass microscope slides (1 cm × 2 cm) were manually diced, cleaned with aqua regia (3:1 HNO_3: H_2SO_4), and rinsed with distilled H_2O. The glass slides were then cleaned by sequential sonication in acetone and 2-propanol followed by drying in a scrubbed air stream and exposure to HMDS vapors.

Each TSMR consisted of a circular quartz crystal 1.4-cm diameter with 0.8-cm diameter gold electrode and a resonant frequency of 10 MHz (International Crystal; Oklahoma City, OK). The CR array chips (2.0 × 1.2 cm) have been described previously.[40] Each array has eight Au/Cr interdigital electrodes (IDEs) arranged in a 4 × 2 pattern on a thermal-SiO_x/Si substrate. The thickness of the Au/Cr metal film is 2000/300 Å. Each IDE has 24 finger pairs with 5 μm widths/spaces, 450 μm length, and 410 μm overlap. The TSMRs and CRs were cleaned by

sequential sonication in acetone and 2-propanol followed by drying in a scrubbed air stream prior to coating.

4.2.3 MPN Film Deposition

MPNs were dissolved in suitable solvents (toluene for C8, DPA, and OPH; dichloromethane for HME; ethanol for TEG; and a 1:1 chloroform/toluene mixture for DTE_5 and DTE_{40}) at concentrations of ~2.5-5 mg/mL. MPN films were drop cast on the reflectance, transmission, and CR substrates. For the reflectance substrates, MPN films were deposited in a criss-cross pattern using a 5 µL syringe (total volume deposited = 20 µL) to maximize surface coverage over the sensing region. For the transmission measurements, the glass slides were coated by placing a droplet of the MPN solution using a 5 µL syringe and allowing the solvent to evaporate at room temperature. To increase the baseline absorbance, another droplet was added in parallel on the opposite side of the glass slide. CRs were coated using a 0.5 µL syringe to create multilayer films with baseline resistances between 0.5-7MΩ. An estimated average film thickness of 240 nm was obtained from our AFM measurements of similarly deposited MPN films.[41]

TSMR devices were coated by airbrushing MPN solutions (~2.5-5 mg/mL) with pressurized air used as the propellant. Due to limited supplies, TEG and DTE_5 were drop cast from their solutions (~2.5 mg/mL). Frequency shifts upon coating were monitored using a phase-lock oscillator (Maxtek, Beaverton, OR) and recorded with Maxtek software on a PC. From the Sauerbrey equation and assuming a nominal density of ~4.3 g/mL for the 4-5 nm MPN types,[41-42] average film thicknesses were ~300 nm. The estimated partition coefficient, K, of each vapor in each MPN was determined from the measured frequency shift at a given

concentration. These K values were then used to estimate mass uptake in the optical probed films.

4.2.4 Exposure Measurements

For reflectance measurements, a microfluidic enclosure, 0.5 mm deep and 0.7 mm wide, was formed from two Si chips and an anti-reflective coated glass slide. The enclosure was sealed to the underlying MPN-coated Si chip using epoxy (Hysol Epoxy Patch 1C, Rocky Hill, CT). Inlet/outlet ports were fitted with deactivated fused-silica capillaries and sealed with epoxy. The sensor was mounted to a metal stage with double sided tape and connected via press-tight connections downstream of the vapor generation chamber used for CR and TSMR testing.

Reflectance sensors were placed in a custom built apparatus that consisted of three discrete laser-diodes (405, 532, and 630 nm) driven by a constant current source, aligned by means of a diffraction grating, and focused through a pinhole onto a single spot on a targeting stage on which the devices are mounted. A schematic of this set-up is given in the Appendix B (Figure B.2). The light reflected from the films was focused through a fixed lens onto a CMOS digital color camera (DCC1645C; Thor Labs, Newton, NJ) that was connected via USB to a PC. The 405, 532, and 630 nm lasers had outputs of 4.5, 10, and 4.5 mW, respectively. The red, green, and blue signals from the camera were recorded by custom written LabView code.

For the transmission measurements, a diced blank glass microscope slide, was placed vertically in the bottom of a 10 mm × 10 mm optical glass cuvette with a septum screw-top lid (Precision Cells Inc., Farmingdale, NY). Absorbance spectra were measured using either a DU800 (Beckman Coulter Inc.; Brea, CA) or a Cary 50 Bio UV-Vis (Varian; Santa Clara, CA) spectrophotometer over the range λ = 400-800 nm at a resolution of 0.15 nm. The blank

spectrum was automatically subtracted using the instrument software. Each MPN-coated glass slide was then placed vertically in the cuvette and the visible absorbance spectrum was measured. Due to the low sensitivity to vapor exposures and for simplicity during initial screening–level testing, films were exposed to six individual vapors at their saturation concentration, C_{sat}, by placing ~2 µL of liquid analyte directly in the cuvette via syringe and replacing the lid. The absorbance spectrum was measured after ~5 min and the cell was purged for another ~5-10 min before recording the recovery spectrum.

Subsequent vapor exposures were performed at 15-50% C_{sat}. Values of 50% C_{sat} concentrations (mg/m^3) for perchloroethylene, toluene, *n*-octane, butyl acetate, 2-butanone, and 2-propanol are listed in Table 4-1. Test atmospheres were generated by passing scrubbed air through a fritted bubbler of the liquid analyte, followed by dilution in a dry, scrubbed air stream. Mass flow controllers were used to maintain a total flow of ~14 L/min. The output stream is reduced to ~30 mL/min by an adjustable split, and passes through a capillary that connects to the sealed cuvette via press-tight connection. Vapor concentrations were confirmed by a flame ionization detector (FID) and are presented as a percentage of C_{sat}. A pre-exposure baseline spectrum was collected prior to exposing the film and then ~5 min after exposure. The cuvette was then purged with clean, dry air for 10 min before collecting another spectra. Triplicate runs were conducted for a subset of vapors. The recovery spectrum was superimposable with the baseline spectrum for virtually all cases. The vapor responses for each film were collected on the same day to minimize any variation from temperature and/or humidity. Duplicate and triplicate runs showed average RSD values were ≤ 5%.

MPN-coated CRs were mounted on custom PC boards and biased with the DC voltage from a battery and connected in series with a reference resistor closely matching that of the

baseline resistance for each individual sensor. The voltage drop was measured by a multiplexer card (model 34970A/34902A, Agilent Technologies, Santa Clara, CA), recorded with Agilent software on a PC, and converted to resistance.[43]

For vapor testing of the MPN-coated TSMRs and CRs, the sensors were placed within an exposure chamber that was equipped with electrical feed throughs and fluidic ports and maintained at a temperature of 25 ± 0.1°C. The CR arrays were placed within the chamber and each TSMR was placed between Viton o-rings in a custom made stainless steel holder. The TSMRs were then placed within the lid of the exposure chamber so that only the sensing area of the TSMR was exposed to the test atmosphere. Test atmospheres were generated by passing scrubbed air through a fritted bubbler of the liquid analyte, followed by dilution in a dry, scrubbed air stream. Mass flow controllers were used to maintain a total chamber flow of ~14 L/min. Vapor concentrations were confirmed by a flame ionization detector (FID) and calibrations typically spanned a ~10-fold concentration range (R^2 values for calibrations of the FID were ≥ 0.99; RSD were ≤ 5%; concentrations ranged from 50 – 5000 ppm).

4.2.5 Data Analysis

Spectral data were imported and analyzed in Microsoft Excel. Each spectrum was smoothed using a 20-point moving average. Response patterns were taken as the normalized fractional change in absorbance, A_λ: ΔA_λ = (A_λ during exposure –A_λ baseline, pre-exposure)/ (Abs_λ baseline, pre-exposure) at 405, 532, and 630 nm.

Chemometric analyses were performed on the optical, CR and TSMR response data. For the optical data, the vector sum of the fractional changes in absorbance at the three discrete wavelengths mentioned above were determined at 0.5 C_{sat}. Response vectors were normalized to

unit length and averaged over each of 2-3 replicates, where such replicates were collected. For the TSMRs and CRs, response vectors were derived from the average sensitivity values for all vapor-sensor pairs. The number of CR or TSMR sensors in an array varied from 2-6 for the TSMRs and from 2-5 for the CRs.

The extent of differences in the magnitude and direction among the vapors for a given film translate into the predicted performance of the MPN type. Principal components analysis (PCA) was performed on the experimental data and then it was extended by using experimental responses as the basis for generating "error-enhanced" response data via Monte Carlo simulation. A simulated data set was generated by a Monte-Carlo method (500 iterations) using R statistical software (version 2.13.1, R Foundation; Boston, MA). Thus, random error was superimposed on the experimental responses by multiplying each response by a fractional value obtained by randomly sampling a Gaussian distribution of mean 1 and a standard deviation of 0.05 for the plasmonic films, corresponding to a proportional random error rate (ε) of 5%. This error rate was representative of the variation in responses obtained over all wavelengths for replicate measurements (based on data collected with C8) and over replicate measurements with the TSMRs and CRs. The fractional value was then multiplied by the original (actual) response to obtain the "error-enhanced" response. The plasmonic films had consistently low sensitivities to all of the vapors tested. In the cases of extremely low responses (those $< 5 \times$ the minimum detectable signal), an additional 1% error was added onto the original response prior to superimposing the random error (ε = 5%). This was done by adding a value generated from randomly sampling a Gaussian distribution of mean 0 and a standard deviation of 0.01.

Average recognition rates (RR) for the individual vapors were estimated by calculating Euclidean distances (ED).[1, 5, 17] If the ED between the simulated and correct library response

vectors was smaller than that between the simulated and alternative vapor library response vectors, then the vapor was considered to be correctly recognized. This process was repeated 500 times for each of the six individual vapors, and the average RR was reported in terms of percentage of those vapors correctly identified. Vapor-specific RR values were then tabulated in a confusion matrix.

4.3 Results & Discussion

4.3.1 Reflectance Measurements

A diagram of the reflectance apparatus is shown in Figure B.2 in Appendix B. The center wavelengths of the lasers were 405, 532, and 630 nm, two of which flanked all of the LSPR λ_{max} values, and a third (i.e., 532 nm) that was in the vicinity of λ_{max} for the MPNs studied here. Exposure of C8, DPA, OPH, and HME drop-cast films to toluene led to decreases in the intensity of reflected light at all three wavelengths. Responses were reversible and varied linearly with vapor concentrations, but gave much lower sensitivities than similarly coated CRs and TSMRs (vida infra).

Responses from films of C8 were investigated in greater detail than those of the other MPNs. Although unique 3-λ response patterns could be achieved for toluene, octane, 2-butanone, butyl acetate, perchloroethylene, and 2-propanol, it was not possible to obtain reproducible results either within a given film over time or among different films. Figure B.3 (Appendix B) shows examples of response patterns for toluene for three similarly drop-cast C8 films. Variations in film morphology undoubtedly contribute to this problem. SEM images of one C8 film and one HME film showed them to be quite non-uniform (Figure B.4; Appendix B), with thickness variations on the order of the probing wavelengths. This would lead to a

significant degree of scattering that could easily account for observed variations in responses among film samples, among different locations within the same film, and upon vapor-induced film swelling. Clearly, net responses were a combination of absorbance and scattering,[24, 30] where the latter was apparently significant and uncontrolled. In an effort to improve film uniformity, a spray-coated C8 film was tested, but there was no apparent improvement: significantly different responses to toluene were obtained at different probed locations across the film (Figure B.3b; Appendix B). Furthermore, the responses of the spray-coated film differed from those of the drop-cast films (Figure B.3; Appendix B.). Neither changing the deposition solvent nor warming or cooling the substrate during deposition resolved the problem. At this point, we abandoned laser reflectance measurements and switched to transmission measurements using a standard UV-vis spectrophotometer with a broad band source that suffered much less from scattering and gave much more reproducible results.

4.3.2 Baseline Absorbance Spectra

Figure 4-2 presents the spectra for all six MPNs both in dilute solution and as dense cast films. It is well known that the position, width, and magnitude of the LSPR absorbance band are dictated by the size, shape, packing order and proximity of the metal nanoparticles as well as the dielectric properties of the surrounding matrix.[30-34] For similarly shaped cores having the same monolayer functionalities, λ_{max} and the magnitude of the absorbance will increase with particle size and decrease with inter-core distance, and the width of the LSPR absorbance will increase with the polydispersity of the core size distribution.[31, 44-46] For densely packed MPN films, the baseline *RI* value can be taken as that of the organic monolayer;[32] λ_{max} shifts to longer values as the *RI* of the monolayer increases.[30-32]

As shown in Figure 4-2a-g the MPN films gave λ_{max} values between 544 and 580 nm, all of which were red shifted by 14-60 nm from their λ_{max} values measured in dilute solution, consistent with previous reports.[31, 47] The order of the λ_{max} values generally follows the order of the monolayer *RI* values. The most obvious exception is DTE_5 for which λ_{max} of the dilute solution and film are both lower than expected. Since the length of the DTE ligand would naturally increase δ in the film, this could explain the decrease in λ_{max} compared to what would be expected due to *RI* alone. The total absorbance level was also lower for DTE_5, which is also consistent with a larger value of δ. The higher λ_{max} value and larger magnitude of absorbance (data not shown) for DTE_{40}, relative to DTE_5, is consistent with its larger core diameter. Although not shown in Figure 4-2, the magnitude of absorbance of the C8 film was higher than that of the other films, which is consistent with it having a smaller average value of δ owing to the well-known tendency for *n*-alkyl groups on adjacent nanoparticles to intercalate.[48]

4.3.3 Responses to Vapors

In a series of preliminary tests, films of each MPN were exposed to a saturated test atmosphere of toluene vapor. With the exception of DPA and OPH, pre- and post-exposure spectra were superimposable, or nearly so. For DPA and OPH, the spectral changes indicated that significant morphological changes had occurred upon exposure (see Figure 4-3). For DPA, the post-exposure λ_{max} was red-shifted by 53 nm, the magnitude of the absorbance was reduced across most of the peak, and the peak became broader. Similar changes occurred to the spectrum of OPH, though λ_{max} was red shifted by only 28 nm. These changes are consistent with a significant degree of agglomeration, which would result in both a larger average particle size and a wider range in particle sizes, consistent with the observed spectral changes. It is not clear why

these particular films were more susceptible to such morphological changes upon vapor exposure. The *K* values listed in Table 4-1 would suggest that C8 and DTE_5 sorb more toluene than the other films, ruling out mass uptake as the primary driver for agglomeration.

Due to the threat of morphological changes at saturated concentrations, all subsequent testing was limited to a maximum of 50% of the saturation vapor concentration, $0.5C_{sat}$, of the six vapors. Freshly prepared MPN films subjected to such exposures were well-behaved; although some shifts in baselines were observed on occasion, these were minor and probably attributable to slight shifts in the position or packing order of the nanoparticles in the films.[49-50]

As shown in Table 4-1, λ_{max} was blue shifted for every vapor-MPN pair tested. This is consistent with all previous reports and reflects the dominant influence of film swelling (increases in δ) on this exposure metric.[24, 28, 30] If *RI* changes were dominant, then PCE and TOL would have caused red shifts in all but the DPA and OPH films or the blue shifts would have been greatly diminished relative to those of the other vapors. *RI* values for the other vapors are lower than those of all of the MPNs and the reduction in RI_{eff} accompanying their sorption would also lead to blue shifts, enhancing the effect of swelling, but there is no strong evidence for such enhancement. Due to the breadth of their LSPR bands the shifts in λ_{max} for DPA and DTE_{40} could not be determined with sufficient precision to have confidence in the values. Decreases in net absorbance across the visible range were also observed in all cases, as shown in the representative spectra for C8 and HME in Figures B.4 and B5 (Appendix B).

Assuming that the values of *K* determined from the TSMR responses at low vapor concentrations are applicable to higher concentrations as well, the relative mass of vapor sorbed by each film, m_{vapor}, can be estimated from the product of *K* and the vapor concentration (i.e., $0.5C_{sat}$ in units of mass/volume). Dividing by the density of the each vapor, the relative mass

uptake can be converted to relative volume uptake, v_{vapor}. If the exact mass of each MPN in each film were known then the actual mass (and volume) of vapor could be determined. As it is, only a relative mass (volume) uptake can be calculated and, therefore, only the volume change expected among the different vapors within a given film can be compared. The values of m_{vapor} and v_{vapor} are compiled in Table 4-1, normalized to the largest mass and volume uptake values, respectively. Although, a rough correlation between m_{vapor} and shifts in λ_{max} is apparent in Table 4-1, there are exceptions with almost every MPN type, which could not be accounted for by the differences in *RI* values between each vapor and MPN. It is known that the volume of vapor taken up by an MPN film does not translate directly into the same degree of swelling in the film.[42] This factor, may be contributing to the lack of a better correlation between vapor uptake volume and the observed shifts in λ_{max}.

Figure 4-4 presents the bar charts that represent the 3-λ response patterns for each vapor-MPN pair, normalized to the largest response among the three wavelengths. In contrast to the other MPNs, responses for DPA and OPH were all positive; absorbances increased for all vapors at all three wavelengths. For DTE_5 the opposite was true, and for C8, HME, TEG and DTE_{40}, while most changes were negative, they all showed at least one case where there was a positive change at one or more wavelengths or one or more vapors. Spectral changes observed for PCE and TOL differ from those of the other analytes. For 3 out of the 7 MPN types tested (C8, TEG, and DTE_{40}), TOL and PCE caused an *increase* in absorbance in the shorter wavelength region, which is puzzling, as theory would predict that a swelling dominated response should cause a net decrease in absorbance.

The large absorbance *increases* for all vapors at all wavelengths with the DPA and OPH films coupled with the lack of any significant shift in λ_{max} is puzzling. Given what we

understand to be the factors affecting responses, RI_{eff} would have to increase and/or δ would have to decrease upon vapor exposure. The former, however, would be accompanied by a shift in λ_{max} which did not occur. Therefore, it must be that these responses arise primarily from changes in δ. Given the anomalous changes in the spectra of these two MPNs indicative of agglomeration, we believe that the normal physical interpretations of such responses are no longer applicable. If agglomeration has indeed occurred, we would expect the MPN film surface to have regions of high and low particle density and for the regions of high particle density to dominate the optical changes upon vapor exposure. The individual nanoparticles would still swell upon vapor exposure, but may do so in such a manner that causes the larger clumps in the film to come closer together. This would effectively decrease the δ governing the response, leading to increases in the overall absorbance. The extent of increase in absorbance seems to be correlated with the values of m_{vapor} for both films, and as discussed below the selectivity exhibited by the DPA film is very low, suggesting responses dictated almost entirely by swelling.

4.3.4 Individual Vapor Recognition with Single Plasmonic Films

For reference, the 7 film-wise 3-λ response patterns, normalized to the wavelength giving the highest response for a given vapor, are presented as bar charts in Figure 4-4. As shown, changes in absorbance differ in both sign and magnitude among vapors for a given film and among wavelengths for a given vapor-film pair. Calibrations were performed over a range of concentrations spanning roughly from 0.15-0.50 C_{sat} for two of the MPN films, C8 and DTE_{40}. As shown by the representative results in Figure B.7 (Appendix B) for C8 with TOL and BAC, absorbance shifts varied linearly with concentration ($R^2 \geq 0.96$).

To assess the diversity of optical responses from each MPN film more definitively, PCA was performed on the normalized vapor-wise 3-λ response vectors for all six test vapors. Results are shown in the two-dimensional score plots of Figure 4-5. In fact, the classification models used ultimately to evaluate diversity employed three PCs, which improved the discrimination achievable with several films despite the third PC accounting for only a small fraction of the total variance in the data in many cases. A representative 3-D PC score plot is presented in Figure B.8 (Appendix B). The elliptical boundaries in Figure 4-5 represent 95% confidence intervals around the centroid for each vapor, derived by iterative Monte Carlo simulations of responses assuming 5% variation in responses, and subsequent plotting of the resultant normalized response vectors. This serves as an aid in assessing the degree of vapor discrimination while accounting for expected pattern variations.

Inspection of the 2-D PC plots in Figure 4-5 confirms what was qualitatively apparent from the bar charts of Figure 4-4. That is, films of DPA, OPH, and DTE_5 show significant overlap in the clusters attributable to the vapors, while films of C8, HME, and DTE_{40} show much less overlap. TEG shows a more moderate degree of overlap.

Monte Carlo simulations were then performed to generate statistical estimates of recognition rates for each vapor assuming 5% variation in responses. Confusion matrices were also generated to evaluate the nature of the classification errors (i.e., the mistakenly assigned vapor identities). Results are summarized in Table 4-2 in terms of the average recognition rate (RR) as well as the minimum and maximum RR values among the six vapors for each film. The average RR values span from 51.5 – 99.9%. We consider an average RR $\geq$ 95% to represent the threshold for "good" performance. Using this criterion, C8, HME, and DTE_{40} perform well. The other four films fall below this performance threshold to varying degrees. These RR values are

consistent with what is depicted in Figure 4-5 (and Figure 4-4). As expected, DPA shows the lowest RR value, followed by OPH and DTE_5, which give similar RR values. Notably, the RR value of 99.9% for DTE_{40} is remarkably high and significantly higher than its 5-nm analogue DTE_5.

To explore further the basis for the discrimination levels calculated on the basis of the 3-λ response vectors, we performed a correlation analysis of the three pairs of wavelengths. It was expected that the pair-wise correlation coefficients, *r*, would reveal any redundancies in responses and that lower *r* values would be associated with higher RR values. Surprisingly, this was not found to be the case. For the C8, HME, and DTE_{40} films, one or more wavelength pairs had a high *r* value, despite their high RR values, and for DTE_{40} all three r values were > 0.90. Furthermore, for the poorly performing DPA and TEG films, at least two of the three wavelength pairs had quite low *r* values. Upon closer inspection, it was found that in all of these cases, the value of *r* belied that actual level of correlation. Figure B.9 (Appendix B) reveals this for several cases. For example, for the C8 film, PCE and TOL gave positive responses at two wavelengths whereas the remaining four vapors gave positive responses at all wavelengths (Figure 4-4). Thus, the vectors for PCE and TOL are positive whereas those for the other vapors are negative and are clustered together (Figure B.9a). Since PCE and TOL are some distance from the rest of the vapors, the linear regression gives an inflated *r* value that fails to capture the true diversity of responses. For DTE_{40}, the BAC vector is significantly separated from the vectors for the remaining 5 vapors and, again, the regression *r* value is inflated and fails to reflect the lack of correlation among the vapor responses (Figure B.9b). Conversely, for DPA the 405-630 nm correlation is dictated by one vapor, TOL, falling off the otherwise linear correlation among the remaining vapors, resulting in an *r* value that does not reflect the correlation among most of the

response vectors (Figure B.9d). Removing the TOL reveals the high correlation among the other vapors: r = 0.99 (Figure B.9e), consistent with the low average RR value. For the HME film, a more careful analysis is necessary. The HME responses at 405 and 630 nm, have a high r value and are actually highly correlated with one another (Figure B.9c). This does not mean, though, that one of these wavelengths is not crucial to the ability of this film to discriminate among the vapor set as the correlation plot in Figure B.9c would suggest. Indeed, if either the response at 405 or 630 nm is removed, the average RR drops to ~85%. By looking at the response patterns in Figure 4-4d, the relative 405/532 nm responses for PCE and IPA are similar and only by adding in the response at 630 nm do these patterns differ. This highlights the shortcomings of using such correlation metrics as predictors of the contributions of individual array elements (i.e., wavelengths in this case) to diversity. These findings are in agreement with those made on the basis of similar analyses we performed of other sensor arrays in Chapter III.[17]

Increasing the core size had a dramatic effect on response diversity, as evidenced by the performance of the DTE_{40} (RR = 99.9%) compared to the DTE_5 (RR = 82%). One hypothesis is that the larger core decreases the contribution of swelling to the net response, allowing the differences in RI among the vapors to play a greater role. Some support for this is found in the response data at 0.5 C_{sat}; sensitivities of the DTE_{40} are generally lower than those of the DTE_5 at the same wavelengths (Tables B.1-B.3).

4.3.5 Comparison of Single Plasmonic Sensing Films vs. 3-TSMR and 3-CR Arrays

Calibration curves for the test vapors with each of the MPN-coated TSMR and CR sensors were linear with forced-zero regression R^2 values > 0.95 in all cases. Note that CR data for the DTE-MPNs could not be collected because films were too highly resistive to get

measurable signals (conduction decreases with increasing δ, but increases with increasing particle size)[51] and TSMR data was not collected for DTE_{40} due to limited supplies. Sensitivity values in $(\Delta f/f)_{ppm}/(mg/m^3)$ for the TSMRs and in $(\Delta R/R)_{ppm}/(mg/m^3)$ for the CRs are tabulated (Table B.4) and these values were used to generate limits of detection (LODs) and relative response patterns (Figure B.10 and B.11) for use in comparing diversity and vapor discrimination capabilities among the TSMR arrays, CR arrays, and optically probed films.

LODs for the TSMRs and CRs are presented in Table B.5 and they range from 1.7 to 367 mg/m^3 among the test vapors. LODs were calculated as $3s/b$, where s is the baseline standard deviation and b is the sensitivity. Although CR sensitivities are generally higher, the LODs are also higher than those of the similarly coated TSMRs due to higher baseline noise levels. The LODs for the C8 plasmonic sensing film are presented in Table B.6 and were derived from the calibration data at the most sensitive wavelength for each vapor. As shown, they are orders of magnitude higher than those for the TSMR and CR sensors.

Notwithstanding the differences in sensitivity, it was of interest to compare the diversity of responses and the capabilities for differentiating vapors on the basis of responses from arrays of TSMRs and CRs of different sizes (i.e., different number of sensors) and individual plasmonic sensor films probed at three wavelengths as well as dual-film plasmonic sensor arrays probed at fewer wavelengths. Arrays of three TSMRs and three CRs were compared to single plasmonic films probed at all three wavelengths, as a test of the hypothesis that the different wavelengths would be as independent from each other as the different MPNs in the TSMR and CR arrays.

Response data from all CR arrays and TSMR arrays were used in PCA and also to generate RR values using Monte Carlo simulations assuming a 5% error rate. The PCA scores plots for the best performing 3-TSMR and 3-CR arrays are shown in Figure 4-6. The RR values

for the top-five best-performing 3-TSMR and 3-CR arrays are presented in Table 4-3. Cluster separation distances (all six vapors are well-separated) are consistent with the high RR values for the best performing 3-TSMR and 3-CR arrays. Among the 5 top-performing 3-TSMR and 3-CR arrays given in Table 4-3, the RR values for the 3-TSMR and 3-CR arrays were > 98% and > 95%, respectively. Thus, there are many arrays that give high RR values. The worst performing arrays give substantially lower RR values (RR ~86%, data not shown). Both of the best performing 3-sensor arrays include the same two film combination, C8 and DPA. Both of the best performing 3-sensor arrays, though, include two out of three of the same films as the worst performing 3-sensor arrays. Still, this emphasizes the importance of judiciously selecting interface materials when optimizing array performance; a process that remains empirical at this point. Among all possible arrays, 60% of the 3-TSMR arrays and 50% of the 3-CR arrays had RR values > 95%. As stated above, there were also three optically probed (plasmonic) MPN films (C8, HME, and DTE_{40}) that gave RR > 95%. Two of these have non-polar monolayer structures and one has a polar structure. The reason for this set of this set of MPNs giving better performance than the others is not apparent and is worthy of further investigation.

4.3.6 Performance of Dual Plasmonic Film Arrays

Arrays of plasmonic sensing films were evaluated next, for the simplest case of two sensing films. The average RR values for the 15 possible dual-film arrays was ≥ 95% (ε = 5%) in all cases. Thus, by combining just two sensing films, discrimination is greatly enhanced. The PCA scores plot for one of the best dual film arrays, C8 + HME, is shown in Figure 4-6c (RR = 100%). Of the 15 possible dual film arrays, 14 gave an average RR > 98% (PCA plots not

shown). The worst dual film array consisting of TEG + C8 slightly confuses BAC for IPA, leading to an average RR of 94.8%.

These dual film arrays perform as well as the 3-TSMR and 3-CR arrays. The performance of the dual film arrays was as also as good as that of the 6-TSMR and 5-CR arrays (similar in array dimension, i.e. number of sensors or measured parameters), which gave RR values of > 99%. The performance of the 6-TSMR and 5-CR arrays does not improve much over the 3-TSMR and 3-CR arrays. This is in agreement with what has been shown previously, illustrating the facile problem of individual vapor recognition.[3, 5-6, 17] Increasing the number of sensors in an array does not necessarily improve the overall performance, and often the performance plateaus at a relatively small array dimension (number of sensors ~ 4-6). [3, 5-6, 17]

Table B.7 lists four different sets of dual-optical film "arrays" where *only a single wavelength was used from each film in the pair*. For each case in Table B.7, the average RR (ε = 5%) among all six individual vapors tested at 50% C_{sat} for each combination is given. Although there is a range of average RR values among these film/λ pairs, each dual film examined had at least one combination of wavelengths that could discriminate among the six individual vapors with an average RR > 95%. The average RR values of the top-performing film/λ pairs were better than the RR values of the top-performing 2-TSMR and 2-CR arrays examined at the same assumed error rate (see Table 4-3 entries for 2-TSMR and 2-CR arrays). The PCA scores plot of one example (C8, 532 nm + HME, 532 nm) is shown in Figure 4-6d. These results suggest that the measurement of optical changes of these plasmonic MPN films is inherently more selective than measurements of conductivity changes (CR) or mass changes (TSMR) upon vapor exposure. Analogous tests were also performed assuming an error rate of 10% instead of 5%. As expected, RR values declined, but the best-performing pairs still had RR values from 92-

99%, indicating that their discriminating power has low to moderate sensitivity to variations in responses.

It bears mentioning that although the discrimination of 6 individual vapors is not trivial, such problems have been successfully solved with many different sensor array technologies. In all such cases, it requires < 5-6 sensors to achieve such performance. The ability to do so with a single sensor and with several different single sensors is unprecedented and noteworthy. However, the more challenging problems of analyzing the components of vapor mixtures needs to be addressed; it is with this type of problem that we expect the plasmonic sensor arrays to excel.

4.4 Conclusions

We conclude that thin films of certain plasmonic monolayer protected Au nanoparticles probed at just a few wavelengths near the LSPR maximum can provide a remarkably high level of discrimination among vapors to which the film is exposed by virtue of reversible changes in absorbance. Specifically, we have shown that *individual* films of three different MPNs can successfully differentiate among 6 vapors at an estimated rate of > 95%. Each of these individual plasmonic films exhibits response diversity comparable to that achievable with the best arrays of three MPN-coated TSMRs or CRs that could be assembled from the set of MPNs examined. This demonstrates that the different probing wavelengths are responding to different aspects of the vapor-MPN interaction. This may represent a path toward simpler sensing platforms requiring fewer devices (interface films). In cases where data from two plasmonic films were combined, each probed at three common wavelengths, an average RR of > 99% could be achieved with many different film pairs, and reducing the number of wavelengths probed to

as low as two (i.e., one per film) afforded a similar level of discrimination as that achieved with 6 wavelengths (i.e., 3 per film).

Although some correlations were observed between the sign and magnitude of exposure and those expected on the basis of estimates of sorption-induced changes in inter-core distances and refractive indexes of the exposed films, there were few clear trends that could form the basis for modeling or predicting responses. Furthermore, it was difficult to achieve a high level of reproducibility within or between different films; and differences in responses as a function of concentration were also observed, albeit at concentrations near saturation. The very low sensitivity observed with all of these films is another shortcoming of this sensing approach. Rough estimates of detection limits derived from a subset of tests performed in this study were in the high ppm range for vapors such as toluene and octane for which other sensors show orders-of-magnitude lower sensitivities. That said, preliminary testing with one of these films on a new sensor technology, an optofluidic ring resonator, gave LODs 3 orders of magnitude lower than those estimated from this study. Applying these films to such sensors and probing at multiple wavelengths may afford sufficient sensitivity and selectivity to be useful for integration in gas chromatographic microsystems (uGC) for generalized multi-vapor air monitoring applications. By reducing the vapor concentrations required to elicit responses, it is expected that reproducibility would improve.

This study was constrained to individual-vapor discriminations, which are relatively facile. The more challenging problems of analyzing the components of binary and ternary mixtures have yet to be addressed and will be the topic of future work. The possibility of creating multi-transducer arrays that combine such optical sensors with sensors that respond to mass and/or changes in film resistance is also worth consideration.

4.5 References

1. Zellers, E. T.; Batterman, S. T.; Han, M.; Patrash, S. J. "Optimal Coating Selection for the Analysis of Organic Vapor Mixtures with Polymer-Coated Surface Acoustic Wave Sensor Arrays," *Anal. Chem.*, **1995**, *67(6)*, 1092-1106.
2. Hsieh, M. D.; Zellers, E. T. "Limits of Recognition for Simple Vapor Mixtures Determined with a Microsensor Array," *Anal. Chem.*, **2004**, *76(7)*, 1885-1895.
3. Jin, C.; Kurzawski, P.; Hierlemann, A.; Zellers, E. T. "Evaluation of Multitransducer Arrays for the Determination of Organic Vapor Mixtures," *Anal. Chem.*, **2008**, *80(1)*, 227-236.
4. Ricco, A. J.; Crooks, R. M.; Osbourn, G. C. "Surface Acoustic Wave Chemical Sensor Arrays: New Chemically Sensitive Interfaces Combined with Novel Cluster Analysis to Detect Volatile Organic Compounds and Mixtures," *Acc. Chem. Res.*, **1998**, *31(5)*, 289-296.
5. Park, J.; Groves, W. A.; Zellers, E. T. "Vapor Recognition with Small Arrays of Polymer-Coated Microsensors. A Comprehensive Analysis," *Anal. Chem.*, **1999**, *71(17)*, 3877-3886.
6. Garcia-Berrios, E.; Gao, T.; Theriot, J.; Woodka, M. D.; Brunschwig, B. S.; Lewis, N. S. "Response and Discrimination Performance of Arrays of Organothiol-Capped Au Nanoparticle Chemiresistive Vapor Sensors," *J. Phys. Chem. C*, **2011**, *115(14)*, 6208-6217.
7. Burl, M. C.; Sisk, B. C.; Vaid, T. P.; Lewis, N. S. "Classification Performance of Carbon Black-Polymer Composite Vapor Detector Arrays as a Function of Array Size and Detector Composition," *Sens. & Actuators B: Chem.*, **2002**, *87*, 130-149.
8. Senesac, L. R.; Dutta, P.; Datskos, P. G.; Sepaniak, M. J. "Analyte Species and Concentration Identification Using Differentially Functionalized Microcantilever Arrays and Artificial Neural Networks," *Anal. Chim. Acta.*, **2006**, *558(1)*, 94-101.
9. Patel, S. V.; Mlsna, E. T.; Fruhberger, B.; Klaassen, E.; Cemalovic, S.; Baselt, D. R. "Chemicapacitive Microsensors for Volatile Organic Compound Detection," *Sens. And Actuators B: Chem.*, **2003**, *96*, 541-553.
10. Patel, S. V.; Jenkins, M. W.; Hughes, R. C.; Yelton, W. G.; Ricco, A. J. "Differentiation of Chemical Components in a Binary Solvent Vapor Mixture Using Carbon/Polymer Composite-Based Chemiresistors," *Anal. Chem.*, **2000**, *72*, 1531-1542.
11. Han, L.; Shi, X.; Wu, W.; Kirk, F. L.; Luo, J.; Wang, L.; Mott, D.; Cousineau, L.; Lim, S. I.; Lu, S.; Zhong, C.-J. "Nanoparticle-Structured Sensing Array Materials and Pattern Recognition for VOC Detection," *Sens. & Actuators B: Chem.*, **2005**, *106*, 431-441.
12. Schierbaum, K. D.; Gerlack, A.; Haug, M.; Göpel, W. "Selective Detection of Organic Molecules with Polymers and Supramolecular Compounds: Application of Capacitance, Quartz Microbalance, and Calorimetric Transducers," *Sens. & Actuators A: Phys.*, **1992**, *31(1-3)*, 130-137.
13. Ulmer, H.; Mitrovics, J.; Weimar, U.; Göpel, W. "Sensor Arrays with Only One or Several Transducer Principles? The Advantage of Hybrid Modular Systems," *Sens. & Actuators B: Chem.*, **2000**, *65(1)*, 79-81.
14. Pardo, M.; Kwong, L. G.; Sberveglieri, G.; Brubaker, K.; Schneider, J. F.; Penrose, W. R.; Stetter, J. R. "Data Analysis for a Hybrid Sensor Array," *Sens. and Actuators B: Chem.*, **2005**, *106(1)*, 136-143.

15. Kurzawski, P.; Hagleitner, C.; Hierlemann, A. “Detection and Discrimination Capabilities of a Multitransducer Single-Chip Gas Sensor System,” *Anal. Chem.*, **2006**, *78*, 6910-6920.
16. Jin, C.; Zellers, E. T. “Chemometric Analysis of Gas Chromatographic Peaks Measured with a Microsensor Array: Methodology and Performance Assessment,” *Sens. and Actuators B: Chem.*, **2009**, *139*, 548-556.
17. Scholten, K.; Wright, L. K.; Zellers, E. T. “Vapor Discrimination with Single- and Multi-Transducer Arrays of Nanoparticle-Coated Chemiresistors and Resonators,” *IEEE Sensors J.*, **2013**, *13(6)*, 2146-2154.
18. Jin, C.; Zellers, E. T. “Limits of Recognition for Binary and Ternary Vapor Mixtures Determined with Multitransducer Arrays,” *Anal. Chem.*, **2008**, *80(1)*, 7283-7293.
19. Potyrailo, R. A.; Morris, W. G. “Multianalyte Chemical Identification and Quantitation Using a Single Radio Frequency Identification Sensor,” *Anal. Chem.*, **2007**, *79*, 45-51.
20. Nagraj, N.; Slocik, J. M.; Phillips, D. M.; Kelley-Loughnane, N.; Naik, R. R.; Potyrailo, R. A. “Selective Sensing of Vapors of Similar Dielectric Constants Using Peptide-Capped Gold Nanoparticles on Individual Multivariable Transducers,” *Analyst*, **2013**, *138*, 4334-4339.
21. Martin, S. J.; Frye, G. C.; Senturia, S. D. “Dynamics and Response of Polymer-Coated Surface Acoustic Wave Devices: Effect of Viscoelastic Properties and Film Resonance,” *Anal. Chem.*, **1994**, *66*, 2201-2219.
22. Frye, G. C.; Martin, S. J. Dual Output Acoustic Wave Sensor for Molecular Identification US Patent 5,076,094 December 31, 1991.
23. Cheng, C-S.; Chen, Y-Q.; Lu, C-J. “Organic Vapour Sensing Using Localized Surface Plasmon Resonance Spectrum of Metallic Nanoparticles Self Assemble Monolayer,” *Talanta*, **2007**, *73*, 358-365.
24. Karakouz, T.; Vaskevich, A.; Rubinstein, I. “Polymer-Coated Gold Island Films as Localized Plasmon Transducers for Gas Sensing,” *J. Phys. Chem. B*, **2008**, *112*, 14530-14538.
25. Potyrailo, R.; Larsen, M.; Riccobono, O. “Detection of Individual Vapors and Their Mixtures Using a Selectivity-Tunable Three-Dimensional Network of Plasmonic Nanoparticles,” *Angew. Chem. Int. Ed.*, **2013**, *52*, 10360-10364.
26. Chen, K-J.; Lu, C-J. “A Vapor Sensor Array Using Multiple Localized Surface Plasmon Resonance Bands in a Single UV-Vis Spectrum,” *Talanta*, **2010**, *81*, 1670-1675.
27. Chen, B.; Liu, C.; Ota, M.; Hayashi, K. “Terpene Detection Based on Localized Surface Plasma Resonance of Thiolate-Modified Au Nanoparticles,” *IEEE Sensors J.*, **2013**, *13(4)*, 1307-1314.
28. Scholten, K.; Reddy, K.; Fan, X.; Zellers, E. T. “Vapor Discrimination by Dual-Laser Reflectance Sensing of a Single Functionalized Nanoparticle Film,” *Anal. Methods*, **2013**, *5*, 4268-4272.
29. Chen, F-Y.; Chang, W-C.; Jian, R-S.; Lu, C-J. “Novel Gas Chromatographic Detector Utilizing the Localized Surface Plasmon Resonance of a Gold Nanoparticle Monolayer Inside a Glass Capillary,” *Anal. Chem.*, **2014**, *86*, 5257-5264.
30. Dalfovo, M. C.; Salvarezza, R. C.; Ibanez, F. J. “Improved Vapor Selectivity and Stability of Localized Surface Plasmon Resonance with a Surfactant-Coated Au Nanoparticles Film,” *Anal. Chem.*, **2012**, *84*, 4886-4892.

31. Wang, L.; Miller, D.; Fan, Q.; Luo, J.; Schadt, M.; Rendeng, Q.; Wang, G. R.; Wang, J.; Kowach, G. R.; Zhong, C-J. "Assessment of Morphological and Optical Properties of Molecularly Mediated Thin Film Assembly of Gold Nanoparticles," *J. Phys. Chem. C*, **2008**, *112*, 2448-2455.
32. Kubo, S.; Diaz, A.; Tang, Y.; Mayer, T. S.; Khoo, I. C.; Mallouk, T. E. "Tunability of the Refractive Index of Gold Nanoparticle Dispersions," *Nano. Lett.*, **2007**, *7(11)*, 3418-3423.
33. Yockell-Lelievre, H.; Gingras, D.; Vallee, R.; Ritcey, A. M. "Coupling of Localized Surface Plasmon Resonance in Self-Organized Polystyrene-Capped Gold Nanoparticle Films," *J. Phys. Chem. C*, **2009**, *113*, 21293-21302.
34. Miller, M.; Lazarides, A. A. "Sensitivity of Metal Nanoparticle Surface Plasmon Resonance to the Dielectric Environment," *J. Phys. Chem. B*, **2005**, *109*, 21556-21565.
35. Rowe, M. P.; Plass, K. E.; Kim, K.; Kurdak, C.; Zellers, E. T.; Matzger, A. J. "Single-Phase Synthesis of Functionalized Gold Nanoparticles," *Chem. Mater.*, **2004**, *16*, 3513-3517.
36. Hostetler, M. J.; Templeton, A. C.; Murray, R. W. "Dynamics of Place-Exchange Reactions on Monolayer-Protected Gold Cluster Molecules,' *Langmuir*, **1999**, *15*, 3782-3789.
37. Lista, M.; Liu, D. Z.; Mulvaney, P. "Phase Transfer of Noble Metal Nanoparticles to Organic Solvents," *Langmuir*, **2014**, *30(8)*, 1932-1938.
38. ACD/Labs. http://www.acdlabs.com/products/percepta/predictors.php (accessed Aug. 2014).
39. ChemSpider. http://www.chemspider.com/ (accessed Aug. 2014).
40. Kim, S. K.; Chang, H.; Zellers, E. T. "Microfabricated Gas Chromatograph for the Selective Determination of Trichloroethylene Vapor at Sub-Parts-Per-Billion Concentrations in Complex Mixtures," *Anal. Chem.*, **2011**, *83(18)*, 7198-7206.
41. Bohrer, F. I.; Covington, E.; Kurdak, C.; Zellers, E. T. "Characterization of Dense Arrays of Chemiresistor Vapor Sensors with Submicrometer Features and Patterned Nanoparticle Interface Layers," *Anal. Chem.*, **2011**, *83*, 3687-3695.
42. Steinecker, W. H. Rowe, M. P.; Zellers, E. T. "Model of Vapor-Induced Resistivity Changes in Gold-Thiolate Monolayer-Protected Nanoparticle Sensor Films," *Anal. Chem.*, **2007**, *79*, 4977-4986.
43. Wright, L. K.; Zellers, E. T. "A Nanoparticle-Coated Chemiresistor Array as Microscale Gas Chromatograph Detector for Explosive Marker Compounds: Flow Rate and Temperature Effects," *Analyst*, **2013**, *138*, 6860-6868.
44. Haiss, W.; Thanh, N. T. K.; Aveyard, J.; Fernig, D. G. "Determination of Size and Concentration of Gold Nanoparticles from UV-Vis Spectra," *Anal. Chem.*, **2007**, *79*, 4215-4221.
45. Link, S.; El-Sayed, M. A. "Size and Temperature Dependence of the Plasmon Absorption of Colloidal Gold Nanoparticles," *J. Phys. Chem. B*, **1999**, *103*, 4212-4217.
46. Njoki, P. N.; Lim, I-I. S.; Mott, D.; Park, H-Y.; Khan, B.; Mishra, S.; Sujakumar, R.; Luo, J.; Zhong, C-J. "Size Correlation of Optical and Spectroscopic Properties for Gold Nanoparticles," *J. Phys. Chem. C*, **2007**, *111*, 14664-14669.
47. Chou, A.; Vernon, K. C.; Piro, L.; Radi, B.; Jaatinen, E. A.; Davis, T. J. "Predicting the Localized Surface Plasmon Resonances of Spherical Nanoparticles on a Substrate: Electrostatic Eigenmode Method," *J. Phys. Chem. C*, **2012**, *116*, 26517-26522.

48. Wuelfing, W. P.; Green, S. J.; Pietron, J. J.; Cliffel, D. E.; Murray, R. W. "Electronic Conductivity of Solid-State, Mixed-Valent Monolayer-Protected Au Clusters," *J. Am. Chem. Soc.*, **2000**, *122*(46), 11465-11472.
49. Bian, K.; Choi, J. J. Kaushik, A.; Clancy, P.; Smilgies, D-M.; Hanrath, T. "Shape-Anisotropy Driven Symmetry Transformations in Nanocrystal Superlattice Polymorphs," *ACS Nano*, **2011**, *5* (4), 2815-2823.
50. Wan, Y.; Goubet, N.; Albouy, P-A.; Schaeffer, N.; Pileni, M-P. "Hierarchy in Au Nanocrystal Ordering in a Supracrystal: II Control of Interparticle Distances," *Langmuir*, **2013**, *29*, 13576-13581.
51. Wang, G. R.; Wang, L.; Rendeng, Q.; Wang, J.; Luo, J.; Zhong, C-J. "Correlation Between Nanostructural Parameters and Conductivity Properties for Molecularly-Mediated Thin Film Assemblies of Gold Nanoparticles," *J. Mater. Chem.*, **2007**, *17*, 457-462.

Table 4-1. Physical properties of the six test compounds, estimated partition coefficients and associated relative mass and volume of each vapor at 50% saturation (C_{sat}), and optical response data of the MPN types tested (also at 50% C_{sat}).

MPN (RI)		Vapor					
		PCE	TOL	OCT	BAC	MEK	IPA
	RI[a]	1.505	1.496	1.398	1.394	1.379	1.377
	ρ[b]	1.620	0.870	0.703	0.883	0.805	0.786
	$0.5\ C_{sat}$[c]	57,900	54,400	33,700	25,000	137,000	53,200
	α[d]	12.07	12.40	15.60	12.57	8.25	6.98
C8	K[e]	1218	1039	1697	648	145	152
(1.452)	m_{vapor}[f]	1.00	0.80	0.81	0.23	0.28	0.11
	v_{vapor}[g]	0.53	0.80	1.00	0.22	0.30	0.13
	$\Delta\lambda_{max}$[h]	-4.5	-7.0	-6.9	-3.1	-2.6	0.0
DPA	K[e]	886	984	1092	927	365	260
(1.659)	m_{vapor}[f]	0.96	1.00	0.69	0.43	0.94	0.26
	v_{vapor}[g]	0.51	0.99	0.84	0.42	1.00	0.28
	$\Delta\lambda_{max}$[h†]	–	–	–	–	–	–
OPH	K[e]	1840	2382	3484	1453	391	318
(1.521)	m_{vapor}[f]	0.82	1.00	0.91	0.28	0.41	0.13
	v_{vapor}[g]	0.39	0.89	1.00	0.25	0.40	0.13
	$\Delta\lambda_{max}$[h]	-1.7	-5.7	-2.0	-2.4	-1.4	-0.1
HME	K[e]	285	368	415	291	125	184
(1.459)	m_{vapor}[f]	0.82	1.00	0.70	0.36	0.86	0.49
	v_{vapor}[g]	0.44	1.00	0.87	0.36	0.93	0.54
	$\Delta\lambda_{max}$[h]	-1.8	-3.6	-0.7	-3.3	-4.4	-0.7
TEG	K[e]	165	269	190	314	111	114
(1.489)	m_{vapor}[f]	0.63	0.96	0.42	0.51	1.00	0.40
	v_{vapor}[g]	0.31	0.89	0.48	0.47	1.00	0.41
	$\Delta\lambda_{max}$[h]	-4.2	-4.9	-0.4	-1.1	-3.9	-2.0
DTE_5	K[e]	3831	7472	6741	3795	989	393
(1.484)	m_{vapor}[f]	0.55	1.00	0.56	0.23	0.33	0.05
	v_{vapor}[g]	0.29	1.00	0.69	0.23	0.36	0.06
	$\Delta\lambda_{max}$[h]	-0.7	-0.8	-0.9	-0.5	-0.3	-0.3
DTE_{40}	$\Delta\lambda_{max}$[h†]	–	–	–	–	–	–
(1.484)							

[a]RI = refractive index; [b]ρ = density of liquid analyte (g/mL); [c]C_{sat} = saturated vapor concentration (mg/m^3); [d]α = polarizability; [e]K = partition coefficient determined by TSMR measurements at a concentration range of 1-10% of C_{sat}; [f]m_{vapor}= relative mass of vapor within film at saturation, estimated by K x 0.5C_{sat},; [g]v_{vapor} = relative sorbed volume of vapor within the film at saturation, estimated by m_{vapor}/ρ; [h]$\Delta\lambda_{max}$ = shift in wavelength (nm) at the LSPR maximum upon vapor exposure, where negative and positive values denote blue and red shifts, respectively. [†]λ_{max} could not be defined due to broad peaks.

Table 4-2. Pair-wise correlation coefficients, r, derived from the average responses of each plasmonic MPN sensor at the three probing wavelengths and average recognition rates (RR, %) derived from Monte Carlo/Euclidean distance classification model analyses (ε = 5%) across all six individual vapors (50% C_{sat}). The range of RRs is also given for each MPN.

MPN Type	Correlation Coefficient (r)			RR_{avg} (%)	RR_{min} (%)	RR_{max} (%)
	405 nm, 532 nm	405 nm, 630 nm	532 nm, 630 nm			
C8	0.96	0.62	0.48	98.4	96.6	100
DPA	0.99	-0.37	-0.42	51.5	21.2	73.4
OPH	0.99	0.95	0.98	81.7	59.2	97.7
HME	0.73	0.96	0.62	95.0	87.6	100
TEG	0.057	0.84	-0.26	86.3	74.8	100
DTE_5	0.98	0.93	0.86	82.0	55.4	98.6
DTE_{40}	0.91	0.98	0.98	99.9	87.4	100

Table 4-3. Recognition rates (RR, %) estimated from Monte Carlo simulations (ε = 5%) followed by PC-based classification of normalized responses from the top-performing 3-TSMR, 3-CR, 2-TSMR, and 2-CR arrays.

Array Composition			RR (%)
3- TSMR			
C8	DPA	DTE_5	99.7
C8	TEG	DTE_5	99.2
DPA	OPH	DTE_5	99.2
HME	TEG	DTE_5	99.1
DPA	TEG	DTE_5	98.7
3-CR			
C8	DPA	HME	99.5
C8	OPH	HME	99.1
C8	HME	TEG	99.1
OPH	HME	TEG	96.2
C8	DPA	TEG	95.4
2-TSMR			
OPH	TEG		96.4
TEG	DTE_5		93.9
C8	DPA		87.7
DPA	OPH		86.9
DPA	DTE_5		86.8
2-CR			
C8	HME		93.3
C8	TEG		92.6
OPH	HME		89.8
C8	DPA		83.7
DPA	OPH		78.9

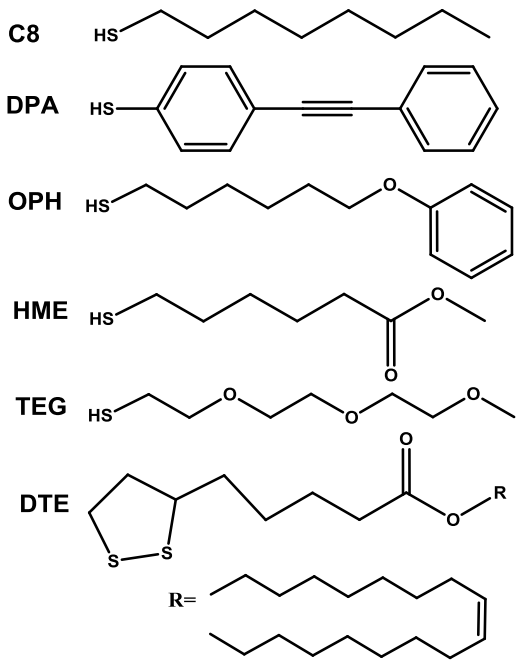

Figure 4-1. Structures of the thiols and the dithiane used in this study.

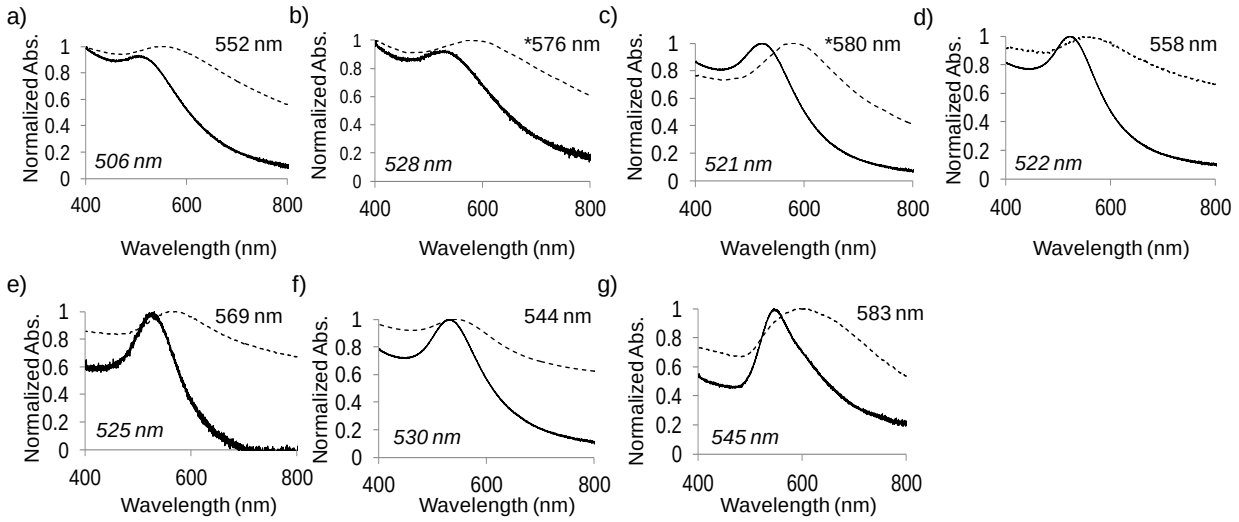

Figure 4-2. Normalized LSPR baseline spectra of (a) C8 (b) DPA (c) OPH (d) HME (e) TEG (f) DTE_5 and (g) DTE_{40}, in the solution phase (solid lines) and as dried films (dashed lines), where the value of λ_{max} for the film is given in the upper right side of each panel and that of the solution phase is given in the lower left of each panel. *λ_{max} of DPA after initial exposure to an atmosphere of saturated toluene shifted to 629 nm; λ_{max} of an additional OPH film started at 613 nm.

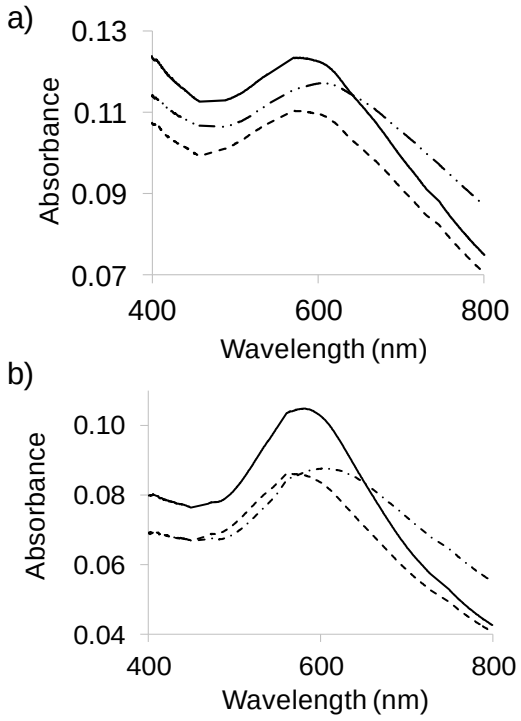

Figure 4-3. LSPR response to a saturated atmosphere of TOL and the incomplete recovery of (a) DPA and (b) OPH films (baseline spectra = solid line; spectra upon dosing = dashed line; spectra after 24 h recovery = dotted-dashed line). All other MPN films tested returned fully or approximately back to the baseline.

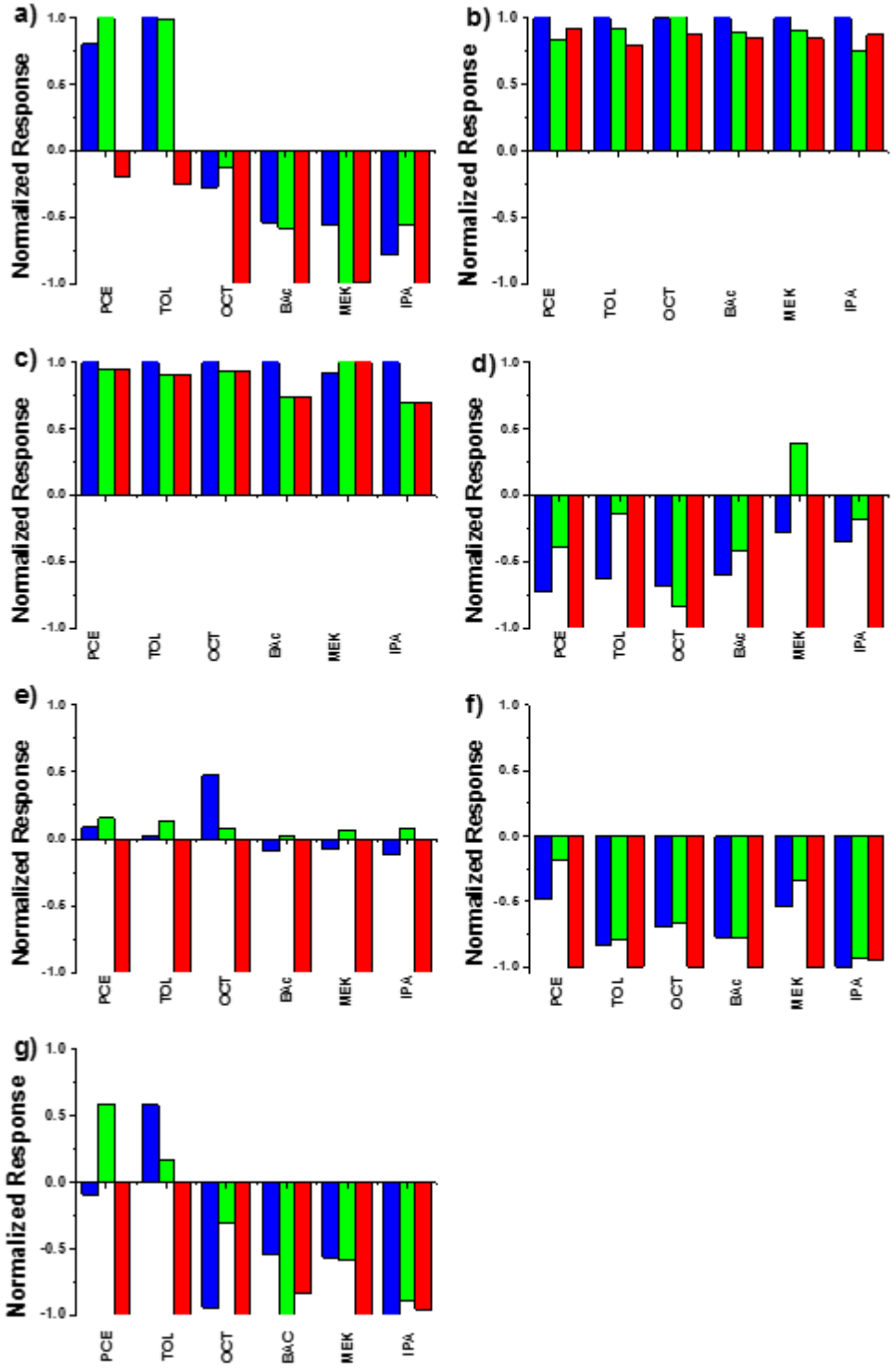

Figure 4-4. Response patterns from transmission measurements of the six plasmonic MPN films exposed to each of six test vapors at 50% C_{sat}. Each 3-wavelength pattern is normalized to the wavelength of largest response for (a) C8 (b) DPA (c) OPH (d) HME (e) TEG (f) DTE_5 and (g) DTE_{40}. Wavelengths: from left to right: blue = 405; green = 532; red = 630.

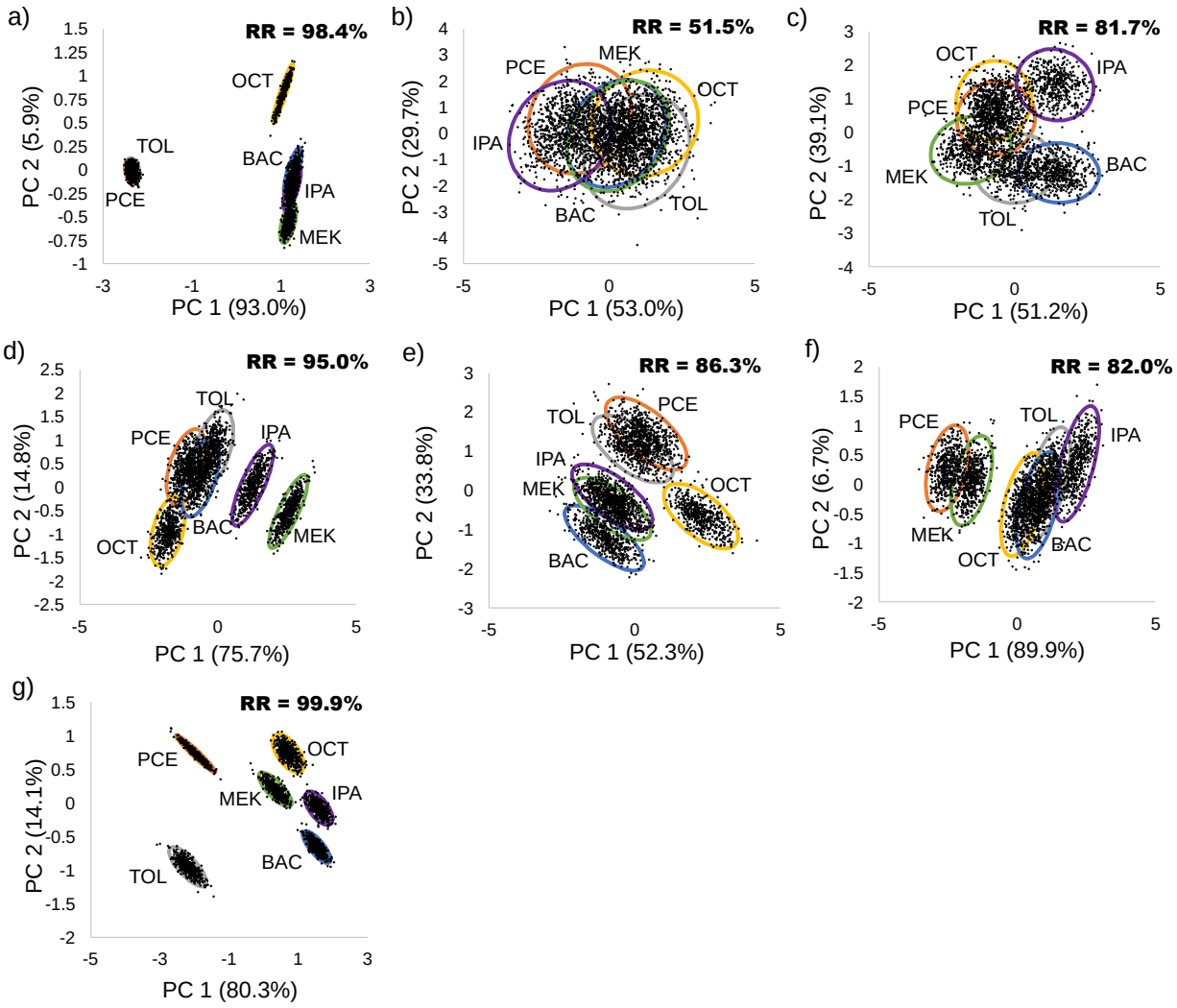

Figure 4-5. Principal components analysis (PCA) scores plots for individual vapors in 50% saturated concentration and the following LSPR sensors: (a) C8 (b) DPA (c) OPH (d) HME (e) TEG (f) DTE_5 and (g) DTE_{40}. The 95% confidence ellipses were calculated from simulated response vectors derived from the experimental data set with 5% random error and 1% baseline noise.

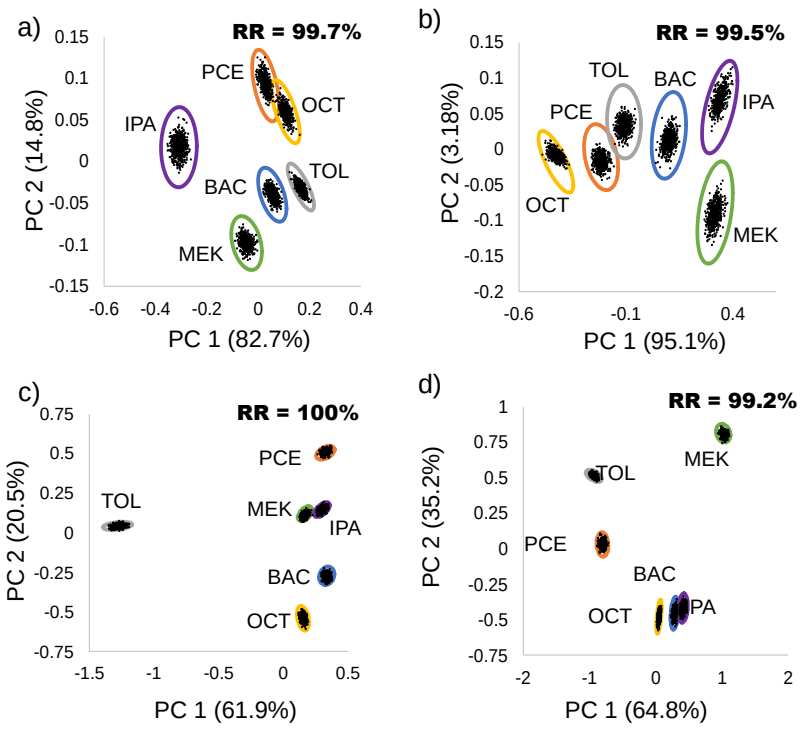

Figure 4-6. Principal components analysis (PCA) scores plots for individual vapors and the best performing (a) 3-TSMR array, C8 + DPA + DTE_5, (b) 3-CR array, C8 + DPA + HME, (c) 2-LSPR array, C8 + HME, and (d) 2-LSPR array (1 wavelength response per MPN film), C8 (532 nm) + HME (532 nm). The 95% confidence ellipses were calculated from simulated response vectors derived from the experimental data set with 5% random error. The LSPR scores plots are based on data collected at 50% C_{sat}.

CHAPTER V

CONCLUSIONS AND FUTURE WORK

5.1 Conclusions

The need to quantitatively analyze volatile and semi-volatile organic compounds (VOCs and SVOCs, respectively) in a complex background is important to today's society, from environmental monitoring to disease diagnosis. In order to determine compounds of interest at the low concentration levels typically encountered in these types of applications, the use of a portable and inexpensive instrument with a sensitive detector is required. Current portable instrumentation falls short of these essential criteria and recent research has been focused on the development of microfabricated gas chromatographs (μGC) utilizing low-power, cost efficient μsensor arrays as the detectors. This dissertation describes a series of projects directed at improving vapor μsensor arrays designed for use as detectors in a μGC for the recognition and quantification of airborne VOCs found in complex mixtures. The specific aims were 1) to optimize the operating conditions of a single nanoparticle-coated chemiresistor (CR) array as a detector in a μGC prototype for the analysis of explosive marker compounds, 2) to determine whether combining sensors operating on different transduction principles into multi-transducer (MT) arrays enhances vapor discrimination, and 3) to investigate the increase in response diversity afforded by use of so-called plasmonic multi-variable (MV) sensors and arrays.

The research presented herein has focused on enhancing vapor discrimination with microsensor arrays that utilize thiolate monolayer-protected gold nanoparticles (MPNs) as

interface layers. Microsensors with interface layers consisting of MPNs with thiolates having different functionalities are assembled into arrays and the differential sorption afforded by the array is equivalent to a crude pattern/spectrum that can assist in identifying various VOCs. The response diversity achieved by these types of sensor arrays is limited by the energies spanned by the non-bonding, reversible interactions governing sorption. Standalone arrays, however, cannot discriminate a mixture of more than three components from lower order mixtures and their individual components. Here, we have investigated several approaches to enhancing the response diversity of sorption-based μsensor arrays. Chapter 2 concerned integrating an MPN-coated chemiresistor (CR) array with an upstream μGC separation module for the detection of explosive marker compounds. Variables, such as temperature and flow rate were optimized in order to detect the marker compounds among a set of interferences. Chapter 3 used an extant data base of responses from MPN-coated CRs and similarly coated thickness shear mode resonators (TSMRs) in chemometric analyses coupled with Monte Carlo simulations to compare single transducer (ST) and MT arrays with respect to response diversity for a set of five individual vapors and their binary mixtures. In Chapter 4, the optical transmission measurements were collected from seven MPN films with different ligand functionalities and gold core sizes exhibiting localized surface plasmon resonance (LSPR).

Each of these independent yet interrelated projects contributed to the overall goals of this dissertation. The major results from the body of this work are summarized briefly below. An MPN-coated CR array was integrated into a μGC for the rapid determinations of trinitrotoluene (TNT) marker compounds for the ultimate use in the screening of luggage and personnel at airports. Changes in flow rate and array temperature resulted in tradeoffs among sensitivity, detectability, and chromatographic resolution of the targets: 2,3-dimethyl-2,3-dinitrobutane

(DMNB), 2,4-dinitroltuene (2,4-DNT), and 2,6-dinitrotoluene (2,6-DNT) from closely eluting interferences. Under the optimized conditions, a complete analysis was completed in < 2 minutes, the two primary targets (2,4-DNT and DMNB) were separated and discriminated from alkanes of similar volatility, and the limits of detection (LOD) were ≤ 4 ng from all sensors in the array. Because the three markers have very low vapor pressures (≤ 10^{-4} kPa), it was necessary to operate the sensor array at temperatures higher than those studied previously to reduce peak broadening due to slow evaporation from the MPN films. Although the operating flow rate is constrained by the injection bandwidth of the preconcentrator/focuser and the chromatographic efficiency, the effect of this variable on the array was evaluated. The following peak parameters were investigated over the range of flow rates (~1-4 mL/min) and temperatures (50-80°C) examined: area (*A*), height (*H*), full width at half maximum ($W_{1/2}$), asymmetry factor (*AF*), and retention time (t_R). The peak metrics used to characterize the sensor performance at a given flow rate and temperature include sensitivity, chromatographic resolution (R_s), limits of detection (LOD).

The medium-term response stability was assessed by calibrating the array to toluene at 30°C and 70°C over the course of 11 days, where sensitivity values and response patterns virtually did not change. On the basis of these findings, the MPN-coated CR arrays were proven to be sufficiently stable in air at 70°C to provide reliable detector performance in μGC field applications using air as the carrier gas. Results showed that increasing the temperature from 55-80°C led to similar decreases in sensitivity (denoted by changes in *A*) among the sensors in the array, increases in the LODs (derived from *H*), and increases in estimated R_s. The decreases in *A* and *H* were expected due to the decreases in the partition coefficients and increases in the diffusion rates in/out of the MPN films at higher temperatures. Increasing the flow rate from

1.1-3.7 mL/min led to decreases in sensitivity and LOD for 2,4-DNT and 2,6-DNT, a net increase in LOD for DMNB, and an increase in R_s. The changes in the performance parameters accompanying changes in flow rate, reflected the influence of multiple factors that led to both vapor- and film-specific flow rate dependencies. These factors include the mass transport within the MPN films, dilution of the air concentrations of the markers with increasing flow rates, and the evaporation rate of the sorbed markers. The rate limiting factor appeared to be the evaporation rate, where alkane interferences of similar volatility did not exhibit the same degree of peak tailing as the marker compounds. Although the slower evaporation rates of the markers was responsible for the lag in mass transport, it should be noted that increased film thickness can also cause slower desorption rates. Taking into account the tradeoffs associated with temperature and flow rate, as well as the factors that affect the performance of the other components of the μGC, a flow rate of 3 mL/min and a temperature of 70°C were selected. These findings have broad implications for any type of sorptive-based sensor arrays used in the detection of semi-volatile organic compounds (SVOCs), i.e. the importance of tightly controlling the temperature and flow rate of operation and controlling the film thickness.

Although this project examined the medium-term stability of these sensor arrays in air at elevated temperatures, the long-term response stability should also be assessed before potential use in a fieldable μGC. Additionally, significant differences in retention time and the degree of peak tailing were observed for the different sensors in the array, arising from differences of evaporation rate on the peak profile. This could have serious implications on detectability if peaks from interferences of similar volatility would overlap with those of the target compounds and on the accuracy of pattern recognition algorithms used to identify the compounds. In order to remediate this problem, the sensor design and film deposition methods should be re-evaluated.

First, the flow path of the sensor array should be re-designed to ensure even mixing of the analytes within the detector cell. Second, a study should be conducted in order to improve the coating method to better control the film thickness, and thus, reduce the impact of this variable on differences in desorption rates.

Chapter 3 used an existing data set of sensor responses from four MPN-coated CRs and four similarly coated thickness shear mode resonators (TSMRs) to five individual vapors to explore whether arrays of vapor sensors from two different types of transducers could provide greater response diversity than arrays of a single transducer (ST) type. The pooled set of 40 vapor-sensor sensitivities was analyzed using principal components regression models in conjunction with Monte Carlo simulations to evaluate the classification performance with different levels of random error superimposed on the sensor responses. Recognition rates (RR) were estimated for the individual vapors and binary mixtures with all possible combinations of ST and multi-transducer (MT) arrays.

Results demonstrated that MT arrays can provide greater diversity than ST arrays of similar dimension, although differences were often marginal and exceptions did occur. The specific sensors included in the MT array were critical. Interestingly, standard correlation metrics fell short of assessing the complementarity between two sensors. The best overall performance was obtained with an MT array of n= 4 sensors, and the performance of MT arrays did not improve for $4 < n \leq 8$. The relatively facile problem of discriminating among a set of individual vapors could be solved using both types of 4-sensor ST arrays and numerous 4-MT arrays (ε = 5%), where the best 4-MT array provided an average RR of 99.7% and the corresponding average RRs for the all-CR and all-TSMR 4-sensor ST arrays were both ~97%. No single array of any type, however, provided universally optimal performance for the 10

binary mixtures, despite the problem being constrained to only whether either or both components were present in the mixture. The best 4-MT array provided an average RR of 74.7% and the corresponding all-CR and all-TSMR 4-sensor ST arrays provided an average RR of ~69% for the 10 binary mixtures from their components. Additionally, six out of the 10 binary mixtures analyzed could not be determined with high enough RRs with any single array. This work highlights the importance of coupling ST and MT arrays with an upstream chromatographic separation module in order to avoid falling victim to the limited vapor recognition capabilities that they offer.

Because it was found that MT arrays of different composition were required to effectively analyze the 10 different binary mixtures, future work could examine the possibility of using a large MT array as a GC detector and down-selecting subsets of an array in order to analyze different overlapping peaks given the mixture composition ahead of time. This could be built into chemometric software routines in such systems. Additionally, MT arrays including different transducers should also be investigated.

In Chapter 4, the plasmonic behavior of the MPN films was exploited by assessing the changes in the absorbance spectrum at three probing wavelengths upon vapor exposure. A set of seven MPN films containing different ligand functionalities and Au core diameters between 4 and 40 nm were exposed to six individual vapors. The swelling-induced increases in the interparticle distance, δ, and changes in the effective refractive index, RI_{eff}, led to spectral shifts that generally differed for each vapor-MPN film pair. Differences in the average particle size, the polydispersity of the particle size, and the ligand affect the LSPR. Normalized response patterns were derived from shift in absorbance at the three probing wavelengths, taking into account the differences in the magnitude and sign of the response at a given wavelength. The

vapor-sensor responses were analyzed using principal components analysis (PCA) in conjunction with Monte Carlo simulations to evaluate the performance of a given film with ε = 5% and average RRs were estimated. The higher value of ε was representative of the variability observed in duplicate measurements among this data set.

Absorbance decreases and blue shifts in the wavelength of maximum absorbance, λ_{max}, were generally observed. This was consistent with theory which predicts such changes upon a decrease of the RI_{eff} and a swelling-induced increase in δ. That blue shifts in λ_{max} still occurred for higher RI analytes, indicated that swelling generally dominated the response.

The performance of the MPN films followed what would be expected on the basis of cluster separation distance in the PCA scores plots. Vapor discrimination was achieved with three individual MPN films (C8, HME, DTE_{40}). Virtually every array consisting of just 2 films could also achieve this level of discrimination (RR > 95%). Furthermore, down selecting the wavelength responses of one 2-film array showed that this level of discrimination could be achieved with as little as one wavelength response from each MPN film in the array. The performance of these arrays was compared to similarly coated 3-CR and 3-TSMR arrays. Results showed that the same level of discrimination achieved with 3-CR and 3-TSMR arrays could be achieved with fewer plasmonic films. These results show promise in miniaturizing these and similar types of sensor arrays.

Although this project was successful in identifying which MPN films to possibly pursue further, several issues arose that deserve mention here, and that should be considered in future work related to MPNs as interface layers for optical sensing. First, differences in film morphology and uniformity are believed to be the reason for inconsistencies in the sensor responses. Responses varied from film to film containing the same MPN type, in which the

magnitude and sign of the response differed. Spin coating was unsuccessful in yielding reproducible responses, despite producing more uniform films. Future studies should look at additional ways to improve the film quality, i.e. investigating additional surface pre-treatments and exploring layer-by-layer self-assembly. Second, these films were not very sensitive. This led to tests being performed at half of the saturated vapor concentration. Increasing the baseline absorbance by stacking multiple films together may increase the sensitivity of these films, which would allow testing at lower concentrations. Lastly, agglomeration apparently occurred with several films upon testing at high concentrations or upon coating. Improving the film uniformity may help to control the agglomeration that occurs upon coating. Future work will investigate why certain MPN types are more prone to agglomeration than others. These tests were performed as a preface to exploring MPN-coated microfabricated optofluidic ring resonators (μOFRRs). Improving the film uniformity is also extremely important to utilizing these materials as interface layers in μOFRRs in order to support the resonating modes used in these devices. Additionally, a bonafide statistical analysis should be performed in order to determine exactly how many and which wavelengths would provide the most complementarity in responses among the MPN types chosen.

In conclusion, this dissertation has addressed many of the advantages, disadvantages, and challenges associated with using MPNs as interface layers in vapor sensor arrays. This research highlighted the performance of MPN-coated sensor arrays when integrated into a μGC and used on multiple transducers. It became evident, however, that differences in film uniformity and film morphology have negative implications on using these materials as interface layers on optical sensors as it stands now. Future work needs to investigate ways to improve the film uniformity, i.e. surface pretreatment and alternative deposition methods, in order to improve the response

reproducibility among different films. This research has made significant contributions to sorption-based sensor arrays using MPN films as interface layers, including the importance of film morphology on the sensor response.

APPENDIX A

SUPPLEMENTARY INFORMATION FOR CH. II

Table A.1. 90-day stability test results showing the extent of drift in average sensitivities for an MPN-coated CR array between Day 1 and Day 90 (see Figure 2-1).

Analyte	Avg. Sensitivity Change	Correlation Coefficient (r^2)[a]
Toluene	+11.7%	0.99
n-Propanol	+34.6%	0.97
2-Butanone	+16.0%	0.99
Octane	+12.0%	0.99
Nitromethane	+1.6%	0.99

[a] determined from linear regression of the sensitivities of all 4 sensors in the array on Day 90 onto to those on Day 1.

Table A.2. Peak asymmetry factors (*AF*) for the marker compounds from each sensor at the lowest and highest temperatures and a flow rate of 1.2 mL/min.

MPN	DMNB		2,6-DNT		2,4-DNT	
	55°C	80°C	55°C	80°C	55°C	80°C
C8	1.8	1.7	1.5	1.3	3.1	2.6
DPA	1.9	1.7	2.2	2.0	3.4	2.6
OPH	2.6	2.2	3.0	2.5	4.3	3.0
HME	1.8	1.5	2.5	2.3	3.9	3.0

Table A.3. Peak asymmetry factors (*AF*) for the marker compounds from each sensor at the lowest and highest flow rates and an array temperature of 70°C.

MPN	DMNB		2,6-DNT		2,4-DNT	
	1.1 mL/min	3.7 mL/min	1.1 mL/min	3.7 mL/min	1.1 mL/min	3.7 mL/min
C8	1.4	1.2	2.5	2.0	2.3	2.0
DPA	1.5	1.4	2.5	2.1	3.2	2.6
OPH	2.1	1.7	4.2	3.0	4.2	3.1
HME	1.7	1.5	2.8	2.5	4.0	3.3

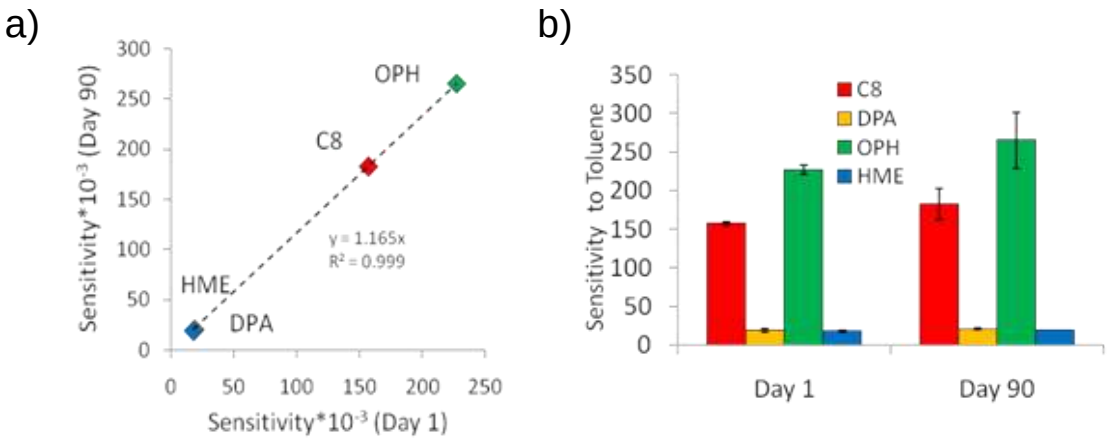

Figure A.1. (a) Correlation of responses to toluene vapor on Day 1 vs. Day 90. Slope of 1.16 reflects the positive drift in sensitivities, but the large correlation coefficient indicates a common-mode source of such drift and the retention of relative sensitivities among the sensors in the array; (b) absolute response patterns among the sensors, confirming the stability of relative sensitivities over time. Similar results were found for the other vapors in Table 2-A.1.

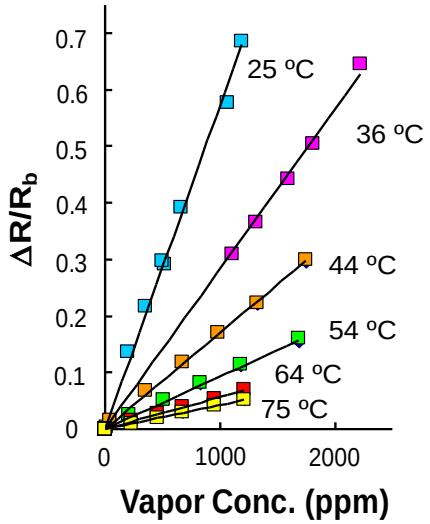

Figure A.2. Calibration curves for 2-propylbenzene from a representative C8-MPN coated CR sensor showing a reduction in sensitivity with increasing temperature but retention of linearity (stability).

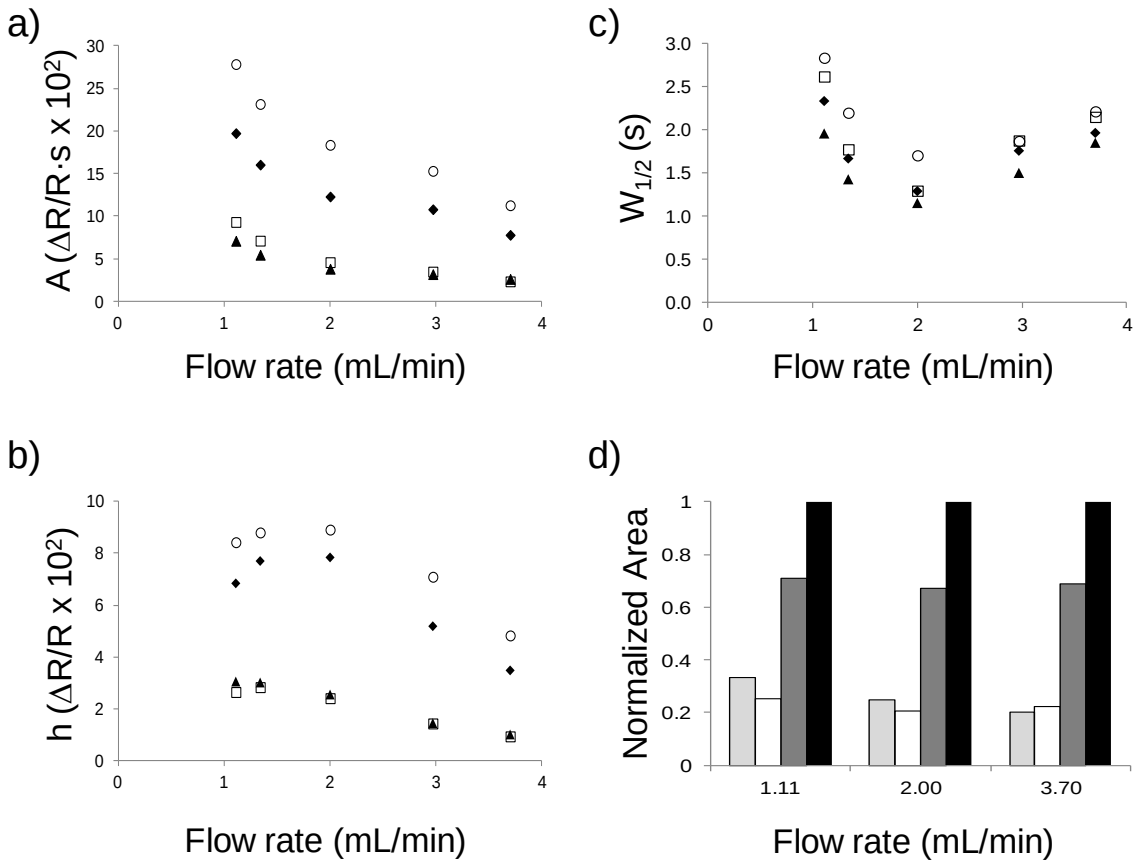

Figure A.3. Effects of flow rate on peak parameters for DMNB: (a) *A*; (b) *H*; (c) $W_{½}$; (d) relative response patterns (from peak areas). Legend: C8 (□), DPA (▲), OPH (♦), HME (○); bar chart, from left to right: C8, DPA, OPH, HME.

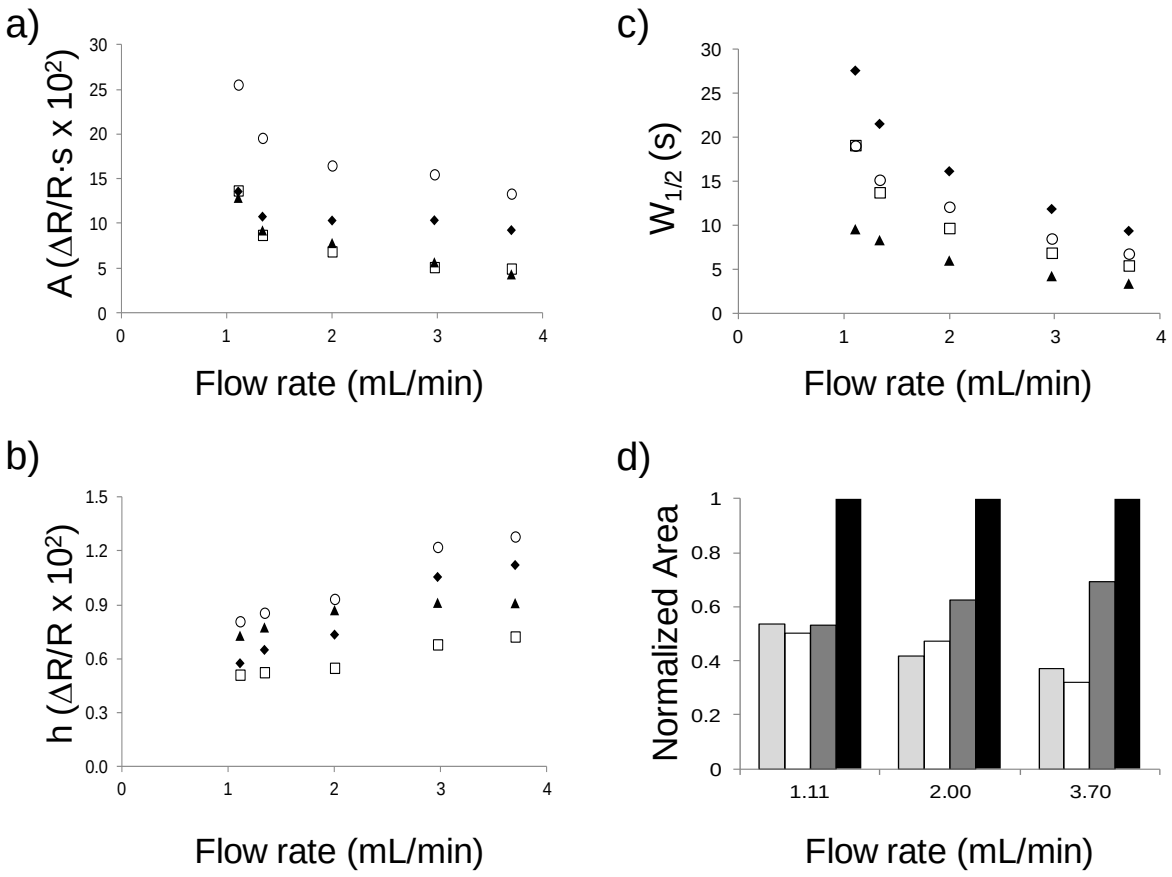

Figure A.4. Effects of flow rate on peak parameters for 2,6-DNT: (a) *A*; (b) *H*; (c) *W½*; (d) relative response patterns (from peak areas). Legend: C8 (□), DPA (▲), OPH (♦), HME (○); bar chart, from left to right: C8, DPA, OPH, HME.

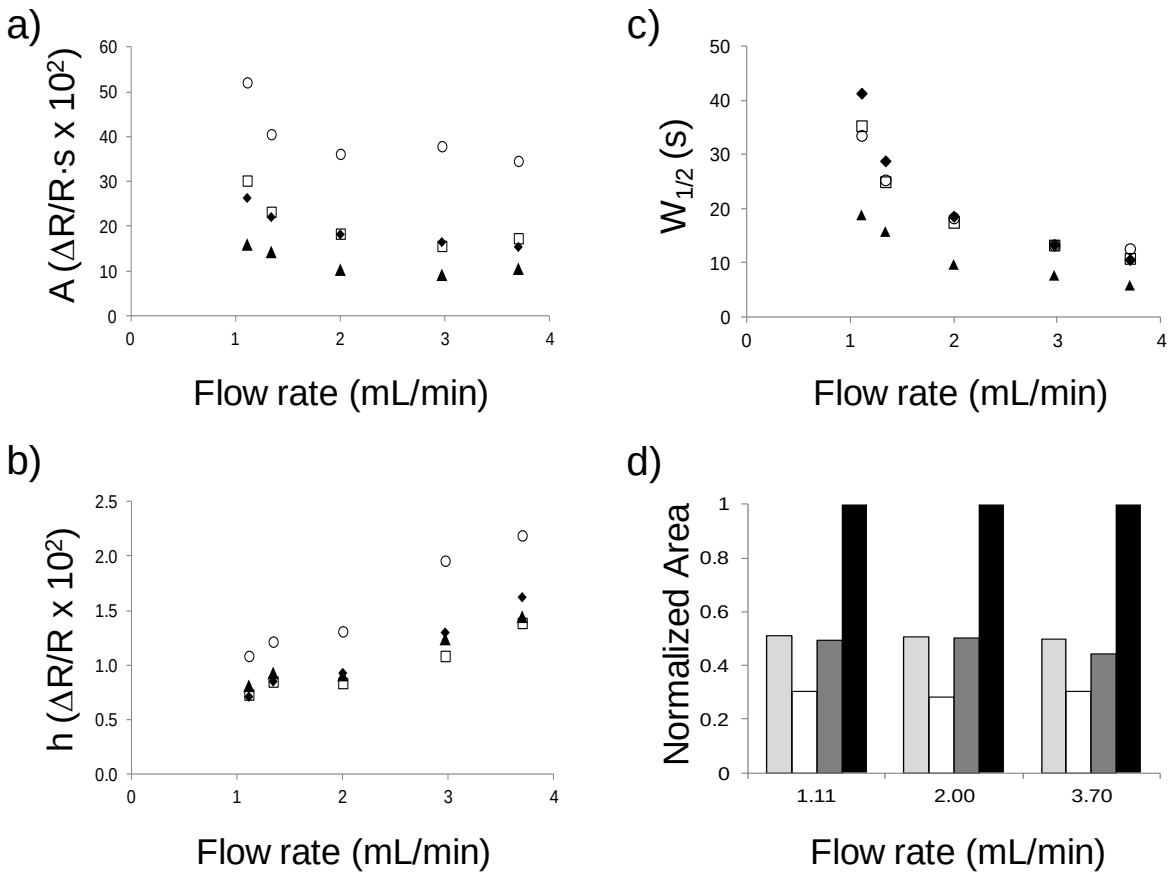

Figure A.5. Effects of flow rate on peak parameters for 2,4-DNT: (a) *A*; (b) *H*; (c) $W_{½}$; (d) relative response patterns (from peak areas). Legend: C8 (□), DPA (▲), OPH (♦), HME (○); bar chart, from left to right: C8, DPA, OPH, HME.

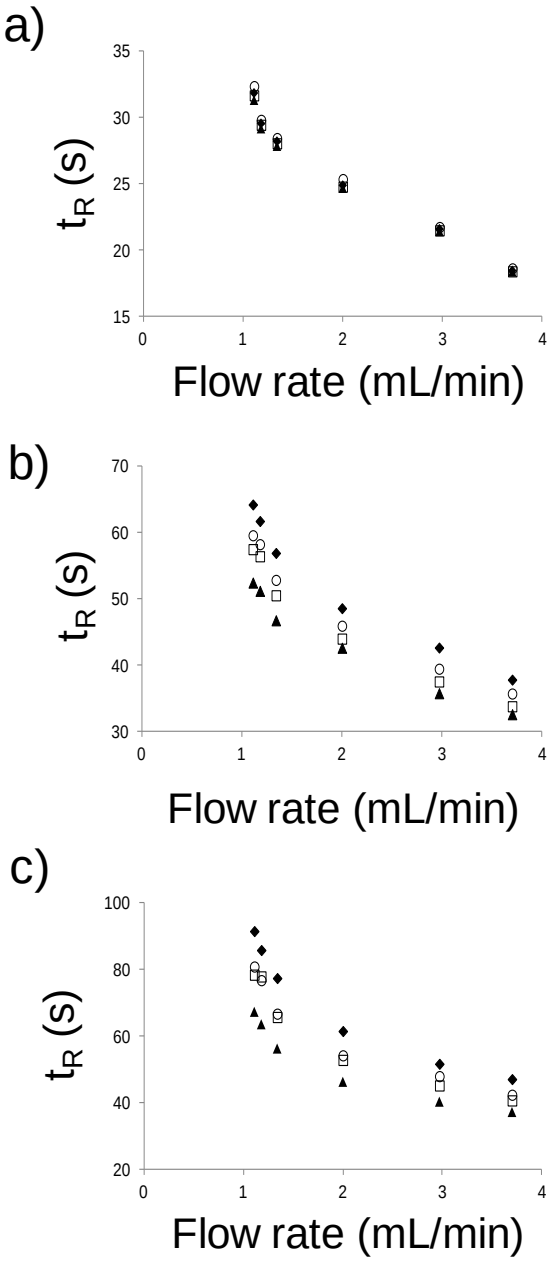

Figure A.6. Effect of flow rate on t_R for (a) DMNB, (b) 2,6-DNT, and (c) 2,4-DNT. Legend: C8 (□), DPA (▲), OPH (♦), HME (○).

APPENDIX B

SUPPLEMENTARY INFORMATION FOR CH. IV

Table B.1. Sensitivities [($\Delta abs/abs_{ppm}$)/ (mg/m^3)] of MPN films probed optically at 405 nm.

Vapor	MPN Type						
	C8	DPA	OPH	HME	TEG	DTE_5	DTE_{40}
PCE	1.08	1.86	2.03	-2.19	0.41	-1.82	-0.02
TOL	1.80	1.81	2.19	-1.69	0.15	-5.62	0.15
OCT	-1.27	1.18	0.44	-1.39	0.94	-4.83	-0.95
BAC	-1.35	1.40	1.70	-1.99	-1.83	-3.10	-1.95
MEK	-0.24	1.11	0.44	-0.39	-0.25	-1.50	-0.29
IPA	-0.30	0.40	0.16	-0.59	-0.54	-1.68	-0.64

Table B.2. Sensitivities [($\Delta abs/abs_{ppm}$)/ (mg/m^3)] of MPN films probed optically at 532 nm.

Vapor	MPN Type						
	C8	DPA	OPH	HME	TEG	DTE_5	DTE_{40}
PCE	1.34	1.56	1.92	-1.18	0.73	-0.69	0.14
TOL	1.77	1.67	1.98	-0.37	1.11	-5.31	0.04
OCT	-0.58	1.18	0.41	-1.72	0.16	-4.64	-0.29
BAC	-1.46	1.25	1.26	-1.38	0.45	-3.12	-3.42
MEK	-0.43	1.01	0.48	0.56	0.20	-0.93	-0.28
IPA	-0.21	0.31	0.11	-0.31	0.36	-1.57	-0.58

Table B.3. Sensitivities [($\Delta abs/abs_{ppm}$)/ (mg/m^3)] of MPN films probed optically at 630 nm.

Vapor	MPN Type						
	C8	DPA	OPH	HME	TEG	DTE_5	DTE_{40}
PCE	-0.25	1.71	1.41	-3.03	-4.70	-3.77	-0.23
TOL	-0.45	8.61	1.15	-2.67	-8.31	-6.70	-0.24
OCT	-4.64	1.03	0.33	-2.05	-1.96	-6.94	-0.93
BAC	-2.51	1.19	0.76	-3.30	-18.92	-4.00	-2.78
MEK	-0.42	0.94	0.29	-1.42	-3.32	-2.79	-0.47
IPA	-0.38	0.35	0.10	-1.72	-4.57	-1.60	-0.61

Table B.4. Sensitivities for the TSMR and CR devices.

	Vapor					
	PCE	TOL	OCT	BAC	MEK	IPA
MPN Type	TSMR[a]					
C8	0.28 (0.99)	0.24 (0.99)	0.39 (0.99)	0.15 (0.99)	0.034 (0.99)	0.035 (0.98)
DPA	0.21 (0.99)	0.23 (0.99)	0.26 (0.99)	0.22 (0.99)	0.087 (0.99)	0.062 (0.99)
OPH	0.35 (0.99)	0.46 (0.99)	0.67 (0.99)	0.28 (0.99)	0.075 (0.99)	0.061 (0.99)
HME	0.066 (0.99)	0.086 (0.97)	0.096 (0.98)	0.068 (0.99)	0.029 (0.98)	0.043 (0.98)
TEG	0.038 (0.99)	0.063 (0.99)	0.044 (0.95)	0.073 (0.99)	0.026 (0.99)	0.027 (0.98)
DTE_5	0.89 (0.96)	1.74 (0.95)	1.57 (0.99)	0.88 (0.98)	0.23 (0.99)	0.091 (0.99)
MPN Type	CR[b]					
C8	1.88 (0.99)	3.84 (0.99)	4.20 (0.99)	2.09 (0.99)	0.62 (0.99)	0.60 (0.99)
DPA	0.48 (0.98)	0.98 (0.99)	0.57 (0.99)	0.87 (0.99)	0.51 (0.99)	0.33 (0.99)
OPH	1.14 (0.99)	2.54 (0.99)	1.89 (0.99)	1.86 (0.99)	0.65 (0.99)	0.34 (0.99)
HME	0.90 (0.99)	2.45 (0.99)	1.05 (0.99)	2.04 (0.99)	0.92 (0.99)	1.02 (0.99)
TEG	1.40 (0.99)	3.32 (0.99)	1.91 (0.99)	3.49 (0.99)	1.25 (0.99)	1.80 (0.99)

[a]TSMR sensitivities are given in $[(\Delta f/f)_{ppm}/(mg/m^3)]$; [b]CR sensitivities are given in $[(\Delta R/R)_{ppm}/(mg/m^3)]$. R^2 values are given in parentheses.

Table B.5. Limits of detection (LOD; mg/m^3) for the TSMR and CR devices.

	Vapor					
	PCE	TOL	OCT	BAC	MEK	IPA
MPN Type	TSMR					
C8	10.7	13	7.7	20.2	90	86
DPA	36	32	29	34	88	122
OPH	3.2	2.5	1.7	4.1	15	19
HME	29	23	20.1	29	67	45
TEG	247	151	215	130	367	357
DTE_5	9.7	4.9	5.5	9.8	38	95
MPN Type	CR					
C8	54	26	24	48	163	168
DPA	60	29	50	33	59	87
OPH	82	37	50	51	144	275
HME	107	39	93	47	104	94
TEG	95	40	69	38	105	74

Table B.6. Limits of detection (LOD) for the test vapors with the C8 film derived from calibrations of transmission measurements.

	Vapor					
	PCE	TOL	OCT	BAC	MEK	IPA
LOD (% C_{sat})	2.1	2.3	1.9	3.3	3.9	7.9
LOD (mg/m^3)	2431	2503	1282	1646	10723	8414

Table B.7. Average RR (%) for dual film, 2-wavelength responses to the six individual vapors tested at 50% C_{sat}; ε = 5%.

$MPN_{1,\lambda1}$	$MPN_{2,\lambda2}$	Avg. RR (%)
TEG_{405}	$C8_{405}$	99.9
TEG_{532}	$C8_{532}$	97.4
TEG_{532}	$C8_{630}$	89.4
TEG_{405}	$C8_{532}$	85.9
TEG_{532}	$C8_{405}$	85.8
TEG_{630}	$C8_{405}$	87.3
TEG_{630}	$C8_{532}$	87.1
TEG_{405}	$C8_{630}$	74.0
TEG_{630}	$C8_{630}$	59.9
TEG_{532}	HME_{532}	100
TEG_{405}	HME_{630}	99.9
TEG_{405}	HME_{532}	91.6
TEG_{630}	HME_{630}	88.9
TEG_{532}	HME_{405}	83.9
TEG_{405}	HME_{405}	83.2
TEG_{630}	HME_{532}	80.1
TEG_{630}	HME_{405}	76.7
TEG_{532}	HME_{630}	76.5
TEG_{405}	$DTE_{5,532}$	97.2
TEG_{405}	$DTE_{5,630}$	91.9
TEG_{405}	$DTE_{5,405}$	91.8
TEG_{630}	$DTE_{5,532}$	85.6
TEG_{630}	$DTE_{5,405}$	83.6
TEG_{532}	$DTE_{5,630}$	83.2
TEG_{532}	$DTE_{5,405}$	74.6
TEG_{630}	$DTE_{5,630}$	70.8
TEG_{532}	$DTE_{5,532}$	70.5
$C8_{532}$	HME_{532}	99.2
$C8_{630}$	HME_{630}	95.9
$C8_{405}$	HME_{405}	94.5
$C8_{532}$	HME_{630}	93.2
$C8_{630}$	HME_{405}	88.7
$C8_{532}$	HME_{405}	85.3
$C8_{405}$	HME_{532}	85.2
$C8_{630}$	HME_{532}	83.4

$C8_{405}$	HME_{630}	81.1

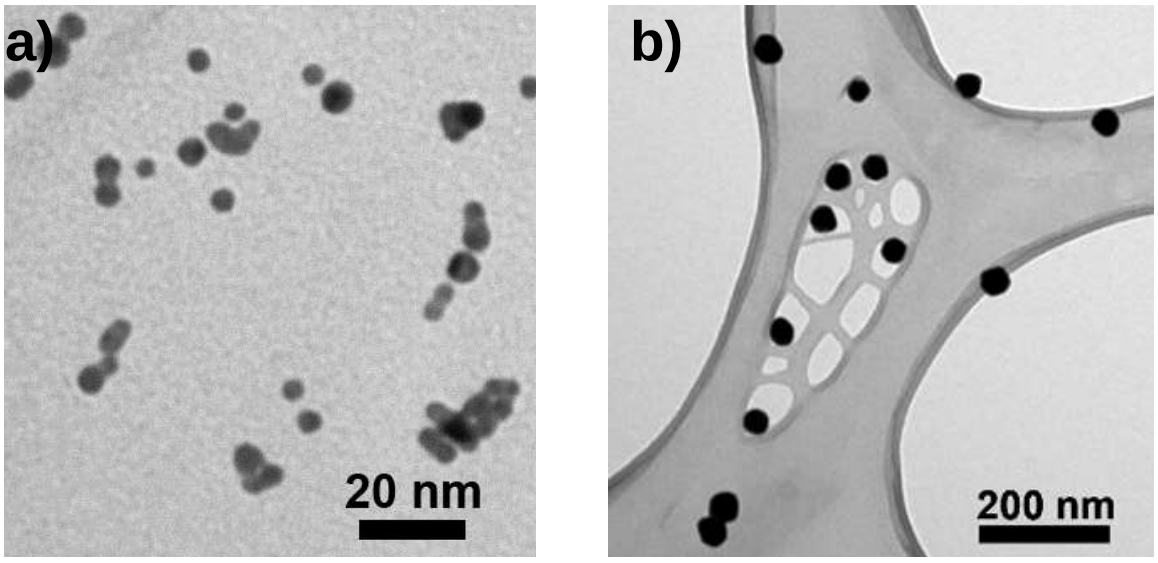

Figure B.1. TEM images of DTE MPNs synthesized by phase-transfer method: (a) 5 nm, (b) 40 nm.

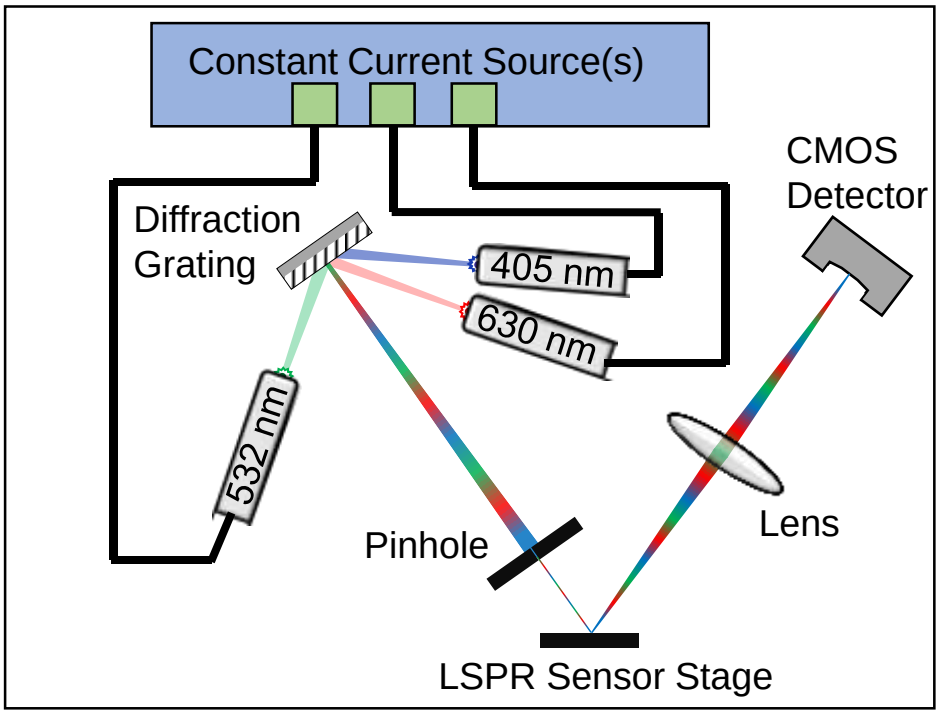

Figure B.2. Diagram of 3-laser reflectance measurement set-up used in preliminary tests to assess the utility of plasmonic MPN films as vapor sensitive interface materials in a multi-variable (multi-wavelength) sensing system.

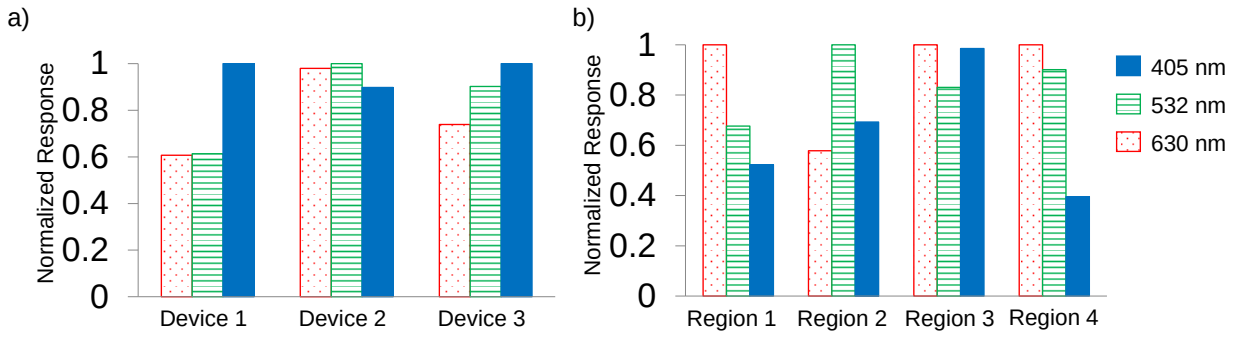

Figure B.3. Normalized response patterns (a) between different C8-drop-cast reflectance sensors and (b) different regions of a C8-spray coated reflectance sensor to toluene, illustrating both inter- and intra-sensor variability due to differences in film morphology and uniformity. Sensors were exposed to toluene vapor ranging from 2000-8000 ppm at a flow rate of 9 mL/min for a total of 5 min, followed by 5 min of purging with a line of scrubbed, dry air at the same flow rate.

a)

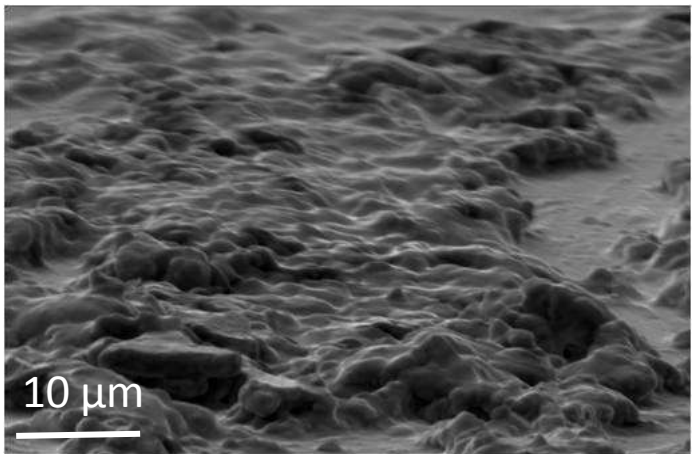

b)

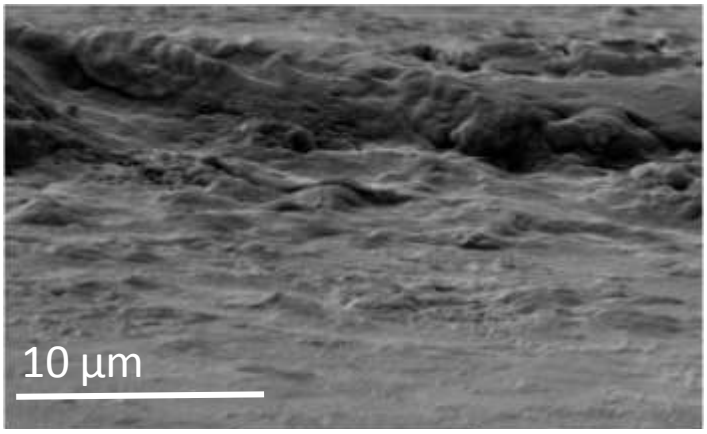

Figure B.4. SEM images of drop-cast (a) C8 and (b) HME films, showing significant variation in film morphology.

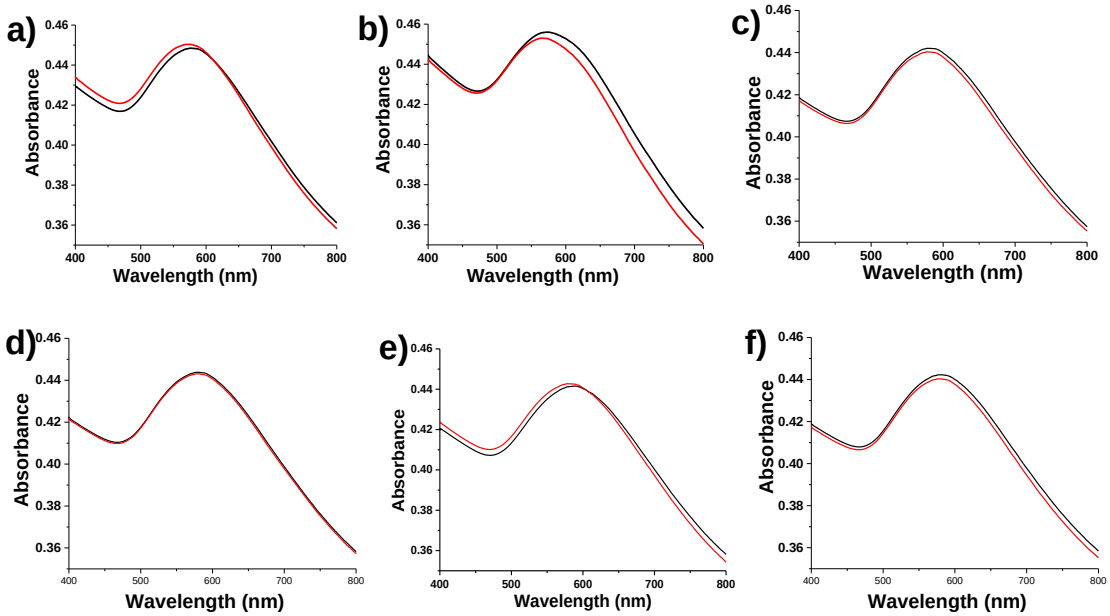

Figure B.5. Raw spectra of C8 before and during exposure to (a) TOL (b) OCT (c) MEK (d) IPA (e) PCE and (f) BAC vapors at $0.5C_{sat}$ (baseline spectra = black solid line; spectra upon dosing = red solid line).

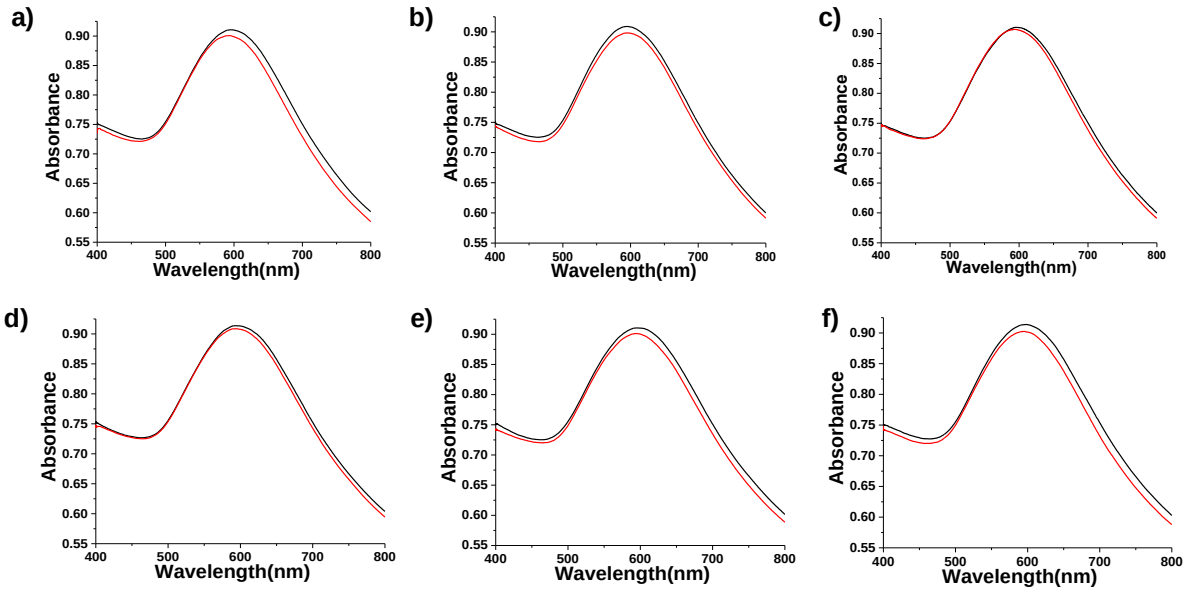

Figure B.6. Raw spectra of HME before and during exposure to (a) TOL (b) OCT (c) MEK (d) IPA (e) PCE and (f) BAC vapors at $0.5C_{sat}$ (baseline spectra = black solid line; spectra upon dosing = red solid line).

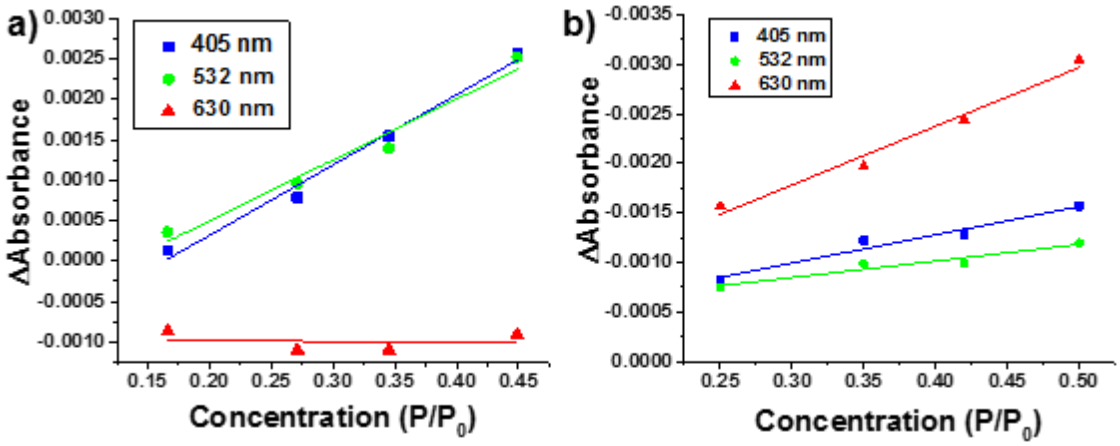

Figure B.7. Calibration curves for C8 exposure to a) TOL and b) BAC showing general trend of linear dependence of absorbance shifts on vapor concentration from 0.15-0.50C_{sat} ($R^2 \geq 0.96$ in all cases).

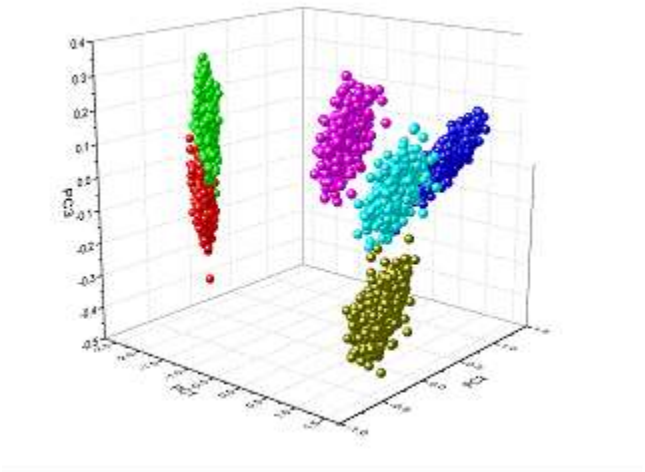

Figure B.8. 3D PCA scores plot for $C8_4$ showing excellent discrimination among the 6 test vapors. Green = PCE; Red = TOL; Gold = MEK; Aqua = IPA; Blue = BAC; pink = OCT.

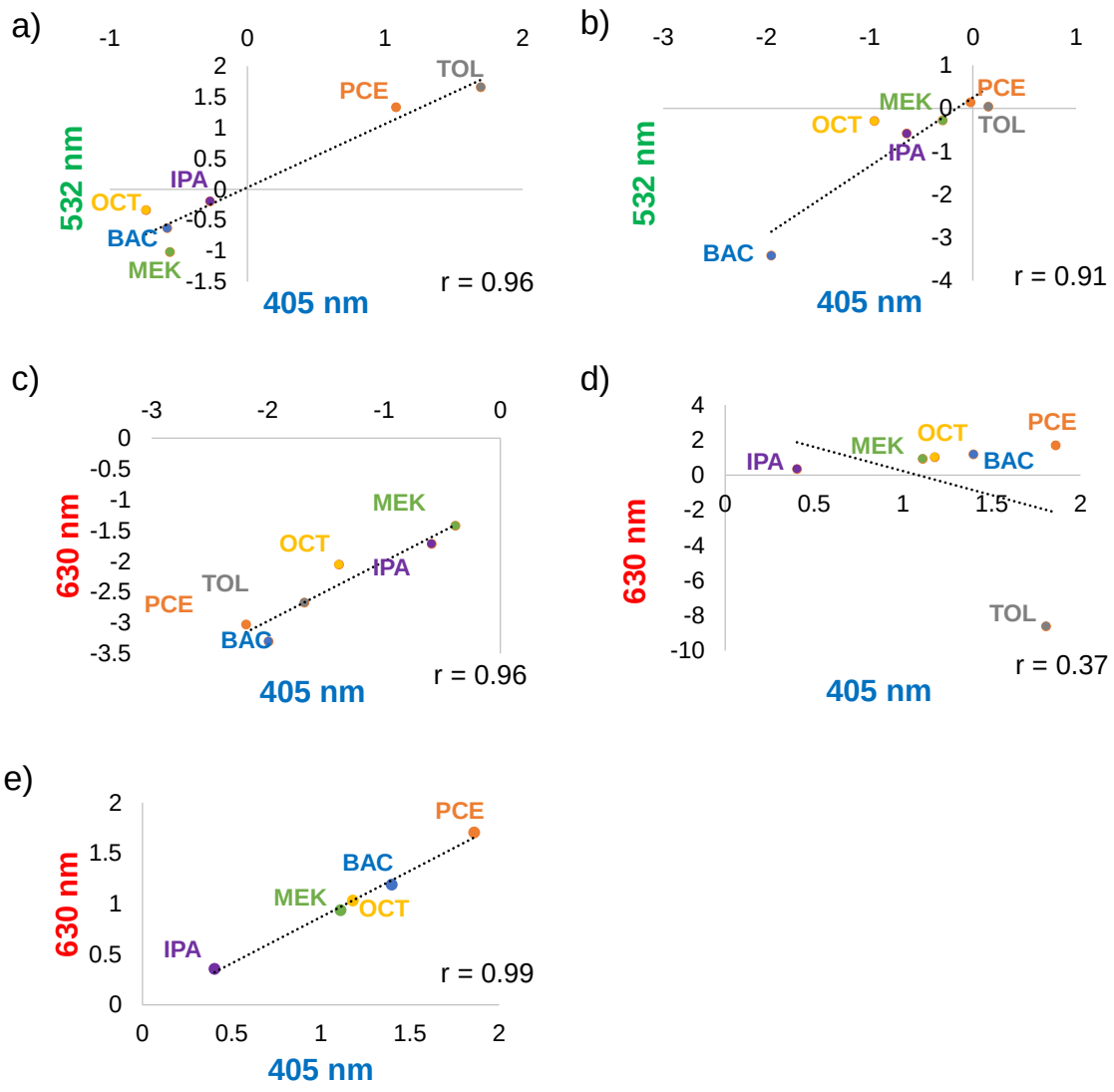

Figure B.9. Correlation plots for (a) C8: 405/ 532 nm (b) DTE_{40}: 405/ 532 nm (c) HME: 405/ 630 nm (d) DPA: 405/ 630 nm and (e) DPA: 405/ 630 nm, without the TOL response. The correlation coefficients, *r*, are given in the lower right of each plot.

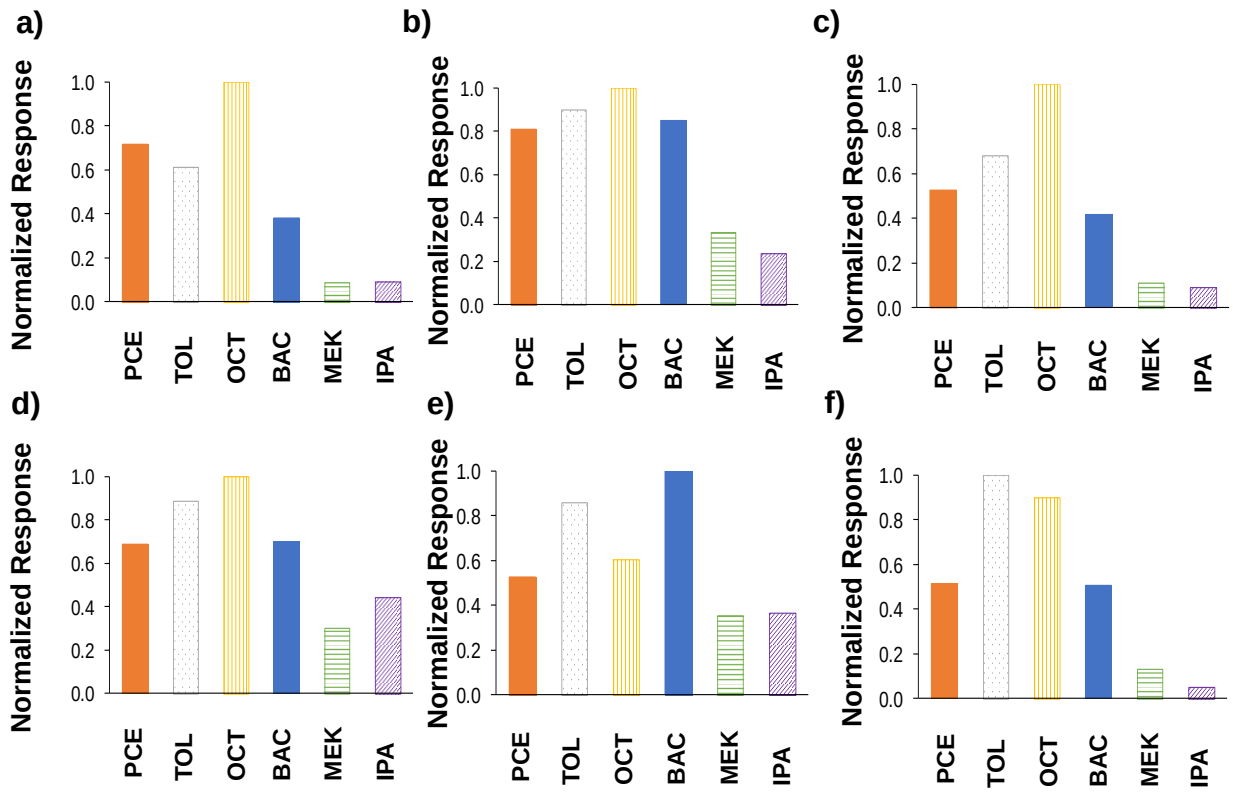

Figure B.10. Normalized sensitivities from the TSMRs coated with: (a) C8 (b) DPA (c) OPH (d) HME (e) TEG and (f) DTE_5 for the six test vapors. Sensitivities are normalized by the vapor giving the largest response.

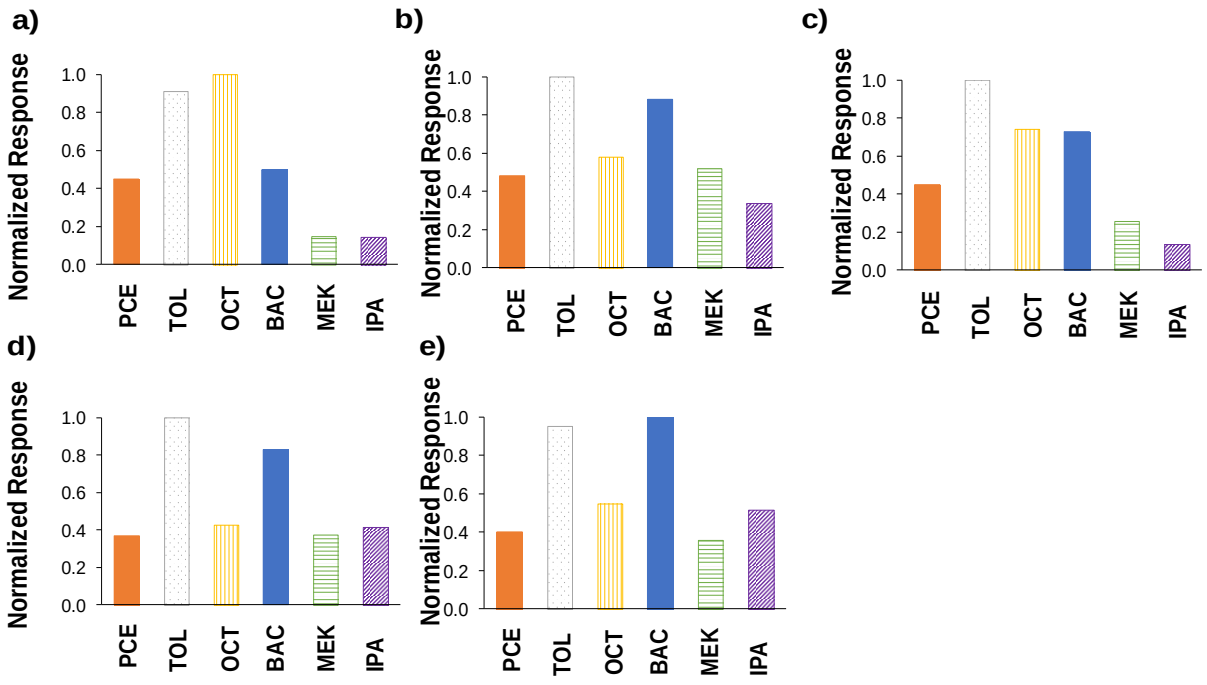

Figure B.11. Normalized sensitivities from the CRs coated with: (a) C8 (b) DPA (c) OPH (d) HME and (e) TEG for the six test vapors. Sensitivities are normalized by the vapor giving the largest response. Note: The size of the DTE ligand restricted the electron tunneling; resistances were too large to measure.